Evaluation of Highly Viscous Liquid Mixing Based on Particle Tracking

Dissertation

Submitted to the

Department of Chemistry

Faculty of Natural Sciences

University of Paderborn, Germany

for the degree

Doctor of Natural Science (Dr. rer. nat.)

by

Bhaskar Bandarapu

Adviser:

Prof. Dr.-Ing. H.-J. Warnecke

Institute of Technical Chemistry and

Chemical Process Engineering

Department of Chemistry

University of Paderborn

Co-adviser:

Prof. Dr. rer. nat. D. Bothe

Chair for Mathematics

Center for Computational Engineering Science (CCES)

RWTH Aachen

To my

Family, Teachers and Friends

Acknowledgements

List of Figures

List of Tables

List of Symbols

Abbreviations

CDS	central differencing scheme
CFD	computational fluid dynamics
CICSAM	comprehensive interface capturing scheme for arbitrary meshes
CS	control surface
CV	control volume
FD	finite difference
FE	finite element
FV	finite volume
QUICK	quadratic upwind interpolation for convective kinematics
RTD	residence time distribution
UDS	upwind differencing scheme
VOF	volume of fluid

Roman Letters

a	acceleration, m/s^2
$\mathbf{A}$	area, m^2
b	source term in discrete equation
c	specie concentration
C_u	Courant number
d	diameter, m

D	diffusion coefficient, m^2/s
D_{ij}	rate of deformation in tensor notation
D	rate of deformation tensor
E	energy, J
f	face
$\mathbf{f}$	body force, N
$\mathbf{F}$	force, N
g	acceleration due to gravity, m/s^2
g_1, g_2, g_3, g_4	nodal co-ordinates
H	higher order terms
I	intensity of segregation
J	diffusion flux, mol/m^{2}s
k	face number
L	characteristic length of macroscopic flow, m
m	molecular mass, kg
n	number of particles
$\mathbf{n}$	unit vector normal to the surface
N_e	Newton number
p	pressure, N/m^2
P_e	Peclet number
P	power, W
$r1, r2$	radii, m
$\mathbf{r}$	position vector, m
S	source term
t	time, s
T_{ij}	stress in tensor notation
T	rate of deformation stress tensor
$\mathbf{u}$	velocity, m/s
$\mathbf{u}_g$	grid velocity, m/s

V	volume, m^3
x, y, z	Cartesian co-ordinates

Greek Symbols

α	VOF coefficient
δ	Kronecker symbol
ϵ	given fraction or threshold
η	kinematic viscosity
γ	constant
Γ	convective term in Navier-Stokes equation
λ	molecular mean free path, m
μ	viscosity, kg/ms
Ω	angular velocity, rpm
ϕ	intensive property
Φ	extensive property
ρ	density, kg/m^3
σ	variance
τ	torque, N-m

Subscripts

ax	axial
Agit	agitation
Diss	dissipation
Kin	kinematic
max	maximum
mix	mixing
0	initial

Contents

Chapter 1

Introduction and Aim of the Work

1.1 Introduction

Industrial fluid mixing in stirred vessels is one of the basic and important requirements of most production systems in bio-chemical, food, pharmaceuticals, polymer, pulp and paper, waste water treatment and petroleum etc industries. The term 'mixing' refers to an operation or process which tend to reduce inhomogenities or gradients in composition, properties or temperature of the material bulk. Fluid mixing is the motion and/or contacting of a single or multiphase process with a liquid continuous phase to achieve a desired process result. Practically, every plant will contain some sort of tank where mixing is carried out by the relative movement of material between the various parts of the whole mass using suitable equipment for the specific operation or process. There are several ways to provide mixing action in a vessel, but this thesis is primarily concerned with the impeller type mixers in stirred vessels.

A study of the mixing process includes several basic considerations. The first is the effect of the vessel on the mixing process. Vessel geometry, dimensions, and the structure may dictate mixer selection and mixing performance. The next is the mixing impeller(s) to be used for a given specific process or operation and it would be a real problem if every new application requires a new impeller design. Thus impellers are usually made in an homologous and in geometrically similar series. Further, the flow

patterns generated by impellers can be divided into two basic types as axial- and radial-flow impellers. Axial-flow impellers produce flow parallel to the impeller shaft where as the radial-flow impellers discharge fluid to the vessel wall in a horizontal or radial direction.

Although mixing is one of the most ancient technological practices, there are still notable achievements to be done. The importance of future mixing and various steps to follow for better understanding of it is clearly demonstrated in a review article [36]. Since mixing is primarily due to the relative motion within the material to be mixed, the efficient design of the mixer gain much appreciation. Most of the available articles based the results on optimising the designs of the mixers focused on the flow field, power consumption and mixing time etc. Ample experimental and numerical data for the design and optimisation of mixers can be found in [55] and additional references given there. However, there is no systematic method for selecting and designing the mixers. Further, the majority of these investigations are concentrated mainly in the turbulent flow regime although many industrial mixing operations are carried out in laminar flow condition.

In laminar mixing, inertial terms in the equations of motion for incompressible fluids are either not present or not important because of their magnitude. The viscous terms in the equations of motion dominate the flow behaviour since viscosity is very large in such fluids. Additionally, rapid mixing or homogeneity cannot be easily obtained for highly viscous liquids since there are no turbulent eddies which enhance mixing by increasing the rotational speed of the agitator. Apart from large viscosities, the low diffusion coefficients are also responsible for laminar mixing to be an area-controlled process. The increase in interfacial area during mixing provides additional area, over which diffusion can act so that mixing can be accomplished. Therefore, the impellers used in laminar mixing are usually full-tank, close-clearance impellers. This means the diameter of such impellers approaches the diameter of the vessel to bring motion to the entire vessel volume. The present thesis contributes for the mixing of highly viscous liquids in close-clearance stirred vessels under laminar flow condition.

The preceeding section introduces the motivation as well as contribution of the current studies.

1.2 Motivation and Contribution

In the past, extensive experiments were carried out by several researchers to realise the effect of various parameters on mixing efficiency (quality) for different mixing devices at variable process conditions and material properties. However, for small changes in the design parameters of the mixers or for the different materials to be studied in the mixer, it is too laborious and expensive to perform experiments each time. On the other hand, technological progress in computers from the past two decades made it easier to explore and apply in engineering sciences. In particular, computer based simulation method "'computational fluid dynamics (CFD)"' has become a widely used tool for analysing, optimising and supporting the design of mixing processes [6, 8, 70].

In general, several numerical methods exist in the literature to assess the quality of mixing and some of the widely known among them are numerical tracer experiments, Lagrangian particle tracking simulations and entropy based calculations. Numerical tracer experiments are extensively used methods to quantify mixing and plenty of information is reported in the literature [55]. Although this method is of increasing importance as a means to analyse mixing processes, there is a principle problem which becomes a severe obstacle in case of highly viscous liquid mixing or, more generally in case of high tracer schmidt numbers. In this situation, a sufficiently accurate solution of the species equation can be spoiled by the effect of so-called numerical diffusion [21]. A way to avoid this problem is to replace the continuous tracer concentration by a number concentration obtained from Lagrangian (i.e. inertia free) particles. This approach does not suffer from artificial diffusion, since the position of tracer particles can be resolved with sub-grid-scale accuracy and the velocity field at these particle positions can be obtained by interpolation from its values at grid points. Please refer to [32,35,50,61,64] for further reading on Lagrangian particle based mixing calculations

for characterisation of different mixers. In addition, entropy based characterisation of mixing also gained much attention in recent years [61, 82]. The definition of entropy is given as a measure of disorder or degree of distributive mixing.

In the present work, theoretical method of calculating intensity of segregation, intensity of mixing and mixing time based on Lagrangian particle tracking is presented. The approach is as follows. The total computational domain is divided into smaller compartments (sub-volumes) and inertia free particles are placed initially in one compartment, say. During the process of particle tracking the resulting number concentrations are recorded and allow for computation of evolution of its variance. Based on the statistical measures, we provide an answer to the number of particles and compartments needed for a reliable assessment of the mixing quality. Further, this method is evaluated using the numerical investigation of mixing in a vessel stirred with an anchor type impeller as well as a specific kneader element operated under laminar flow condition for highly viscous liquids. Mixing times were calculated for both mixers based on evolution of intensity of segregation. Finally, a mapping matrix method is elaborated to evaluate the quality of mixing. This mapping method employs a transition matrix, which describes how many particles are advected from one compartment to the other compartment in a particular period of time. With the aid of this transition matrix one can compute variance evolutions and mixing times using vector multiplications with significantly less computational effort.

1.3   Organisation of the Thesis

The contents of the each chapter are briefly described in this section. Where relevant, the key problems addressed in the chapters are highlighted, and regarded them as the important contributions of the work. The present thesis contains six chapters, including an introduction (Chapter 1) and conclusions (Chapter 6). Since this work contributes for the modelling and simulation of mixing in stirred vessels, it first starts with the mathematical formulation. Chapter 2 presents an overview on the basic

equations of fluid flow. These governing equations are developed based on continuum hypothesis, according to which the physical quantities are considered to be the continuous functions of space and time. The resultant system of equations are presented both in integral form as well as in differential form.

In Chapter 3 detailed information on numerical techniques was provided. A finite volume based commercial CFD - tool is used in the current studies and hence a comprehensive description is supplied on this method. A spatial and temporal discretization schemes are elaborated to solve the governing transport equations. Simulation of mixing in stirred vessels is always a challenging task as it involves complicated design mechanism. Different available numerical methods (e.g. rotating reference frame, moving mesh) to model flow in mixing vessels are emphasized and employed on simple reference geometry. Finally, torque computation in a simple Couette-flow between two rotating cylinders is discussed and compared with the analytical results.

The numerical analysis in one of the ancient yet widely used mixing apparatus, anchor mixer is addressed in Chapter 4. A review on the relevant literature is also given there. Detailed flow field computations are carried out and torque is computed for partly filled vessel stirred with anchor type impeller. The torque computation procedure is given and the power number is explained. With ever increasing demand for the estimation of mixing quality based on the numerical methods, there exists a severe obstacle in the form of numerical diffusion when numerical tracer experiments are carried out especially for highly viscous liquids. A method of avoiding this problem is addressed in this chapter based on Lagrangian particle tracking. Additionally, an answer for the minimum number of particles as well as number of compartments is provided with the aid of statistical measures and finally evaluation of mixing in anchor mixer is performed using particle tracking.

Chapter 5 extends the Lagrangian particle tracking simulation to investigate mixing in a specific kneader element. A summary on the relevant literature for kneader, single and double screw extruder is given there. Further, a mapping matrix method is presented which employs a transition matrix to describe the advection of particle in a

particular period of time. This transition matrix allows to estimate the mixing quality with significantly less computational efforts. The comparison of simulation data with mapping matrix is presented. A summary and outlook of the thesis is presented in Chapter 6.

Chapter 2

Mathematical Formulation

2.1 Introduction

The first step in dealing with the problems related to hydro or fluid dynamics, is to understand the physical background and describe them using mathematical equations. These equations are derived by postulating the continuum i.e., continuous hypothesis which allows to use the representation of physical quantities such as velocity, pressure, density and temperature. These quantities are considered to be continuous functions of space in the fluid and of time. Of course, a similar hypothesis is made in the mechanics of solids, and the two subjects together are often designated as continuum mechanics. If λ is the molecular mean free path and L is the characteristic length of macroscopic flow, then the ratio λ/L is called Knudsen number. The assumption of continuum hypothesis is valid at macroscopic level (if $\lambda/L \ll 1$) to represent transport phenomena in gases, liqiuds and solids. However, contiunuum hypothesis breaks down on the molecular or microscopic level (if $\lambda/L \leq 1$) where each fluid is descrete with its properties fluctuating randomly and are not in local equilibrium. This is due to the fact that the molecules in such a process do not get sufficient time and space to come to local equilibrium.

Nevertheless, the vast majority of phenomena encountered in fluid mechanics fall well within the continuum domain. This situation is illustrated in Fig. 2.1, where the
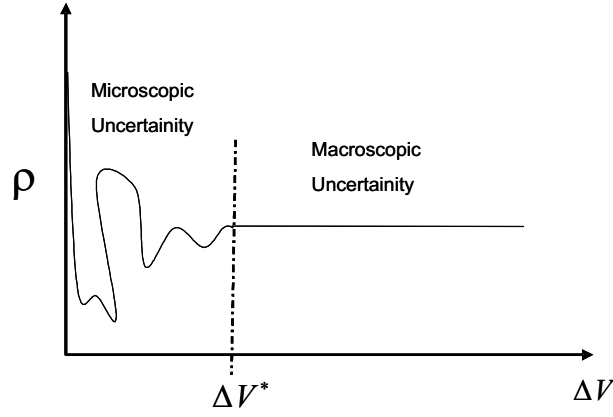
Figure 2.1: Illustration of continuum hypothesis, where the density ρ is calculated from molecular mass Δm within a given volume ΔV.

density ρ is calculated from molecular mass Δm within a given volume ΔV. If ΔV is very large, ρ is affected by the inhomogeneities in the fluid itself. As ΔV becomes smaller, and almost uniform density is reached independent of ΔV. In continuum approximation, the point density is defined as that value of ρ which occurs at the smallest magnitude of ΔV, before statistical fluctuations becomes significant. This limiting volume is ΔV^*, below which molecular variations may be important and above which aggregate variations may be important. Thus, the density ρ of a fluid now becomes:

$$\rho = \lim_{\Delta V \to \Delta V^*} \frac{\Delta m}{\Delta V} \; . \tag{2.1}$$

 In the present work, the dimensions of interest are very large compared to microscopic level, and hence it is assumed that the behaviour of the fluid in terms of macroscopic properties. In this case, the continuum hypothesis is valid as a statistical average of corresponding properties of a large numbers of molecules. Now, on this basis it is possible to establish equations governing the motion of the fluid which are independant as far as their form is concerned.

2.2 Governing Equations of Fluid Flow

In this section, the mathematical statements of two fundamental physical principles are developed upon which most of the fluid mechanics is based and they are conservation of mass and momentum. Additionally, conservation of species equation is also formulated. The derivations of governing transport equations of fluid flow given here are based on the lecture notes of [13] and other references [4, 21, 81]. Before delving into the elaborations of the equations, it is worth a while to mention some of the advantages and disadvantages of mathematical modeling in academic or industrial research. Inspite of the high initial investment in mathematical modeling, especially as relates to experiments:

- serves as an alternative to experiments

- is cheaper and faster

- can be used in planning experiments

- is used in parameter investigation to answer "'what if"' questions

- provides information about certain transport phenomena that are otherwise difficult to measure experimentally.

2.2.1 Basic Concepts

All the fluid mechanics is governed by conservation of mass, momentum, energy and other constitutive equations. These can be mathematically expressed in many ways and are briefly discussed here.

Differential Element Approach

Consider an infinitesimally small fluid element in the flow field with a differential volume ΔV. The fluid element may be fixed in space and fluid is moving through it or it may be moving along the stream line with a velocity equal to the flow velocity

at each point. The fundamental physical principles applied to this small fluid element leads directly in terms of deformation rate in partial differential equation form. The partial differential equations obtained directly from the fluid element fixed in space are in conservation form whereas the partial differential equations obtained directly from the moving fluid element are in nonconservation form.

Control Volume Approach

Consider an arbitrary closed volume drawn within a finite region of the general flow field. This volume defines a control volume CV, and a closed surface which bounds the control volume is the control surface CS. The control volume may be fixed in space with the fluid moving through it or the control volume may be moving with the fluid such that the same fluid particles are always inside it. The fundamental physical principles applied to the fluid inside the control volume and the fluid crossing the control surface gives the transport equations in integral form. Of course, on the manipulation of these integral forms of transport equations generates partial differential equations. The integral form of the equations obtained from the finite control volume fixed in space are in conservation form whereas, the equations obtained directly from the finite control volume moving with the fluid are in nonconservation form. The control volume approach is considered to be mathematically more rigorous as it does not assume the solution to be continuous before hand. However, both the methods of formulation gives the final form of the equations which are independant of the method of derivation. In this chapter we will focus on integral form (i.e., control volume approach) of the equations since most of the commercial CFD codes are based on finite volume method.

Time Derivatives

Let us consider a fluid element moving along a curve C as shown in Fig. 2.2. When this fluid element moves from point 1 to 2, one of its velocity components changes from u_1 at t_1 to u_2 at t_2. The time rate of change of velocity of the fluid element as t_2
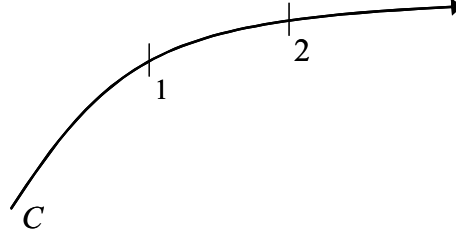
Figure 2.2: Description of time derivatives. Assume that a fluid element is moving along a curve C through points 1 and 2.

approaches t_1 becomes:

$$\lim_{t_2 \to t_1} \frac{u_2 - u_1}{t_2 - t_1} = \frac{du}{dt} . \tag{2.2}$$

Here, $\frac{du}{dt}$ is known as the total derivative and is defined as the time rate of change of velocity of the given fluid element as it moves from point 1 to 2. This kind of description of fluid flow is called Lagrangian flow analysis. It is convenient to use fixed coordinate system and measure the velocity with respect to the coordinate system as it is difficult to follow the fluid element. Therefore, the difference in velocities between successive fluid elements which arrive at a point 1, seperated by time difference Δt, is given by:

$$\lim_{\Delta t \to 0} \frac{u_1(t + \Delta t) - u_1(t)}{\Delta t} = \frac{\partial u}{\partial t} . \tag{2.3}$$

Here, $\frac{\partial u}{\partial t}$ is known as the partial derivative and is defined as the time rate of change of velocity at a fixed point 1. This kind of description of fluid flow is called Eulerian flow analysis. Thus, $\frac{du}{dt}$ and $\frac{\partial u}{\partial t}$ are physically and numerically different quantities. Similarly:

$$\lim_{\Delta x \to 0} \frac{u_1(x + \Delta x) - u_1(t)}{\Delta x} = \frac{\partial u}{\partial x} , \tag{2.4}$$

where $\frac{\partial u}{\partial x}$ is the partial derivative and is defined as the time rate of change of velocity at a given instant of time t. Furthermore, both Lagrangian and Eulerian flow analysis can be related as follows. Since $u = u(\mathbf{x}, t)$:

$$\frac{du}{dt} = \frac{\partial u}{\partial t} + \frac{\partial u}{\partial x} \frac{dx}{dt} + \frac{\partial u}{\partial y} \frac{dy}{dt} + \frac{\partial u}{\partial z} \frac{dz}{dt} , \tag{2.5}$$
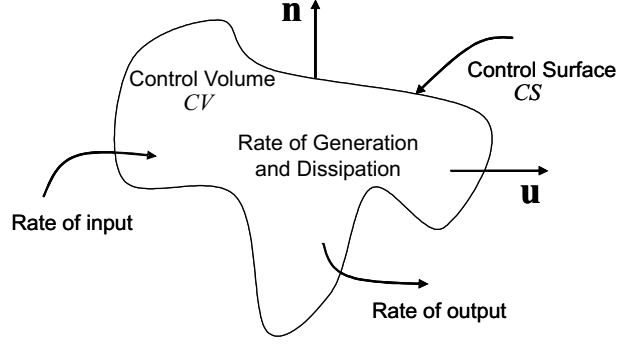
Figure 2.3: Schematic representation of the Reynolds transport theorem.

where $(x, y, z) = \mathbf{x}$ is the coordinate of the fluid element being followed at instant t. Therefore:

$$\frac{du}{dt} = \frac{\partial u}{\partial t} + u\frac{\partial u}{\partial x} + v\frac{\partial u}{\partial y} + w\frac{\partial u}{\partial z}\,, \tag{2.6}$$

can be written and $(u, v, w) = \mathbf{u}$ is specified. Additionally, the vector operator ∇ in three dimensional cartesian coordiante system is defined as:

$$\nabla = \mathbf{i}\frac{\partial}{\partial x} + \mathbf{j}\frac{\partial}{\partial y} + \mathbf{k}\frac{\partial}{\partial z}\,. \tag{2.7}$$

Finally, we write:

$$\frac{du}{dt} = \frac{\partial u}{\partial t} + \mathbf{u}\cdot\nabla u\,. \tag{2.8}$$

In the above equation $\frac{du}{dt}$ is the total derivative, which is the time rate of change of velocity of a moving fluid element; $\frac{\partial u}{\partial t}$ is the local derivative, which is the time rate of change of velocity at a fixed point; $(\mathbf{u}\cdot\nabla u)$ is the convective derivative also commonly known as substantial derivative, which is the time rate of change of velocity due to the movement of fluid element from one location to another location in the flow field.

Reynolds Transport Theorem

Consider a system with a control volume CV fixed in space and enclosed with a control surface CS as shown in Fig. 2.3. Reynolds transport theorem states that the rate of change of an extensive property Φ within the system is equal to sum of the rate of

change of Φ within the control volume and the net rate of Φ through the control surface. Let ϕ be an intensive property and is defined as Φ per unit mass of the fluid. Since Φ is defined with respect to a fixed mass of the fluid, the conservation laws (mass and momentum) are also applicable to ϕ. Then, the relation between Φ and ϕ can be written as:

$$\Phi = \int_{CV} \rho\,\phi\,dV \tag{2.9}$$

where ρ is the density of the fluid. Let $\mathbf{u}$ be the velocity and $\mathbf{n}$ be a unit normal drawn outward on CS. The Reynolds transport theorem can be stated as:

$$
\begin{array}{ccc}
\text{Rate of change} & = & \text{Net outflow of } \Phi \text{ at} \\
\text{of } \Phi \text{ in time} & & \text{the control surface}
\end{array}
\;+\;
\begin{array}{c}
\text{Rate of change of } \Phi \\
\text{by generation and dis-} \\
\text{sipation}
\end{array}\,.
$$

Mathematically this means:

$$\frac{d\Phi}{dt} = \int_{CS} \rho\,\phi\,\mathbf{u}\cdot\mathbf{n}\,dS + \int_{CV} \frac{\partial}{\partial t}\left(\rho\,\phi\right)dV\,. \tag{2.10}$$

The above equation is often called the Reynolds transport equation or control volume equation.

2.2.2 Continuity Equation

Continuity equation is based on the law of conservation of mass, according to which the mass of a closed system remains constant regardless of the processes acting inside the system. This means that matter changes from one form to another form but neither created nor destroyed. For example, for any chemical reaction in a closed system, the mass of the reactants must be equal to the mass of the products.

The integral form of the continuity equation is obtained directly from Reynold's transport theorem [Eq. 2.10], by setting $\frac{d\Phi}{dt}=0$ and $\phi=1$:

$$\int_{CV} \frac{\partial\rho}{\partial t}\,dV + \int_{CS} \rho\,\mathbf{u}\cdot\mathbf{n}\,dS = 0\,. \tag{2.11}$$

In vector calculus, Gauss divergence thoerem (which states that the flux of a vector field on a surface is equal to the volume integral of the divergence on the region inside the surface) is used to transform the surface integral into volume integral. Therefore, using Gauss divergence theorem, surface integral in Eq. 2.11 can be expressed as a volume integral:

$$\int_{CS} \rho \, \mathbf{u} \cdot \mathbf{n} \, dS = \int_{CV} \nabla \cdot \rho \, \mathbf{u} \, dV. \tag{2.12}$$

Replacing surface integral in Eq. 2.11 using Eq. 2.12, gives:

$$\int_{CV} \left(\frac{\partial \rho}{\partial t} + \nabla \cdot \rho \, \mathbf{u} \right) dV = 0 \,, \tag{2.13}$$

for any arbitrary control volume CV. Allowing the control volume to become infinitesinally small, leads to a differential coordinate free form of the continuity equation:

$$\frac{\partial \rho}{\partial t} + \nabla \cdot \rho \, \mathbf{u} = 0 \,. \tag{2.14}$$

In the above, the velocity vector $\mathbf{u}$ represents three velocity components in cartesian coordinate system. Expressions in cylindrical and spherical coordinate systems for the continuity equation can be found in many text books [11,57]. Continuity equation represented in tensor form:

$$\frac{\partial \rho}{\partial t} + \frac{\partial (\rho \, u_i)}{\partial x_i} = 0 \,, \tag{2.15}$$

where x_i (i=1,2,3) are the Cartesian coordinates and u_i are the corresponding Cartesian components of the velocity vector $\mathbf{u}$. In many applications involving liquids, the density ρ is constant and the flow is said to be incompressible. For such flows, Eq. 2.14 can be simplified as:

$$\nabla \cdot \mathbf{u} = 0 \,. \tag{2.16}$$

The flows representing the above equation are called divergence free.

2.2.3   Momentum Equation

The momentum of a point mass m with velocity u is given simply by mu. The momentum equation is based on conservation of momentum, according to which the rate of change of (linear) momentum of a fluid element is equal to the sum of the forces acting on it, which is nothing but Newton's second law of motion.

Rate of change of momentum = Sum of all relevant forces.

Therefore:

$$\frac{d}{dt}(m\,\mathbf{u}) = \mathbf{F} \quad \text{or alternatively,} \quad \mathbf{F} = m\,\mathbf{a} \quad \text{for} \quad m = \text{const}\,,$$

where $\mathbf{a}$ is an acceleration. The integral form of the momentum equation is obtained directly from Reynold's transport theorem [Eq. 2.10], by substituting $\frac{d\Phi}{dt} = \sum \mathbf{F}$ and $\phi = \mathbf{u}$:

$$\int_{CV} \frac{\partial}{\partial t}(\rho\,\mathbf{u})\,dV + \int_{CS} \rho\,\mathbf{u}\,\mathbf{u}\cdot\mathbf{n}\,dS = \sum \mathbf{F}\,. \tag{2.17}$$

Here, $\mathbf{F}$ represents all the relevant forces and they are:

- **surface forces**: which act directly on the surface of the fluid element (pressure, shear and normal stresses, surface tension etc.);

- **body forces**: which act directly on the volumetric mass of the fluid element (gravitational, centrifugal, Coriolis, electromagnetic etc.).

For Newtonian fluids, the molecular rate of momentum transport can be written as:

$$\mathsf{T} = -\left(p + \frac{2}{3}\mu\,\nabla\cdot\mathbf{u}\right)\mathsf{I} + 2\,\mu\,\mathsf{D}\,, \tag{2.18}$$

where T is the stress tensor, p is the static pressure, μ is the dynamic viscosity, I is the unit vector and D is the rate of deformation tensor. The rate of deformation tensor D is defined as:

$$\mathsf{D} = \frac{1}{2}\left[\nabla\,\mathbf{u} + (\nabla\,\mathbf{u})^{\mathsf{T}}\right]\,. \tag{2.19}$$

The above two [Eq. 2.18 and Eq. 2.19] equations in tensor notation gives:

$$T_{ij} = -\left(p + \frac{2}{3}\,\mu\,\frac{\partial u_j}{\partial x_j}\right)\delta_{ij} + 2\,\mu\,D_{ij}\,, \tag{2.20}$$

$$D_{ij} = \frac{1}{2}\left(\frac{\partial u_i}{\partial x_j} + \frac{\partial u_j}{\partial x_i}\right), \tag{2.21}$$

where δ_{ij} is Kronecker symbol (δ_{ij} =1 if i=j and δ_{ij}=0 otherwise).

Finally, the integral form of the momentum conservation equation with the body forces represented by $\mathbf{f}$ becomes:

$$\int\limits_{CV} \frac{\partial}{\partial t}\,(\rho\,\mathbf{u})\,dV + \int\limits_{CS} \rho\,\mathbf{u}\,\mathbf{u}\cdot\mathbf{n}\,dS = \int\limits_{CS} \mathsf{T}\cdot\mathbf{n}\,dS + \int\limits_{CV} \rho\,\mathbf{f}\,. \tag{2.22}$$

By applying Gauss divergence theorem to the convective (2nd term) and diffusive (3rd term) flux terms in the above equation, results:

$$\frac{\partial(\rho\,\mathbf{u})}{\partial t} + \nabla\cdot(\rho\,\mathbf{u}\,\mathbf{u}) = \nabla\cdot\mathsf{T} + \rho\,\mathbf{f}\,. \tag{2.23}$$

The above equation represents a coordinate-free form of the momentum conservation equation. The momentum conservation equation [Eq. 2.23] together with the continuity equation [Eq. 2.14] are popularly known as *Navier-Stokes* equations.

2.2.4   Species Equation

In addition to the continuity and momentum equations, if a problem involves transport of mass then an additional species concentration equation needs to be solved. The conservation equation for species transport takes the general form:

$$\int\limits_{CV} \frac{\partial}{\partial t}\,(\rho\,c)\,dV + \int\limits_{CS} \rho\,c\,\mathbf{u}\cdot\mathbf{n}\,dS = -\int\limits_{CS} J\cdot\mathbf{n}\,dS\,, \tag{2.24}$$

in the absence of a chemical reaction. Here, c is the specie concentration and J is the diffusion flux of the species. Diffusion flux arises due to the concentration gradients and is defined by Fick's first law of diffusion. According to this:

$$J = -D\,\frac{\partial c}{\partial x}\,, \tag{2.25}$$

where D is the diffusion coefficient.

Present thesis do not deal with the problems related to heat transfer and hence the energy conservation equation is not discussed here. It is clear from the above equations that they all have common terms and it is useful to write the conservation equations in one general form. Thus, the integral form of the generic transport equation with ϕ as a variable gives:

$$\int_{CV} \frac{\partial}{\partial t}(\rho\,\phi)\,dV + \int_{CS} \rho\,\phi\,\mathbf{u}\cdot\mathbf{n}\,dS = -\int_{CS} \Gamma\,\Delta\,\phi\cdot\mathbf{n}\,dS + \int_{CV} S_\phi\,dV\,. \tag{2.26}$$

The coordinate-free form of the above equation yields:

$$\frac{\partial(\rho\,\phi)}{\partial t} + \nabla\cdot(\rho\,\phi\,\mathbf{u}) = -\nabla\cdot(\Gamma\,\Delta\,\phi) + S_\phi\,. \tag{2.27}$$

The Eq. 2.27 highlights the various transport processes: *the rate of change* and the *convective* terms on the left hand side whereas the *diffusive* and the *source* terms on the right hand side. The next chapter deals with the numerical methods which are used to solve the transport equations derived in this chapter.

Chapter 3

Numerical Methodology

3.1 Introduction

Experimental methods are popular and desirable in science and engineering and they also provide a deep understanding of important concepts about a particular problem. But sometimes it becomes very difficult to establish an experimental model. Moreover, the flows and related phenomena described by integro-differential equations cannot be solved analytically except in some special cases. In such instances, numerical methods are mandatory. Solution of transport equations using numerical method is known as computation. The advantages of computation are low cost, faster than experimental method, gives local values compared to experiments where only global values are available and ability to simulate both ideal and real conditions. However, it might be difficult to obtain numerical solution for problems involving complex geometries, non-linearities, sensitive variations. In addition, it can be difficult to develop mathematical model for some processes like combustion, multi-phase flows, non-Newtonian flows, complex turbulent flows etc. Even if the problem is modelled, it is difficult to determine how reliable is the modelled equation. Thus verification of the model has to be done from the results of corresponding experiments. The fundamental equations of the fluid flow have been derived in Chapter 2 and simplification of these equations are used to realize the fluid flow. The simplified equations are usually based on a combination of

approximations and dimensional analysis.

Inspite of the limitations, some numerical methods are used to obtain an approximate solution for the transport equations. For this puprose, one need to follow a discretization method which approximates the differential equations by a system of algebraic equations which can be then solved on a computer. This method is called Computational Fluid Dynamics (CFD). The first step in CFD is the development of mathematical model which contains set of differential equations and boundary conditions based on the conservation principles. Next step is the division of solution domain into a small finite number of sub domains (numerical grid or descrete points) at which the variables are calculated. This numerical grid is generated depending on the problem and can be of structured or unstructured. A suitable discretization method (finite difference, finite volume or finite element etc) is chosen to solve the mathematical model at the descrete points in space and time. Discretization methods applied at descrete points yields a system of non-linear algebraic equations and an iterative method is used to solve these non-linear algebraic equations. Based on the accuracy and efficiency of the solution, one needs to set the convergence criteria for the iterative method. Finally, post processing of the solution into a physically realistic result completes the numerical investigation of any fluid flow. Since discretization plays very important role in numerical methodology, the following section is dedicated to finite volume descitization method which is used in the present thesis.

3.2   Finite Volume Method

Basically, there are three well-known discretization schemes which are finite difference (FD), finite volume (FV) and finite element (FE) available to solve a mathematical model. Finite difference method is the oldest method available and the partial derivatives are approximated by the nodal values of variables using Taylor series expansion at each grid point resulting in algebraic equation. Finite difference method is very simple and effective for simple geometries. In finite volume method whole domain is

discritized into small volumes and differential equation is integrated and terms are approximated to obtain algebraic equation at each control volume. In finite element method complete domain is divided into finite elements that are generally unstructured. In this method differential equation is multiplied by a weight function before integration. Unknown variable is approximated by a shape function and substituted in the weighted integral equation.

Finite volume method is popular among the engineers and scientists because each term in this method has a physical meaning. The solution domain is divided into a finite number of small control volumes called computational cells where the flow variables are defined. This is usually done at the geometric centre of the a control-volume and this approach is called colocated cell-centered arrangement. The differential form of the governing equations are first integrated over the individual computational cells to transform the flux terms into surface integrals and then approximated in terms of the cell-centred nodal values of the dependent variables.

The integral form of the generic transport equation with ϕ as a variable is given as:

$$\int\limits_{CV} \frac{\partial}{\partial t}\left(\rho\,\phi\right)dV + \int\limits_{CS} \rho\,\phi\,\mathbf{u}\cdot\mathbf{n}\,dS = \int\limits_{CS} \Gamma\,\Delta\,\phi\cdot\mathbf{n}\,dS + \int\limits_{CV} S_\phi\,dV\,. \qquad (3.1)$$

Eq. 3.1 applies to each control volume as well as to the complete solution domain. To obtain an algebraic equation for each control volume, the surface and volume integrals need to be approximated using discretization techniques. The discretization of each term in the Eq. 3.1 is performed based on the name convention depicted in Fig. 3.1. In the current formulation, each control volume centre has six immediate neighbours which get involved in each term of the generic transport equation. The control volume surface is subdivided into six plane faces denoted by e,w,n,s,t and b to represent east, west, north, south, top and bottom directions with respect to the central node P as shown in Fig. 3.1.
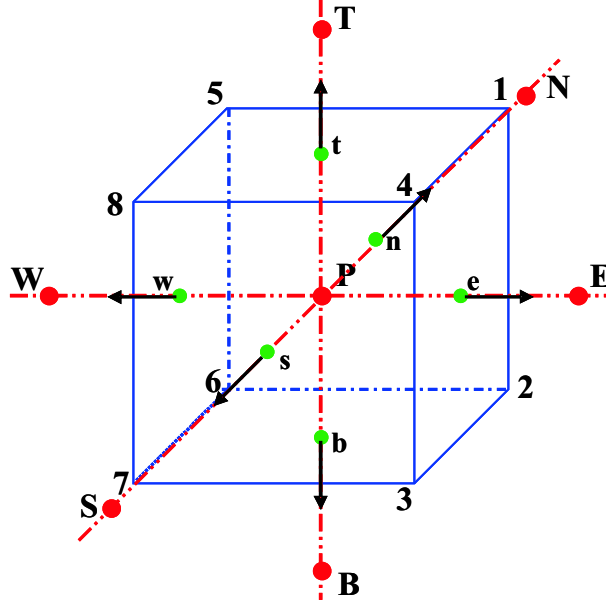
Figure 3.1: Illustration of control volume approach with three dimensional discretization notation.

3.2.1   Spatial Discretization

The second and third terms of the Eq. 3.1 are contributions due to the convection $(\rho \phi \mathbf{u} \cdot \mathbf{n})$ and diffusion $(\Gamma \Delta \phi \cdot \mathbf{n})$. The net flux through the control volume boundary is the sum of integrals over the six control volume faces, this means:

$$\int\limits_{CS} f \, dS = \sum_k \int\limits_{CS_k} f \, dS \,, \tag{3.2}$$

where f is the component of the convective or diffusive vector in the direction normal to the control volume face. One would need to know f to calculate the surface integral in Eq. 3.2 and therefore the cell face values are approximated in terms of the nodal (cell centred) values. Similarly the source term in Eq. 3.1 requires integration over the volume of a control volume. A second-order approximation is used to replace the volume integral by the product of the mean and the volume of a control volume. Thus, the volume integral is approximated as the value at the centre of a control volume as:

$$S_P = \int\limits_{CV} S \, dV = \overline{S} \, \Delta V \approx S_P \, \Delta V \,, \tag{3.3}$$

where S_P is for the value of S at the control volume centre. No interpolation is necessary to calculate S_P since all variables are available at node P.

The approximations to the integrals also require the values of the variables at locations other than control volume centres. Assume that $\mathbf{u}$, ρ and Γ are known at all locations. The value of ϕ and its gradient normal to the cell face at one or more locations on the control volume surface are needed to calculate convective and diffusive fluxes. The volume integrals of the source term also require these values. Hence, ϕ has to be expressed in terms of the nodal values by interpolation methods. There are several interpolation methods availabal for approximating ϕ and some of the frequently used among them are described below.

Upwind Differencing Scheme (UDS)

In this interpolation method, ϕ_e is approximated using a forward or backward difference approximation depending on the flow direction. If the flow is in positive direction $(\mathbf{u} \cdot \mathbf{n})_e > 0$, approximation for ϕ_e gives:

$$\phi_e = \phi_P \,,$$

if the flow is in negative direction $(\mathbf{u} \cdot \mathbf{n})_e < 0$, approximation for ϕ_e gives:

$$\phi_e = \phi_E \,.$$

For the flow in positive direction, Taylor series expansion about P is given as:

$$\phi_e = \phi_P + (x_e - x_P) \left(\frac{\partial \phi}{\partial x} \right)_P + \frac{(x_e - x_P)^2}{2} \left(\frac{\partial^2 \phi}{\partial x^2} \right)_P + H \,, \tag{3.4}$$

where H denotes higher-order terms. This approximation retains only the first term on the right hand side of the Eq. 3.4, so it is a first order scheme. Although UDS approximation never yields oscillatory solutions, it is numerically diffusive due to Taylor series truncation error.

Central Differencing Scheme (CDS)

Central differencing approximation for the value at control volume face centre is linear interpolation between two nearest neighbouring nodes, irrespective of flow direction.

Approximation for ϕ_e at location e is given as:

$$\phi_e = \phi_E \lambda_e + \phi_P (1 - \lambda_e) \,, \tag{3.5}$$

where the linear interpolation factor λ_e is defined as:

$$\lambda_e = \frac{x_e - x_p}{x_E - x_P} \,.$$

The Taylor series expansion for CDS gives:

$$\phi_e = \phi_E \lambda_e + \phi_P (1 - \lambda_e) - \frac{(x_e - x_P)(x_E - x_e)}{2} \left(\frac{\partial^2 \phi}{\partial x^2} \right)_P + H \,. \tag{3.6}$$

This is the simplest second order accurate and is most widely used scheme. This scheme may produce oscillatory solution because of the large variations of the fluxes between the neighbouring points, but produces less numerical diffusion.

Quadratic Upwind Interpolation for Convective Kinematics (QUICK)

The quadratic upstream interpolation for convective kinetics (QUICK) scheme [41] is a third order scheme which fits parabola through two points upstream and one point downstream to get an interpolated value. Approximation for ϕ_e is given according to the nature of convection. If the flow is in positive direction:

$$\phi_e = \phi_P + g_1(\phi_E - \phi_P) + g_2(\phi_P - \phi_W) \,,$$

and if the flow is in negative direction:

$$\phi_e = \phi_E + g_3(\phi_P - \phi_E) + g_4(\phi_E - \phi_{EE}) \,,$$

where the coefficients g_1, g_2, g_3 and g_4 are nodal coordinates. Details of the expressions of these coefficients can be found in [21]. The Taylor expansion of this scheme gives:

$$\phi_e = \frac{6}{8}\phi_P + \frac{3}{8}\phi_E - \frac{1}{8}\phi_W - \frac{3(\Delta x)^3}{48} \left(\frac{\partial^3 \phi}{\partial x^3} \right)_P + H \,. \tag{3.7}$$

The first three terms on the right hand side represent the QUICK approximation, while the last term is the principal truncation error. As we can see, this quadratic

interpolation has a third order truncation error.

Diffusive term is generally discretized using CDS approximation whereas convective term can be discretized by any scheme depending on the strength of the convection. A dimensionless number, the Peclet number:

$$Pe = \frac{\rho u}{(\Gamma/\delta x)} \,, \tag{3.8}$$

which is the ratio of strength of convection to diffusion, is introduced. At high Pe number, results produced from CDS are oscillatory because convection is high and the complete contribution comes from the upstream point, nothing comes from the downstream point. Therefore if the flow is convection dominated then the upwind differencing (backward or forward) scheme should be used. Note that QUICK scheme should not be used for all-tetrahedral meshes and that it can be dispersive.

Finally, the spatial discrete equation takes the general linearised form:

$$a_P \phi_P = \sum_{nb} a_{nb} \phi_{nb} + b \,. \tag{3.9}$$

where a_P denotes the contribution of fluxes and other terms at the control volume centre and a_{nb} are the coefficients of the neighbouring nodes (east, west, north, south, top and bottom). The term b denotes the source term of the discrete equation.

3.2.2 Temporal Discretization

Essentially, there are two temporal discretization schemes available to perform the transient simulations and they are the first order fully-implicit scheme and second order Crank-Nicolson scheme. Under fully-implicit formulation, the fluxes prevailing over the time interval are calculated from the new time-level values of the variables. The first term in Eq. 3.1 represents the time derivative and on discretization of it using fully-implicit scheme gives:

$$T1 = \frac{(\rho\,\phi V)_P^{n+1} - (\rho\,\phi V)_P^n}{\Delta t} \,, \tag{3.10}$$

where the superscripts n and $n + 1$ refer to old and new time levels respectively, seperated by an interval Δt.

In principle, the fully implicit scheme allows any magnitude of time step to be used, but for transient problems, Δt must be small enough to limit the temporal approximation errors to acceptable levels. In Crank-Nicolson scheme, the point at $n + 1/2$ is used as the expansion point for the second-order formulation. This scheme is liable to generate unbound extrema and this trend can be improved by the use of smaller Δt.

3.2.3 Boundary Conditions

All CFD problems are defined in terms of initial and boundary conditions. In order to solve the set of algebraic-equations, one need to estimate the boundary fluxes either explicitly or in terms of the variables at inner nodes. The most commonly used boundary conditions have been described here.

- **Inlet**: The realization of this boundary condition is relatively easier, where the destribution of mass flux and fluid properties are known.

- **Outlet**: The total mass flux from all inlet planes should be equal to the total mass flux from all outlet planes. This means, the gradients of all variables along the flow direction at the outflow surface are taken to be zero and the exit mass flow is fixed from overall mass conservation criterion.

- **Symmetry**: The symmetry or zero-gradient boundary condition is a common type of boundary condition in all CFD solvers. The conditions at the symmetry boundary are, no flow and no scalar flux across the boundary. In the implementation, normal velocities and normal gradients of all other variables are set to zero at a symmetry boundary.

- **Slip surface**: A slip surface is impermeable to flow across it but offers no resistance to tangential motion and is usually appropriate for inviscid flow calculations and it can also be used for free surface flows. Slip condition is implemented

by setting the mass and tangential momentum fluxes to zero at cell faces as well as zero normal velocity and zero normal gradients for all other variables except pressure.

- **Wall**: The wall boundary condition is the most encountered boundary condition in general fluid flow problems. The no-slip boundary condition is applied directly in the case of laminar flows and certian turbulence models via wall functions is used in the case of turbulent flows. A wall moving at a known velocity may also be prescribed to account for rotating flow problems.

3.3 Rotating and Moving Meshes

In the present thesis as well as in many practical applications of fluid dynamics, fluid motion is induced or governed by relative movement between stator and rotor. This is usually accompanied by the strong characteristic unsteadiness in the flow pattern. Important examples where such flows occur are:

- kneaders, single and twin screw extruders

- mixing vessels

- rotary and reciprocating engines

- turbomachinary, axial and centrifugal pumps

- ship and aircraft propellers.

The mostly used mixing equipment is stirrer. In the case of axi-symmetric geometries, the computational domain can be made fixed in space using rotating coordinate system. The similar idea is applied in case of sliding interface technique for non-symmetric vessels. In this case the computational domain is divided into partial domains and the domains with the rotating parts are calculated using rotating reference frame. Several CFD codes offer modeling of flows involving rotating bodies. In the present work, a

finite volume based commercial code Star-CD from CD-adapco is used to investigate flows in stirred vessels. Major features available in Star-CD for rotating geometries are rotating reference frame method and general mesh motion [1]. A brief discussion of these features is given in this section with an example.

3.3.1   Rotating Reference Frame

In the problems of stirred vessels, the impeller is generally rotated with certain speed. The influence of rotation can be realized either by prescribing tangential speed at the boundary cells or by transforming the equations to a rotating frame of reference. Velocities and accelerations recognized by an observer in a rotating frame of reference are different from that recognized by an observer at rest in an inertial or fixed frame of reference. To futher elaborate, consider a fluid in rotation about some fixed axis with an angular velocity ($\mathbf{\Omega}$). Let (x_1, y_1, z_1) be the fixed coordinate system and (x_2, y_2, z_2) be the rotating frame of reference. The fixed axis of rotation is common to both the coordinate systems, i.e., z_1 and z_2 coincide. The transformations relating the two coordinate systems are:

$$
\begin{aligned}
x_1 &= x_2 \cos(\mathbf{\Omega}t) + y_2 \sin(\mathbf{\Omega}t) \\
y_1 &= y_2 \cos(\mathbf{\Omega}t) - x_2 \sin(\mathbf{\Omega}t) \\
z_1 &= z_2 \,,
\end{aligned}
$$

and,

$$
\begin{aligned}
x_2 &= -x_1 \sin(\mathbf{\Omega}t) + y_1 \cos(\mathbf{\Omega}t) \\
y_2 &= -y_1 \sin(\mathbf{\Omega}t) + x_1 \cos(\mathbf{\Omega}t) \\
z_2 &= z_1 \,.
\end{aligned}
$$

In order to calculate velocities and accelerations in rotating reference frame, again consider a fluid element with position vector $\mathbf{r}$ in inertial frame of reference and observe the motion of this fluid element in rotating reference frame which rotates with a

constant angular velocity ($\mathbf{\Omega}$). Then, the equation of motion in inertial frame is obtained by time derivative on $\mathbf{r}$ and read as:

$$\frac{d\mathbf{r}}{dt} = \mathbf{\Omega} \times \mathbf{r} \,.$$

The time derivative of $\mathbf{r}$ in rotating reference frame has two components, one from inertial reference frame and another from its own rotation. The above equation is re-written in rotating reference frame by adding instantaneous velocity $\mathbf{u}'$ as:

$$\frac{d\mathbf{r}}{dt} = \mathbf{u} = \mathbf{u}' + \mathbf{\Omega} \times \mathbf{r} \,.$$

The second time derivative operating on position vector $\mathbf{r}$ gives an acceleration as:

$$\begin{aligned} \mathbf{a} &= \left(\frac{d^2\mathbf{r}}{dt^2}\right) = \left(\frac{d\mathbf{u}}{dt}\right) \\ &= \left(\frac{d}{dt'} + \mathbf{\Omega}\times\right)(\mathbf{\Omega} \times \mathbf{r}) \end{aligned}$$

After simplification and re-arranging the above equation yields:

$$\mathbf{a}' = \mathbf{a} - \underbrace{\mathbf{\Omega} \times (\mathbf{\Omega} \times \mathbf{r})}_{I} - \underbrace{2\mathbf{\Omega} \times \mathbf{u}'}_{II} , \tag{3.11}$$

where the terms $I = \mathbf{\Omega} \times (\mathbf{\Omega} \times \mathbf{r})$ and $II = 2\mathbf{\Omega} \times \mathbf{u}$ are centrifugal and Coriolis accelerations respectively. The centrifugal and Coriolis accelerations result in fictitious forces in rotating reference frame. Adopting the above mentioned transformation procedure, the momentum equations in rotating reference frame are modified by taking into account Coriolis and centrifugal force terms. The Navier-Stokes equations written for use in a rotating reference frame at constant angular velocity ($\mathbf{\Omega}$) then read as [80]:

$$\frac{\partial \mathbf{u}}{\partial t} + (\mathbf{u} \cdot \nabla)\mathbf{u} + \mathbf{\Omega} \times (\mathbf{\Omega} \times \mathbf{r}) + 2\mathbf{\Omega} \times \mathbf{u} = -\frac{1}{\rho}\nabla p + \nu\nabla^2\mathbf{u} + \frac{1}{\rho}\mathbf{b} \,. \tag{3.12}$$

Note that in the above Eq. 3.12 the prime symbol $'$ is deliberately omitted. The continuity equaion ($\nabla \cdot \mathbf{u} = 0$) is invariant under the given transformation.

The rotating reference frame feature of Star-CD enables to model cases where the entire mesh is rotating at a contant angular velocity around a prescribed axis as well as different mesh blocks moving with different angular velocities around different rotating

axes. This means, there are two types of rotational motion that may be simulated, corresponding to:

- Global rotation, using single rotating reference frame.

- Region wise mesh rotation using multiple reference frames.

Global Rotation

This is the simple rotation where the entire mesh rotates with a prescribed angular velocity ($\mathbf{\Omega}$) about a given axis. The main features of this type are:

- The axis of orientation and sense of rotation are defined by the z-axis of a local coordinate system and the convention that $\mathbf{\Omega}$ obeys right hand rule.

- Selection of this feature adds the Coriolis and centrifugal force terms to the momentum equations and yields Eq. 3.12.

Region Wise Mesh Rotation

This feature allows different mesh blocks within the model to rotate at different angular velocities, i.e. the rotational source terms added to the relevant equations depending on the local spin and axis of rotation. The basic idea here is to calculate relative mesh rotation by activating the appropriate rotational terms at cells within each specified region, without rotating the entire mesh. Then it is possible to have multiple adjoining rotating regions, each with its own rotational speed.

3.3.2   Mesh Motion

In a number of situations it is convenient for the computatonal grid to follow moving boundaries rather than rotating the entire mesh. In this case of moving grids, the time coordinate has to be transformed in a way similar to the space transformation. A brief description of a moving grid system is given below. On the basis of the rules of

partial differentiation, the total time derivative from the Lagrangian view point reads:

$$\frac{d\phi}{dt} = \frac{\partial\phi}{\partial t} + \frac{\partial\phi}{\partial x_i}\frac{dx_i}{dt}\,, \tag{3.13}$$

where the left hand side is the time rate of change of ϕ of a given fluid element when it moves from one point to the other point. The first term on the right hand side is the time rate of change of ϕ at a fixed point. The quantity $\frac{\partial\phi}{\partial x_i}$ is the time rate of change of ϕ at a given instant of time and $\frac{dx_i}{dt}$ is the grid velocity $\mathbf{u}_g$. Therefore, Eq. 3.13 can now be written as:

$$\frac{\partial\phi}{\partial t} = \frac{d\phi}{dt} - \mathbf{u}_g\frac{\partial\phi}{\partial x_i}\,. \tag{3.14}$$

The above Eq. 3.14 can be referred as *Arbitrary Lagrangian-Eulerian* (ALE) formulation for moving grids. The conservation form of the ALE is obtained with the help of the *geometric* or *space conservation law* (SCL), which ensures that the rate of change of volume is consistent with net volume flux due to grid movement [18]:

$$\frac{d}{dt}\int_{CV}\phi\,dV - \int_{CS}\phi\,\mathbf{u}_b\cdot\mathbf{n}\,dS = 0\,. \tag{3.15}$$

The generic transport Eq. 3.1 in finite-volume formulation using Eq. 3.15 for moving grids yield:

$$\frac{d}{dt}\int_{CV}\rho\,\phi\,dV + \int_{CS}\rho\,\phi\,(\mathbf{u}-\mathbf{u}_b)\cdot\mathbf{n}\,dS = \int_{CS}\Gamma\,\Delta\,\phi\cdot\mathbf{n}\,dS + \int_{CV}S_\phi\,dV\,. \tag{3.16}$$

The above equations are used if the control volume does not move. If the boundary moves with the same velocity as the fluid, the mass flux through the control volume face will be zero. If this is true for all control volume faces, then the same fluid remains in the control volume and becomes a control mass. The resulting conservation equation describes the Lagrangian fluid motion.

Star-CD offers several methods to carry out moving mesh simulations. Of course, the mesh motion is not entirely arbitrary; there are certain limits on the degree of distortion that can be tolerated, imposed on accuracy and stability requirements. The moving mesh feature in Star-CD is activated by command MVGRID and changes in

grid movement can be specified either by change grid operation in the EVENTS command module, or by user defined function included in subroutine NEWXYZ. In this subroutine, the geometry of the model can be varied by defining vertex coordinates as the function of time. There are several methods to apply above mentioned operations. They are:

- Cell layer addition or removal.

- Sliding mesh.

- Cell attachement and change of fluid.

- Mesh region inclusion or exclusion.

Sliding mesh method is utilized in the present thesis and therefore, it is described here. The detailed information of other methods can be found in [1].

Sliding Mesh

Various methods of implementing sliding mesh are regular sliding interface, arbitrary sliding interface (ASI) and automatic events generation. The regular sliding interface method combines both the cell attachment and the change grid operation of the EVENTS command module. The ASI approach involves re-computing boundary face matches at each time step, and may thus be slightly slower than using ATTACH events. Automatic events generation is a simplified procedure for generating a transient moving mesh model, starting from a stationary mesh built at a given position of the impeller blade. The events, moving grid commands, attach boundaries and any other required user subroutines are generated in a single command. The next section expands the rotating reference frame and sliding (moving) method with the aid of a simple example.

(a) Vertical   (b) Horizontal
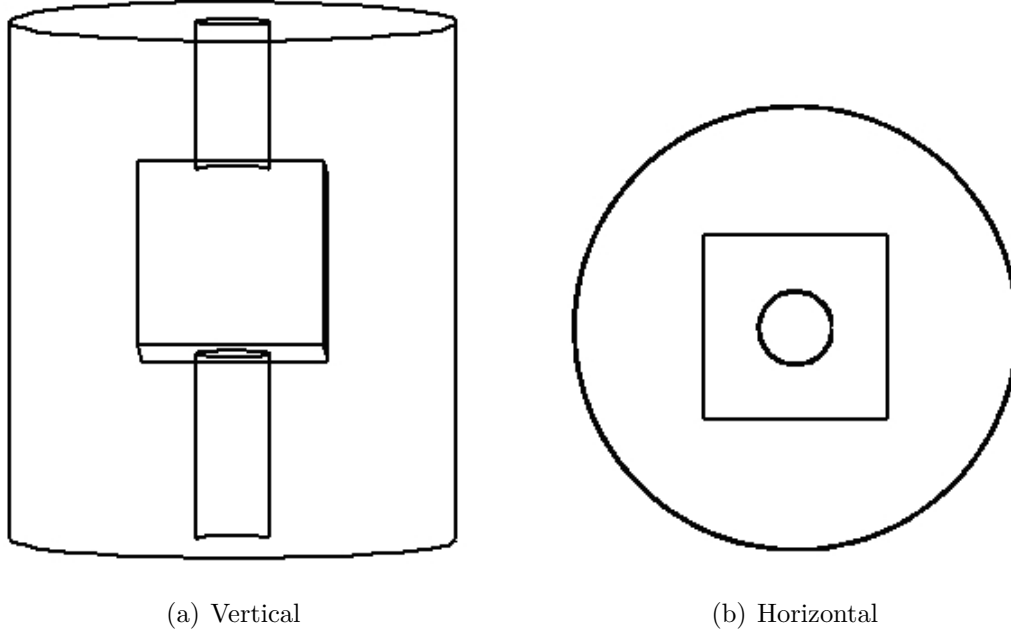
Figure 3.2: Schematic of the simple reference geometry considered for rotating and sliding mesh analysis.

3.3.3 Simple Reference Geometry

The purpose of using simple reference geometry is to apply and compare rotating reference frame simulations with moving mesh simulations. The geometrical configuration used in the present study contains two concentric cylinders height 7 m, outer cylinder radius 3 m and inner cylinder radius 0.5 m. Each side of the cube is 2.5 m and is attached to the inner cylinder (shaft) as shown in Fig. 3.2.

Simulation

The simulation methods employed for the simple reference geometry are the rotating reference frame and the moving mesh with change grid operation. In the first case, the entire mesh is rotated with an angular velocity of 10 rpm. Since the boundaries of the rotating domain assumed to be rotating with the same angular velocity, an opposite spin of the same angular velocity is defined on inner walls to make them stationary. In the moving mesh case where the grid (cell vertices) is changed at each time step using change grid operation with events. No-slip boundary conditions are used at the outer,

top, bottom and inner walls. All fluid motion is caused by the rotation of the cube and shaft. The unstructured mesh contains approximately 50000 grid nodes is generated using Star-Design and the numerical simulations are performed with Star-CD v 3.22. A time step of 0.01s is used in the simulations and 1200 time steps were performed in each case corresponding to two rotations of the shaft. Estimated calculation time is one hour per rotation on an AMD Athlon XP, 3200+ and 1GB RAM single processor.

(a) After 6 sec (one rotation)   (b) After 6 sec (one rotation)
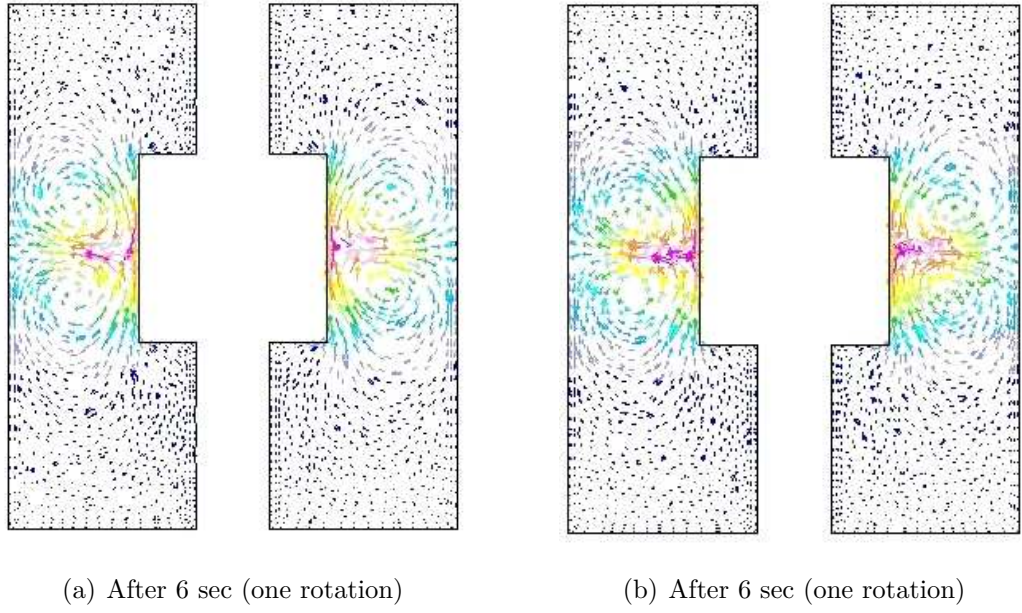
Figure 3.3: Section plots of velocity vectors after one rotation of the impeller in moving mesh (left) and rotating reference frame (right) simulations.

Results and Discussions

Fig. 3.3 shows the section plots of velocity magnitudes after one rotation of the impeller in the simple reference geometry. The flow pattern is shown by means of velocity vectors. The length of the vectors is proportional to the magnitude of the liquid velocity. As expected, two circulation loops can be seen around the impeller in both cases.

Fig. 3.4 shows the section plots of the velocity magnitude fields in both moving

(a) After 3 sec

(b) After 3 sec

(c) After 6 sec

(d) After 6 sec

(e) After 12 sec

(f) After 12 sec
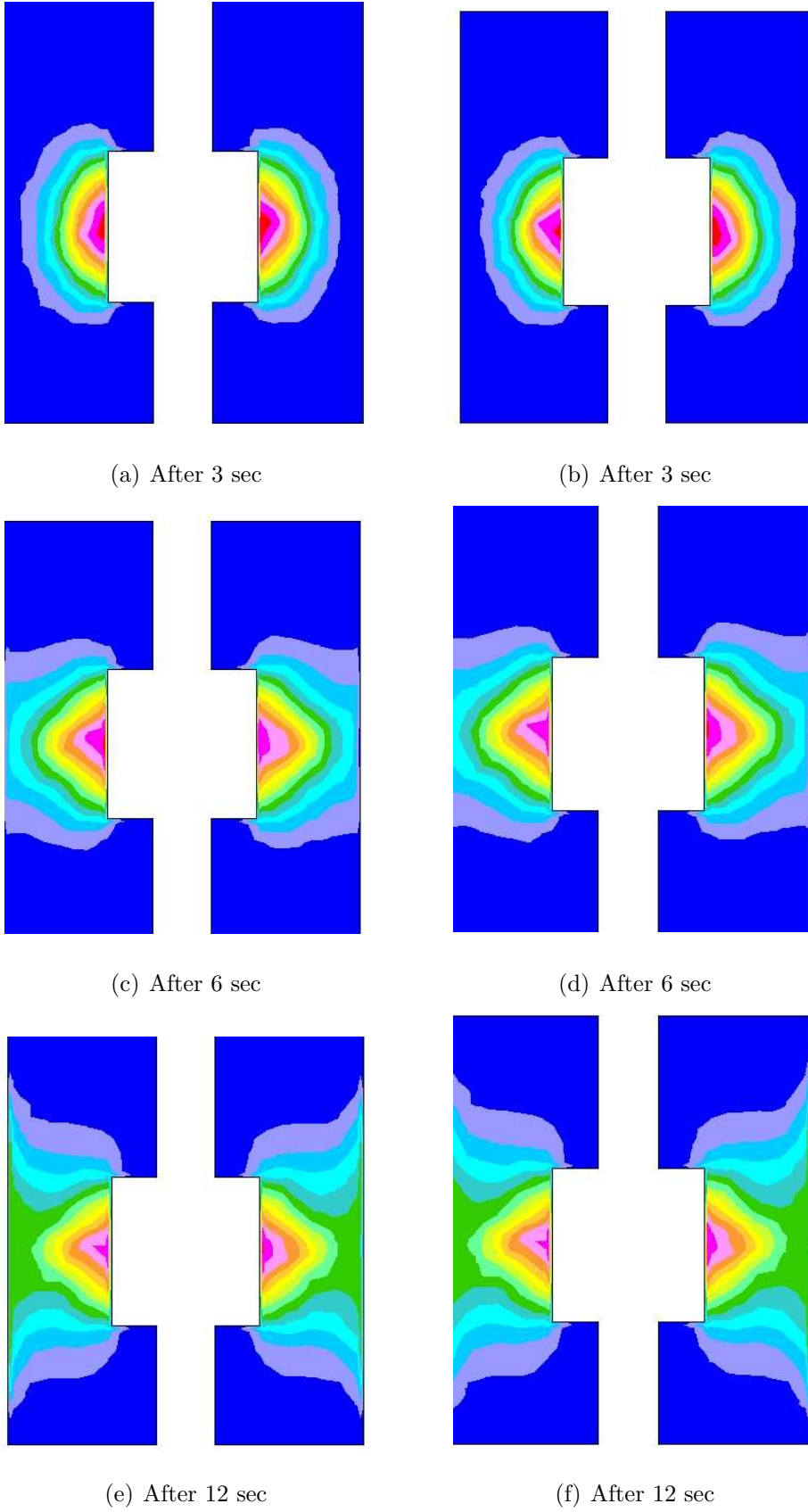
Figure 3.4: Contour section plots of velocity magnitudes at different time intervals in both moving (left) and rotating reference frame (right) simulations.

mesh and rotating reference frame simulations at different time steps. The flow pattern
is shown by means of contour plots. Since the motion of the fluid is governed by the
movement of the impeller (cube and shaft together), the highest velocities are found
near the impeller tip and the velocities are lower near the outer cylinder wall. Moving
mesh simulation results are shown on the left side while the rotating reference frame
simulation results are shown on right side. In Fig. 3.4 (a) and (b) are observed after 3
sec, i.e. after half of the roation of the impeller. As one can see, the flow is very week
away from the impeller. The velocity profiles are shown after one rotation in Fig. 3.4 (c)
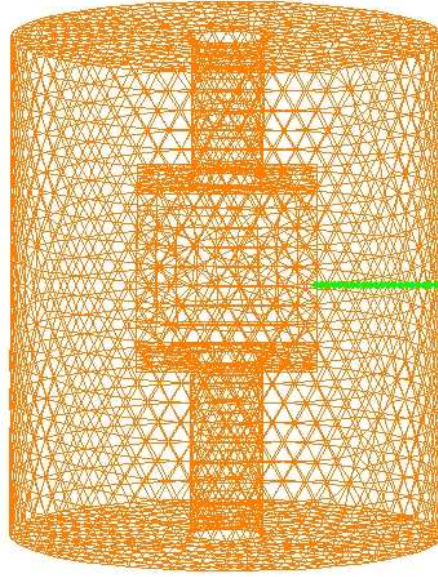
Figure 3.5: Computational sensor points to extract quantitative information for better
comparison of the velocity magnitudes.

and (d). At this instance, the flow field becomes stronger and developing towards the
wall of the outer cylinder. After two rotations, much stronger flow fields are observed
in Fig. 3.4 (e) and (f). The principle reflection in both the moving mesh and rotating
reference frame simulations is that the results show very good coincidence with each
other. For more quantitative validation of the simulation results, 20 computational
sensing points are considered starting from the impeller wall to the outer cylinder wall
in radial direction as shown in Fig. 3.5. A very good agreement is noticed for for
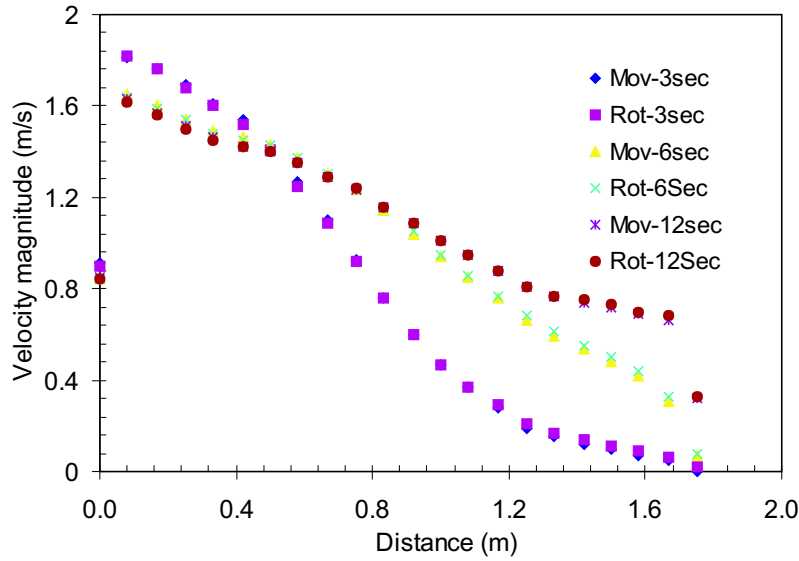
Figure 3.6: Quantitative comparison of velocity magnitudes computed both in moving mesh and rotating reference frame simulations.

the simulation results of both the moving mesh and the rotating reference frame as depicted in Fig. 3.6. It can also be seen that as the time proceeds, more uniform profiles are achieved. From the above simulations, it is evident that both the moving mesh and the rotating reference frame simulation give similar results. However, the moving mesh calculations needs longer computational time than the rotational reference frame. Therefore, the rotating reference frame method is utilized to accurately predict the time dependant flows in stirred vessels. The following section explores the utilisation of Star-CD to compute torque in rotating system by considering a simple Couette-flow between two concentric rotating cylinders.

3.4 Torque Computation in a Couette-Flow

3.4.1 Introduction

Couette-flow refers to the laminar flow of a fluid between two concentric cylinders, one of which is moving relative to the other. Couette-flow reactors are the widely used

devices in chemical process industries especially due to their mixing properties. In this section, the torque computation in a Couette-flow reactor using Star-CD are presented. These computations are compared with the theoretically calculated torque as well as torque computed using other well known commercial code Fluent. The simulations and calculations are carried out for the different rotational speeds of the outer cylinder. In the present investigations, a steady tangential laminar flow is considered between

(a)   (b)
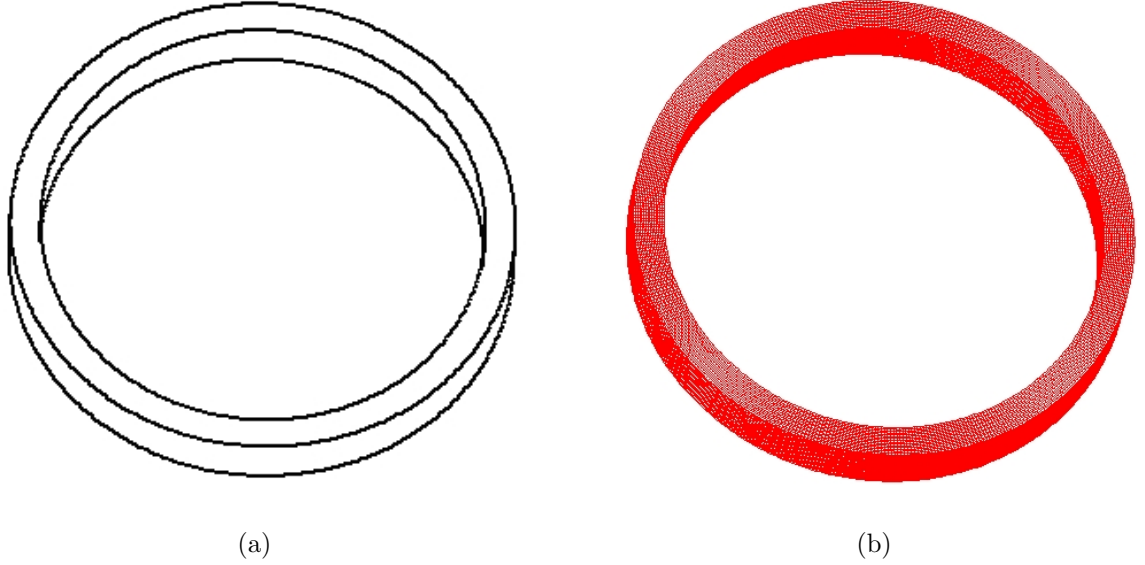
Figure 3.7: Schematic of (a) the Couette-flow geometry and (b) the computational grid which contains 207,000 hexahedral control volumes.

two vertical concentric cylinders shown in Fig. 3.7. The fluid with constant density and viscosity is used as a working fluid. The analytical solution for torque when outer cylinder rotates with an angular speed Ω, is given as [22]

$$\tau = 4\pi\mu L\Omega r_2^2 \left[\frac{(r_1^2/r_2^2)}{1 - (r_1^2/r_2^2)} \right]. \tag{3.17}$$

Where τ is the torque in N-m, μ is the viscosity of the liquid in kg/m-s, L is the height of the cylinders in m, r_1 is the radius of the inner cylinder in m and r_2 is the radius of the outer cylinder in m. The diameters of the inner and outer cylinders are 71 mm, 80.7 mm respectively and both have the same height of 9.7 mm.

Table 3.1: Comparison of torques calculated theoretically and using Fluent.

Angular Velocity	*Torque (Theoretical)*	*Torque (Fluent)*	*Percentage Deviation*
rad/s	*N − m*	*N − m*	*%*
0.1	6.82E-08	6.82E-08	0.00
0.2	1.36E-07	1.37E-07	0.73
0.3	2.05E-07	2.05E-07	0,00
0.4	2.73E-07	2.74E-07	0.37
0.5	3.41E-07	3.43E-07	0.59
0.55	3.75E-07	3.78E-07	0.79
0.6	4.09E-07	4.13E-07	0.97
0.65	4.43E-07	4.48E-07	1.12
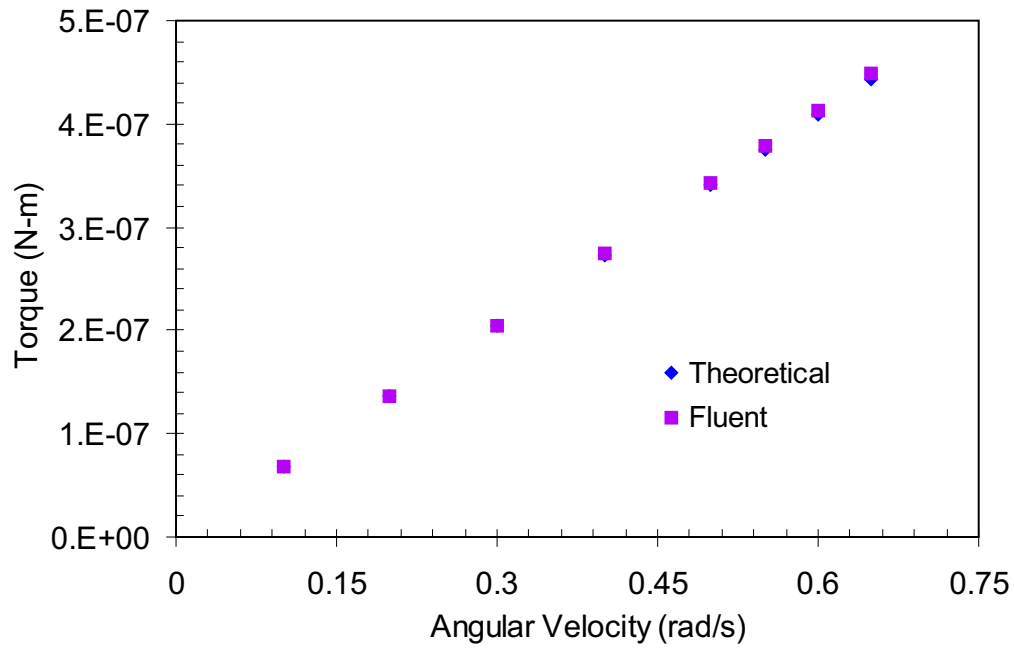
Figure 3.8: Comparison of theoretically calculated torque with torque computed using Fluent.

Table 3.2: Comparison of torques calculated theoretically and using Star-CD.

Angular Velocity rad/s	Torque (Theoretical) N − m	Torque (Star − CD) N − m	Percentage Deviation %
0.1	6.80E-08	5.82E-08	14.4
0.2	1.36E-07	1.26E-07	7.35
0.3	2.04E-07	1.94E-07	4.9
0.4	2.72E-07	2.57E-07	5.51
0.5	3.40E-07	3.30E-07	2.94
0.55	3.74E-07	3.67E-07	1.87
0.6	4.08E-07	3.99E-07	2.21
0.65	4.42E-07	4.31E-07	2.49
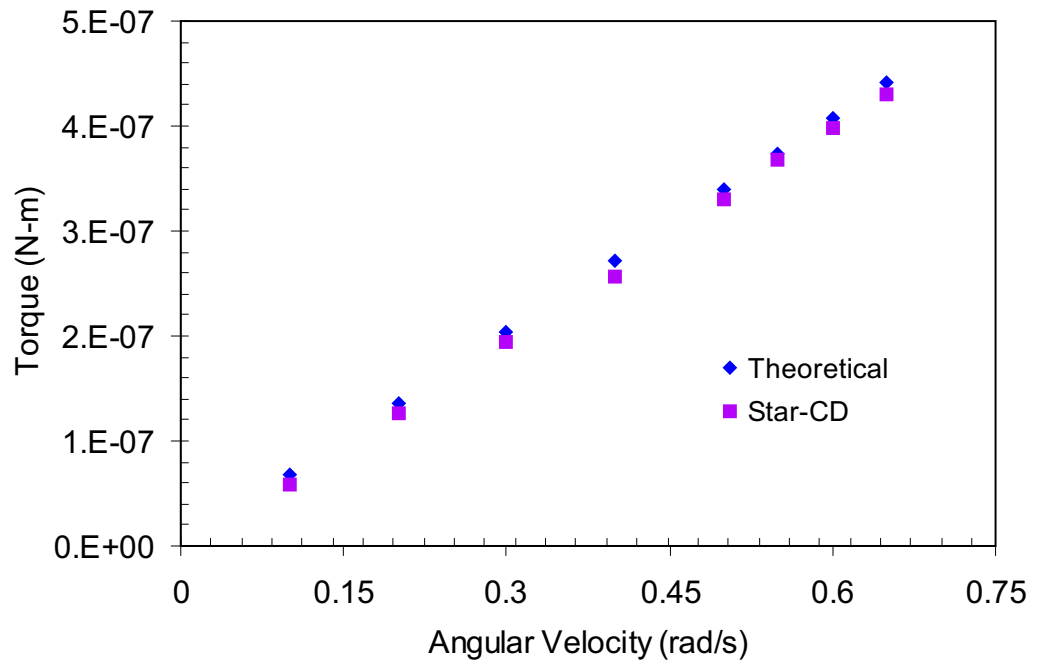
Figure 3.9: Comparison of theoretically calculated torque with torque computed using Star-CD.

Table 3.3: Comparison of torques calculated theoretically and using Star-CD for highly viscous liquid.

Angular Velocity	*Torque (Theoretical)*	*Torque (Star − CD)*	*Percentage Deviation*
rad/s	*N − m*	*N − m*	*%*
0.3	2.04E-03	2.05E-03	0.49
0.35	2.38E-03	2.39E-03	0.42
0.4	2.72E-03	2.73E-03	0.37
0.45	3.06E-03	3.07E-03	0.33
0.5	3.40E-03	3.42E-03	0.58
0.55	3.74E-03	3.76E-03	0.53
0.6	4.08E-03	4.10E-03	0.49
0.65	4.42E-03	4.44E-03	0.45
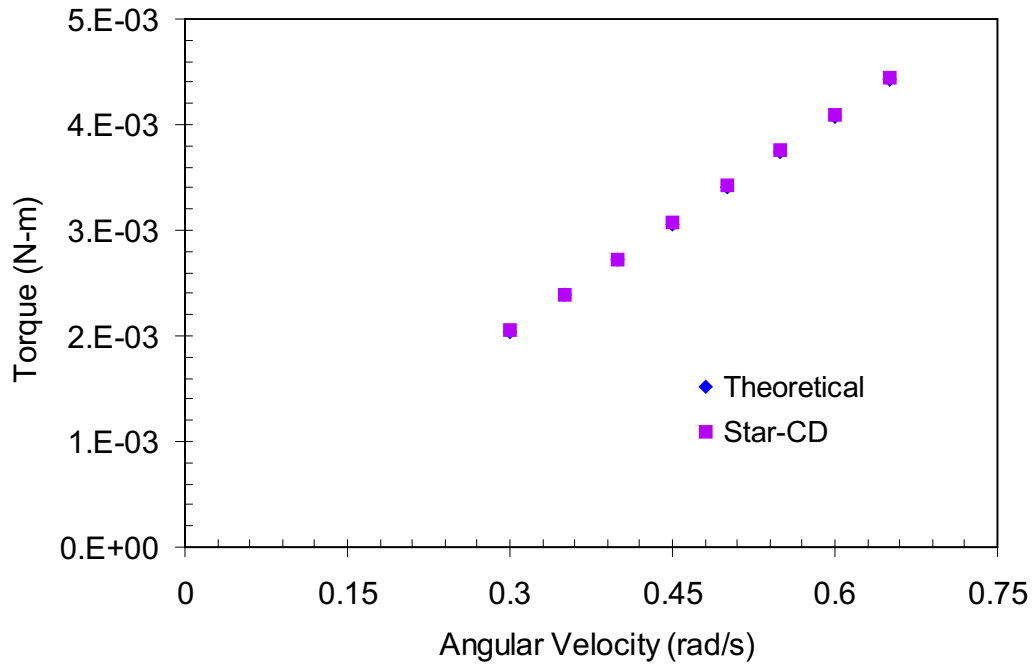
Figure 3.10: Comparison of theoretically calculated torque with torque computed using Star-CD for highly viscous liquid.

3.4.2 Simulation

To compute the torque in couette-flow reactor, numerical calculations were performed using the two widely used commercial CFD softwares Star-CD and Fluent. These computations are compared with the theoretically calculated values. A viscosity of $0.001\,kg/m\,s$ is used in the calculations of Star-CD and $0.00103\,kg/m\,s$ is used in the case for Fluent calculations.

Star-CD

A 3-dimensional block structured grid with 207,000 computational cells were generated using Pro-STAR. A steady, laminar, isothermal simulations were performed at different Reynolds numbers corresponding to different angular velocities. The torque was computed once the convergence is obtained. The detailed method of calculating torque using Star-CD is given in section 4.2.2.

Fluent

For the simulations using Fluent, the results were taken from [29]. Wall shear stress over the area is calculated after convergence is achieved. Integration of wall shear stress over the area of the inner cylinder and multiplied with the the radius of the inner cylinder gives the torque required to rotate the inner cylinder.

3.4.3 Results and Discussions

The theoretical values for the torque and the torque calculated using Star-CD are tabulated in Table 3.2. Fig. 3.9 shows a comparison between the theoretical value and the torque calculated using Star-CD. It can be observed in this figure that there exists a small discrepancy in these values. Where as the variation between the torque [Table 3.1, Fig. 3.8] obtained using Fluent and the theoretically calculated torque are in good agreement. After a carefull observation of the results, it can be seen that the percentage of deviation of the torque values obtained using Fluent from the theoretical

torque values is in the order of one. But the percentage of deviation of the torque values calulated using Star-CD from the theoretical torque values is in the range 2-15. From this we can be seen that the Fluent is more appropriate than Star-CD for this particular case of the torque computation in a couette-flow reactor. However, the intensity of deviation decreases when highly viscous liquids are considered in the investigations. These findings can be found in Table 3.3 and Fig. 3.10. It is believed from these observations that Star-CD predicts values close to theoretical values at high viscosity of the liquids.

Chapter 4

CFD-Analysis of Anchor Mixer

4.1   Introduction

Fluid mixing in a stirred vessel agitated with an anchor impeller is discussed in this chapter. The anchor impeller has a simple and basic configuration suited for mixing of highly viscous liquids, and is widely used in the chemical and food industries. The principle advantages of anchor mixer are that it prevents sticking of pasty materials, and promotes good heat transfer with the wall because of close clearance between the impeller and vessel wall. Because of its unique advantages, the detailed analysis of the flow around the vertical blades of an anchor impeller gains much appreciation. This analysis includes information regarding power consumption, mixing and heat transfer. Some of the early experimental studies on flows in an anchor mixer were reported in [9,60]. They provided the detailed description of the power input and flow fields with Newtonian and non-Newtonian fluids. Early two-dimensional numerical investigations were developed by [39] using an iterative method. This paper reports the flow of highly viscous fluids in anchor mixer and gives information on flow characteristics. Extensive three-dimensional numerical analyses were then followed during early 90s [2, 10, 33, 34, 59, 74]. Inspite of the importance of anchor mixer in process industries, there are only few studies in the literature which deal with this mixer type. The majority of works for stirred vessels refer to six-blade Rushton turbines and paddle
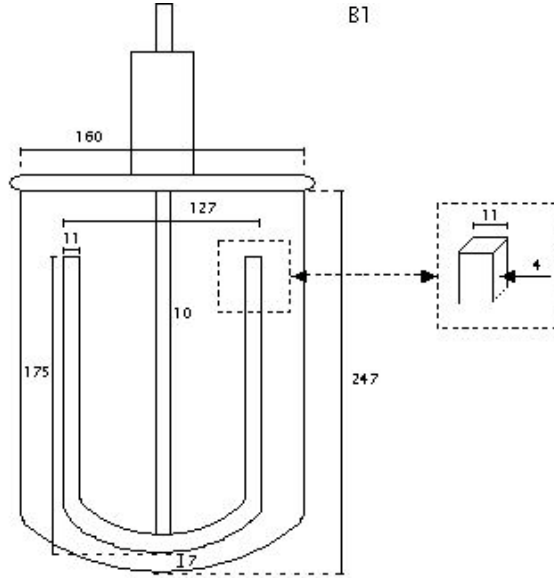
Figure 4.1: Schematic representation of anchor mixer, where all the dimensions are in mm (Geometrical configuration is received from BASF AG, Ludwigshafen).

type impeller mixers under turbulent flow condition. This work contributes for the simulation of anchor mixer.

4.2   Analysis of Partly Filled Anchor Mixer

The present section deals with a three-dimensional analysis of a partly filled anchor mixer which is shown in Fig. 4.1. Since the vessel is partly filled, Volume of Fluid (VOF) method is used to account for the free surface flow. One of the leading commercial CFD codes Star-CD from CD-Adapco has been used for flow field analysis, torque computation and power number calculations. The flow considered here is laminar, Newtonian and time dependant in a two arm anchor type stirrer fixed to a shaft and placed at the centre of the vessel. Simulation procedure addresses the numerical solution of the three-dimensional Navier-Stokes equations in rotating reference frame coordinates with additional centrifugal and Coriolis force terms [Eq. 3.12].

4.2.1 Volume of Fluid (VOF) Method

Since the mixer is partly filled with the liquid, the free surface flow has to be accounted for the analysis of two-phase mixing inside the anchor mixer. Therefore, this problem is solved using Volume of Fluid (VOF) method to implicitly track the residence region of two immiscible flows. According to this, the interface between the liquid and the gas is captured at successive time steps and is represented by the distribution of a passive scalar α_l, which is defined as the ratio of volume of liquid to the total volume of the fluid (liquid and gas) in a computational cell. It was further assumed that the fluids are incompressible and have a considerable density difference. Based on phase-related conservation, advection of the disperse phase is governed by an additional transport equation for the volume fraction α_l of this phase:

$$\frac{\partial \alpha_l}{\partial t} + \nabla \cdot (\alpha_l \mathbf{u}) = 0 \,, \tag{4.1}$$

determining the temporal propagation of the phase with respect to the flow field. Hence, the balance equations of the mass and momentum in addition to Eq. 4.1 can then be solved for both phases simultaneously. Using VOF method, the disperse liquid phase corresponds to the region where α_l has the value 1 and the continuous phase has the value of 0, while the interface is located within the grid cells for which $0 < \alpha_l < 1$. Therefore, cells with $0 < \alpha_l < 1$ comprise both the disperse and continuous phase. To further clarify this approach, Fig. 4.2 represents the distribution of α_l inside the calculation domain. In order to maintain the interface sharpness, Eq. 4.1 is solved using a higher order compressive scheme, the so-called Compressive Interface Capturing Scheme for Arbitrary Meshes (CICSAM). A requirement for this scheme is that the Courant number Cu of the flow should not exceed a certain limit Cu^* (0.3 in this case). Otherwise the scheme is not able to maintain a sharp interface. The Courant number Cu is defined as:

$$Cu = \frac{U \cdot \Delta t}{\Delta x} \,. \tag{4.2}$$

Figure 4.2: Cell occupation of liquid phase $(0 < \alpha_l < 1)$ in a surrounding gas phase $(\alpha_l=0)$ based on the VOF-method.

The physical properties (density ρ and viscosity μ) of the mixture are expressed as functions of the phase properties and are as follows:

$$\rho = \rho_l \alpha_l + \rho_g (1 - \alpha_l), \tag{4.3}$$

$$\mu = \mu_l \alpha_l + \mu_g (1 - \alpha_l). \tag{4.4}$$

4.2.2   Problem Specification and Numerical Approach

For the analysis, a concave-bottom cylindrical vessel with an anchor type stirre fixed to a shaft and placed at the centre of the vessel is considered. An unstructured tetrahedral mesh Fig. 4.3 is generated using ICEM-CFD and exported to Star-CD for numerical analysis. The total number of computational cells used in these investigations are approximately 300,000. The simulations were perfomed with different mesh refinement and sufficient care has been taken in setting the solver parameters such as discretization schemes, time step size etc. A viscosity of 27.25 Pas and density of 1120 kg/m^3 are assigned for the liquid phase and air is considered as the gas phase with viscosity 1.8551E-05 Pas and density of 1.184 kg/m^3. The vessel is filled initially with the liquid upto a level of 148 mm and the stirrer rotates at an angular speed of 50 rpm.
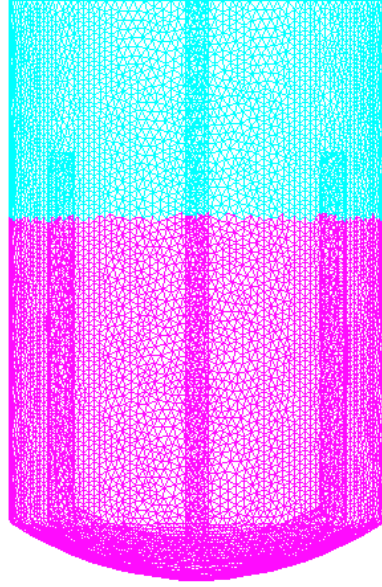
Figure 4.3: Computational grid which consists of approximately 300,000 tetrahedral control volumes generated using ICEM-CFD tool. Mesh with magenta colour (below) correspond to liquid phase and the one with aqua colour (above) correspond to gas phase.

After solving the transport equations for velocity and pressure fields, torque and power numbers are calculated based on the the formulae given in the next sections.

Torque

Torque or the moment of force is an axial vector quantity that represents the magnitude of rotational or angular force applied to a rotational system at a distance from the axis of rotation. This force is determined by linear force multiplied with the radius. More generally, torque can also be defined as the rate of change of angular momentum.

Mathematically, the torque on a particle which has the position $\mathbf{r}$ in some reference frame, can be represented as:

$$\boldsymbol{\tau} = \mathbf{r} \times \mathbf{F}_t \,. \tag{4.5}$$

Alternatively, if a force of magnitude F is at an angle θ from the distance r within

the plane perpendicular to the rotation axis, then from the definition of cross product, the magnitude of the torque arising is:

$$\boldsymbol{\tau} = rF\sin\theta\,. \tag{4.6}$$

The expression for computing flow induced forces on the wall cell faces are given below. Shear force:

$$\mathbf{F}_s = \tau_w A_b \mathbf{t}\,, \tag{4.7}$$

pressure force:

$$\mathbf{F}_p = p_b A_b \mathbf{n}_b\,, \tag{4.8}$$

total force:

$$\mathbf{F}_t = \mathbf{F}_s + \mathbf{F}_p\,, \tag{4.9}$$

and hence the total torque is given by:

$$\boldsymbol{\tau} = \mathbf{r} \times \mathbf{F}_t\,, \tag{4.10}$$

Power Number

The information provided in this section is based on [14]. The mechanical energy balance is to be analysed for the first estimation of the mixing efficiency. It should be noted that this mechanical energy is transferred in two different ways. On one hand, the mechanical energy can be transferred through the inner boundaries, i.e., through the agitation with the moving wall (ex. stirrer, extruder and kneader) and on the other hand the mechanical energy can be transferred over outer boundaries i.e., through pressure drops along the flow direction (ex. static mixer). Scalar multiplication of the Navier-Stokes equations by the velocity, and integration over the considered control volume $V(t)$ in the mixing domain gives the following relation:

$$\dot{E}_{Kin} = P_{Flow} + P_{Agit} - P_{Diss}\,. \tag{4.11}$$

The power transferred due to the flow:

$$P_{Flow} = \Delta p \dot{V} + \int_{A_{in}} \frac{\rho}{2} |\mathbf{u}|^2 V_{ax} dA - \int_{A_{out}} \frac{\rho}{2} |\mathbf{u}|^2 V_{ax} dA \,, \tag{4.12}$$

The power induced due to the mechanical agitation or mixing:

$$P_{Agit} = \int_{A_{mix}(t)} \left(\eta \mathbf{u} \cdot \frac{\partial \mathbf{u}}{\partial \mathbf{n}} - \mathbf{pu} \cdot \mathbf{n} \right) dA \,, \tag{4.13}$$

and the dissipated power:

$$P_{Diss} = \eta \int_V |\nabla \mathbf{u}|^2 \, dV \,. \tag{4.14}$$

Here, $A_{mix}(t)$ denotes the surface area of the moving inner boundary (mixing part), Δp is the pressure drop between the inlet and outlet, $\dot{V}$ is the volume flux through the mixing apparatus and V_{ax} is the component of velocity in axial direction. Eqs. 4.12-4.14 are true under the following consideration that the inlet and outlet surfaces are planar and their velocity vectors have to be perpendicular to them. Additionally, inlet and outlets are governed by constant pressure. For simplification, the formulation is considered only for Newtonian fluids. In the general case, shear stress due to the stress tensor have to be considered [72].

Depending on the mixing process, either Eq. 4.12 or Eq. 4.13 have to be considered. In the case where the moving walls exists, the considered volume domain depends on time. In quasi steady state, where the kinetic energy is constant and hence Eq. 4.11 can be reduced to:

$$P_{Diss} = P_{Flow} + P_{Agit} \,. \tag{4.15}$$

Further simplification of the Eq. 4.15 depends on the specific application. For batch mixing processes in a mixing equipment with moving parts, P_{Flow} can be neglected. Where as in the pressure driven flow mixing with agitation P_{Agit} can be ignored. The term on left hand side in Eq. 4.15 corresponds to the dissipation term and is a required quantity for the integral estimation of mixing efficiency due to convection. For the case, where the flow can be calculated, this dissipation term can be determined using

CFD-simulations. Depending on the complexity of the geometry, topology and scaling of the mixing equipment, valid numerical calculation of the complete flow field can be very demanding. Unfortunately, such kind of calculation even with the present computational advancements cannot be possible. This is true for complex geometries with self-cleaning and intermeshing (e.g. kneaders, extruders) design mechanisms.

Generally, computation of mixing mechanisms in extruders are difficult. However, computation of single screw extruder can be done using appropriate moving or rotating reference frame by considering as a channel flow [56]. Twin screw extruders cannot be modelled using the sliding mesh technique because of the ovelapping of the two screws. The fictitious domain method developed by [27] during the last years and is shown appropriate [26]. The flow calculation in kneaders is even more difficult because of the close clearance between the kneading pins. Recently, new techniques of overlapping meshes have been developed [21, 30]. On the basis of Chimera methods, individual meshes are devoted for each single moving objects. These moving meshes are linked by a common back ground mesh. Because of above mentioned difficulties, experimental data is important to develop correlations. As an integral parameter, the total dissipated power P_{Diss} is the fundamental parameter. In order to obtain a valid correlation depending on the type of the mixing equipment, the parameters influencing the power have to be determined. For example, in case of paddle impeller in which the shearing term in Eq. 4.13 can be neglected and Eq. 4.13 can be simplified as:

$$\eta \int_V |\mathbf{u}|^2 \, dV = \int_{A_{mix}(t)} p\mathbf{u} \cdot \mathbf{n_{mix}dA} \, , \tag{4.16}$$

where $\mathbf{n_{mix}}$ is the outward normal vector of the mixing surface. For a thin paddle impeller, the product of the pressure drop between the blades with the normal component of the velocity has to be integrated. The pressure drop:

$$\Delta p = \frac{\rho}{2} U^2 \sim \frac{\rho}{2} d^2 n^2 \, , \tag{4.17}$$

with the blade diameter d and the rotational speed n can be estimated. Since the

normal velocity is proportional to dn and the surface is also proportional to d^2, follows:

$$\int_{A_{mix}(t)} p\mathbf{u} \cdot \mathbf{n_{mix}} d\mathbf{A} \sim \rho \mathbf{d^5 n^3} \,. \tag{4.18}$$

This gives the following equation for the dissipated power:

$$P_{Diss} = Ne\rho d^5 n^3 \,, \tag{4.19}$$

with the dimensionless number Ne called Newton number, relating the resistance force to inertia force. According to Eq. 4.19, higher Newton number is advantageous because the same power is dissipated by a smaller rotational speed.

If a force is allowed to act through a distance, it is doing mechanical work. Similarly, if torque is allowed to act through a rotational distance, it is doing work. However, time and rotational distance are related by the angular speed where each revolution results in the circumference of the circle being travelled by the force that is generating the torque. This means that torque that is causing the angular speed to increase is doing work and the generated power may be calculated as:

$$P = 2\pi N\boldsymbol{\tau} \,, \tag{4.20}$$

where N is the rotational speed. From Eq. 4.19 and Eq. 4.20, we obtain the relation between power number and torque as:

$$Ne = \frac{2\pi N}{\rho d^5 n^3}\boldsymbol{\tau} \,. \tag{4.21}$$

4.2.3 Results and Discussions

For the preliminary investigations in the partly filled anchor mixer, calculations were performed for two complete iterations. The results presented here correspond to the time instant after one complete rotation of the anchor. Fig. 4.4 shows the free surface flow field with computational grid and anchor stirrer at an instant of time. A corresponding horizontal cross section with flow field and a rearrangement of the interface is illustrated in Fig. 4.5. Here, it is clearly seen that the stirrer takes the
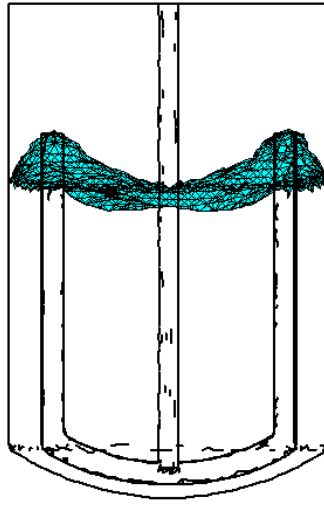
Figure 4.4: Computational grid together with the mixer geometry at the interface between liquid and gas at an instant of time.
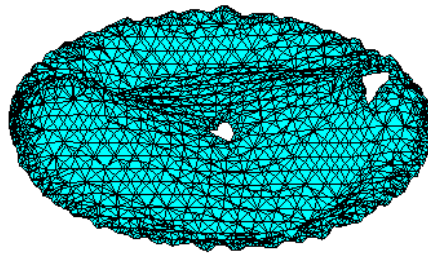
Figure 4.5: Computational grid at the interface between liquid and gas at an instant of time.
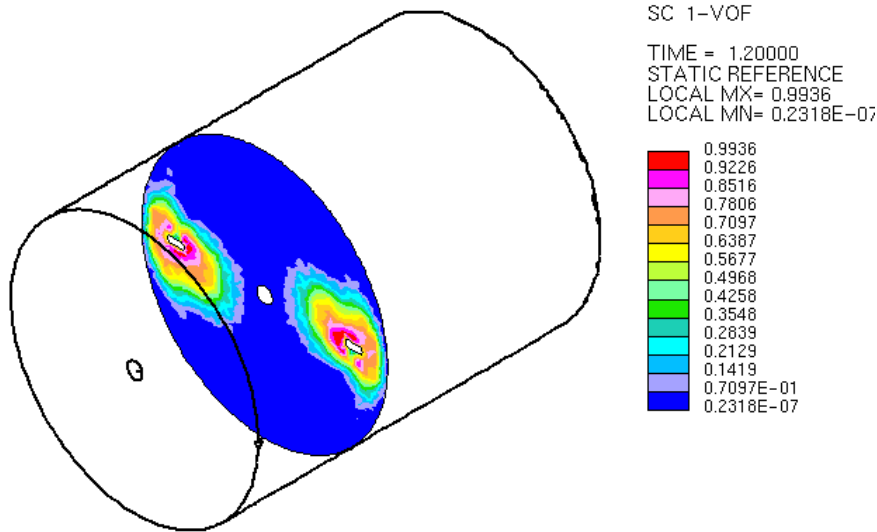
Figure 4.6: Representation of concentration of scalar variable in a mixer vessel stirred with anchor.

interface along with it while moving there by the exchange between the two phases makes possible. Fig. 4.6 demonstrates the contour plot of the volume fraction in horizontal cross section. This profile shows a sharp interface between the liquid and gas phase. Since the stirrer rotates counter clock-wise direction, one can notice the crest on the front side and the trough behind the stirrer. Velocity contours along the two-dimensional vertical and horizontal cross sections at the centre of the vessel are shown in Fig. 4.7. These contours show a maximum velocity field around the stirrer arms and a minimum velocity field outwards the centre of the vessel, which are expected from the physical nature of the flow. These high velocity gradients results in the flow field yields higher shear rates, which ultimately are responsible for reliable mixing.

The pressure distribution inside the mixer is presented in Fig. 4.8. The high pressure arises at the front of the stirrer and the low pressure behind the stirrer and also in the rest of the regions inside the whole domain. Fig. 4.9 demonstrates the evolution of torque with respect to time for a stirrer speed of 50 rpm. As time proceeds at the initial state, torque decreases abruptly and reaches a constant value. At the
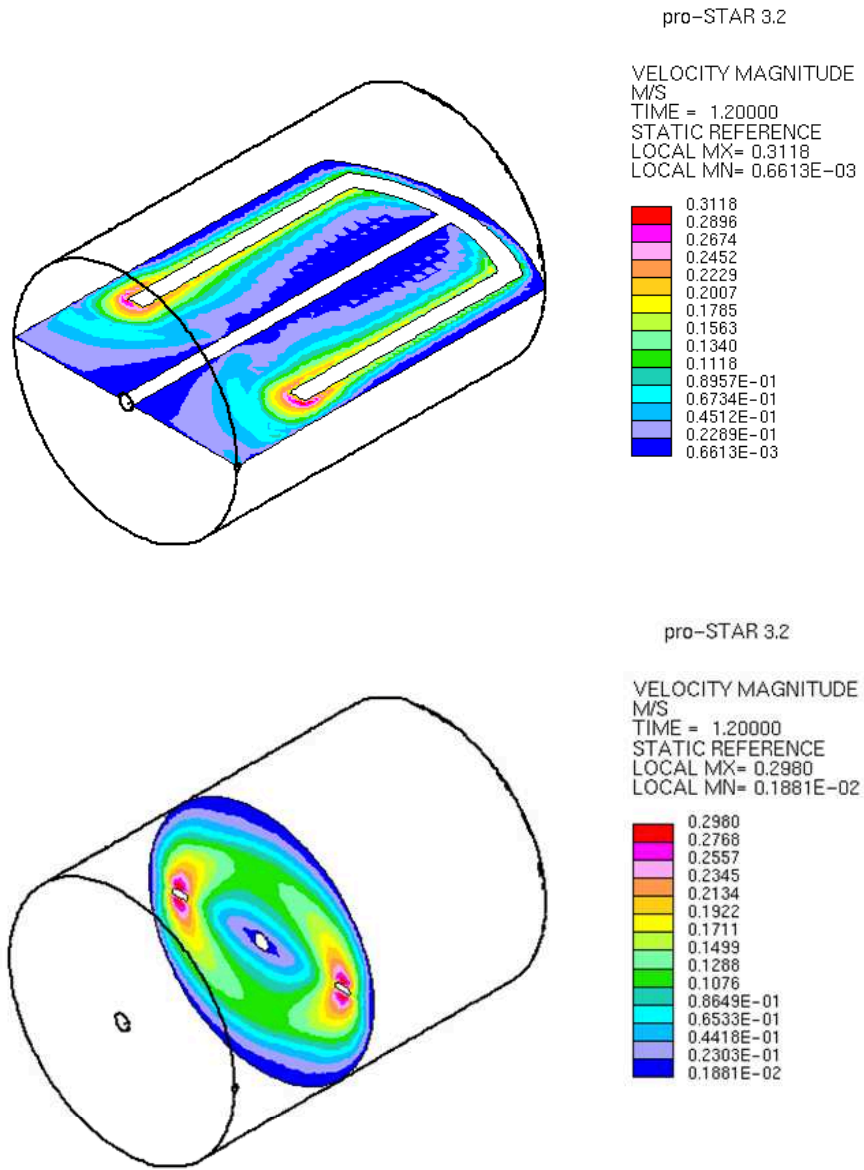
Figure 4.7: Contour plots of the velocity magnitudes in a mixed vessel stirred with anchor. High velocity magnitudes can be seen arround the anchor arms.
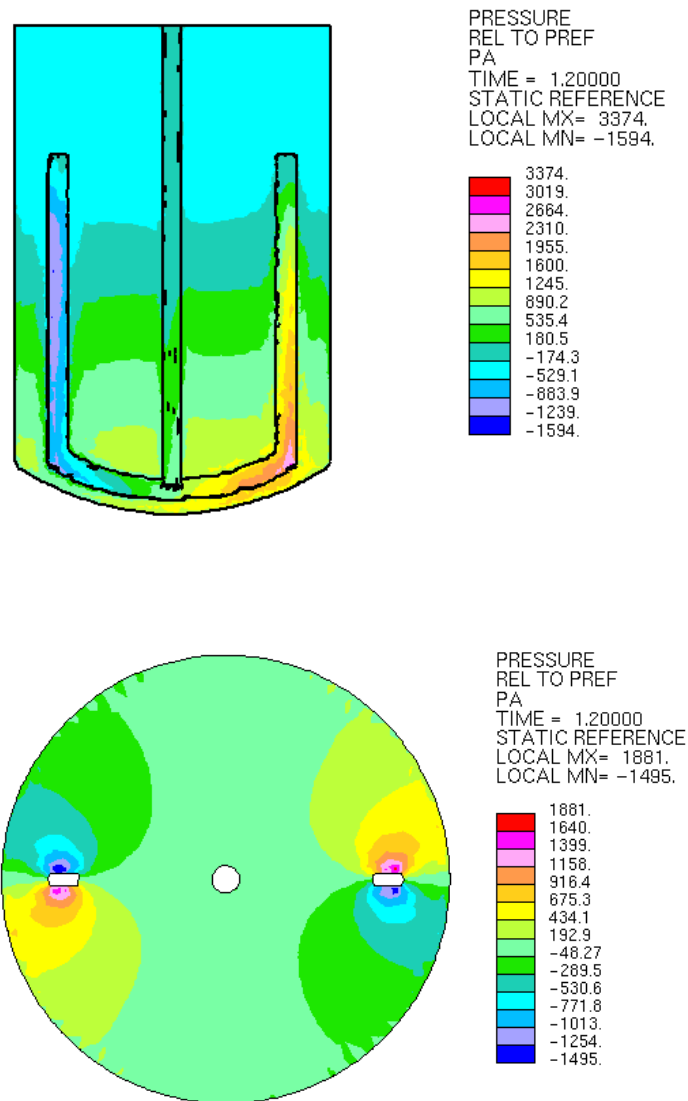
Figure 4.8: Pressure distribution in anchor mixer. High pressure results at the front of the stirrer and low pressure behind the stirrer.
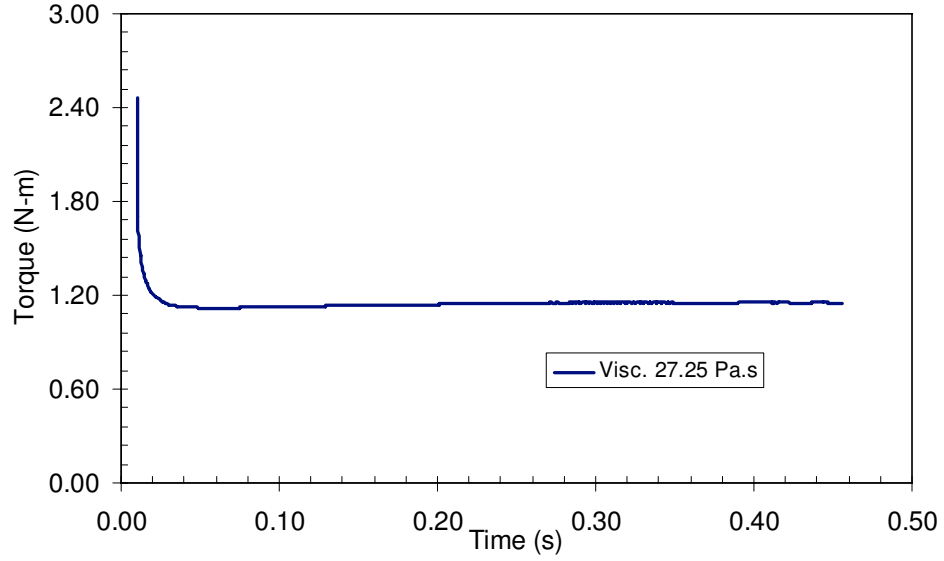
Figure 4.9: Time evolution of torque in anchor mixer.

onset of motion ($t = 0$), torque is at the maximum due to vessel resistance against the fluid and stirrer motion. Torque reaches constant within a short time at high viscosities, which is clearly observed in Fig. 4.10. Power number is expected to show the same trend in its behaviour, since power or Newton number is the product of torque and some constant quantity as shown in Eq. 4.21. There exists several ways for the numerical investigation of mixing in stirred vessels. The well known among them are numerical tracer experiments, Lagrangian particle tracking and entroy based measures. Though numerical tracers experiments are widely used technique, it induces numerical diffusion when dealing with highly viscous liquids. To avoid this, the present studies were carried out based on Lagrangian particle tracking. In the preceeding section, the highlights of this approach is emphasized and elaborated.

4.3 Particle Tracking

While numerical tracer experiments are of increasing importance as a means to analyze mixing processes, there is a principle problem which becomes severe obstacle in case of highly viscous liquid mixing or, more precisely, in case of highly schmidt numbers.
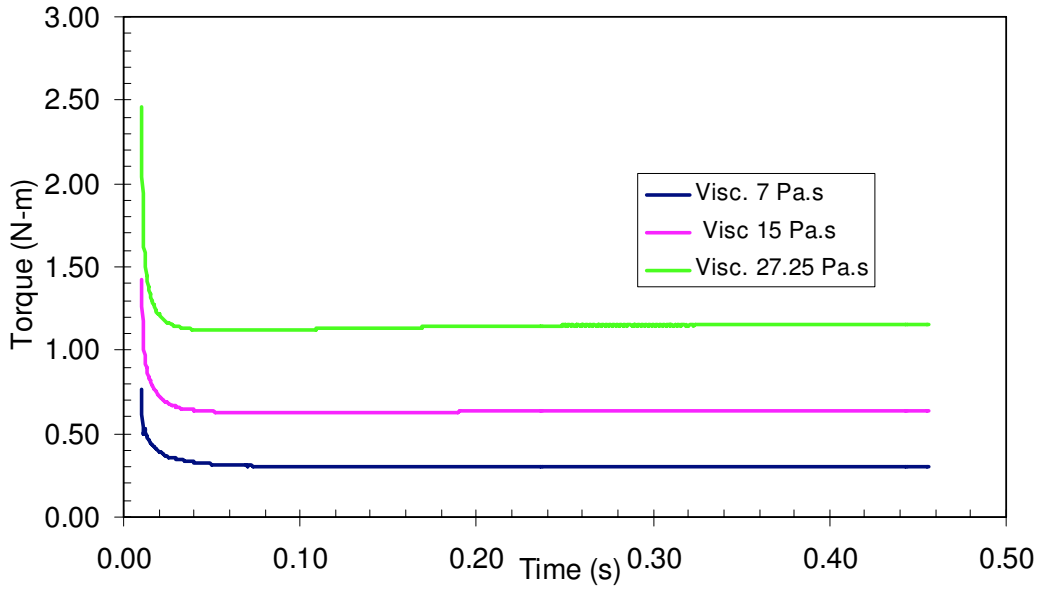
Figure 4.10: Time evolution of torque in anchor mixer for various viscosities.

In this situation, a sufficiency of the species transport equation can be spoiled by the effect of so-called numerical diffusion, i.e. the artificially generated smoothing of a tracer profile due to errors from the discretisation, and the numerical method can be much stronger than the true physical diffusion. In fact, almost all of the mixing that is observed in a numerical simulation may then be artificial. To show the intensity of numerical diffusion we performed simple test case in a lid driven cavity flow. Fig. 4.11 shows the influence of solver settings on numerical diffusion i.e., the so called discretization. The left hand side figure shows the tracer profile under the approximation of 1st order discretization (UDS) and yields produces numerical diffusion due to Taylor series truncation error [Eq. 3.4]. The figure on the right hand side depicts the tracer profile under the approximation of 2nd order discretization (CDS) and numerically less diffusive because the approximation is second order [Eq. 3.5]. One way to reduce this numerical diffusion is to refine the mesh as fine as possible as shown in Fig. 4.12. But the problem with mesh refinement is that it is numerically very expensive and the numerical diffusion is only minimized and not keep off.

A way to avoid this problem is to replace the continuous tracer concentration by
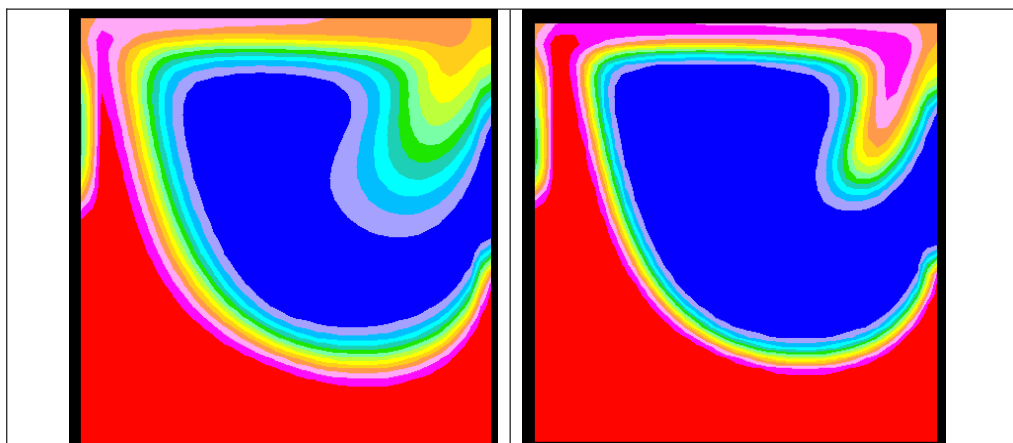
Figure 4.11: Influence of solver settings on numerical diffusion. 1st order discretization (left) and 2nd order discretization (right).
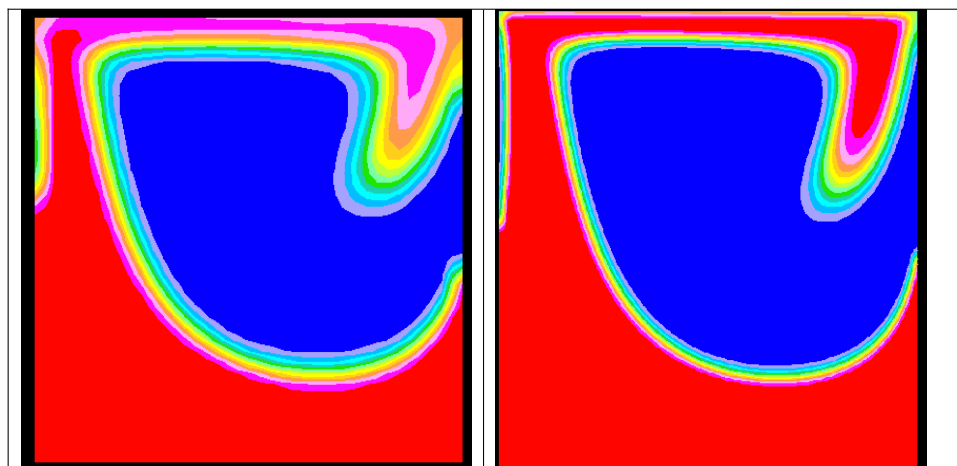
Figure 4.12: Influence of computational mesh refinement on numerical diffusion. Coarse mesh (left) and fine mesh (right).
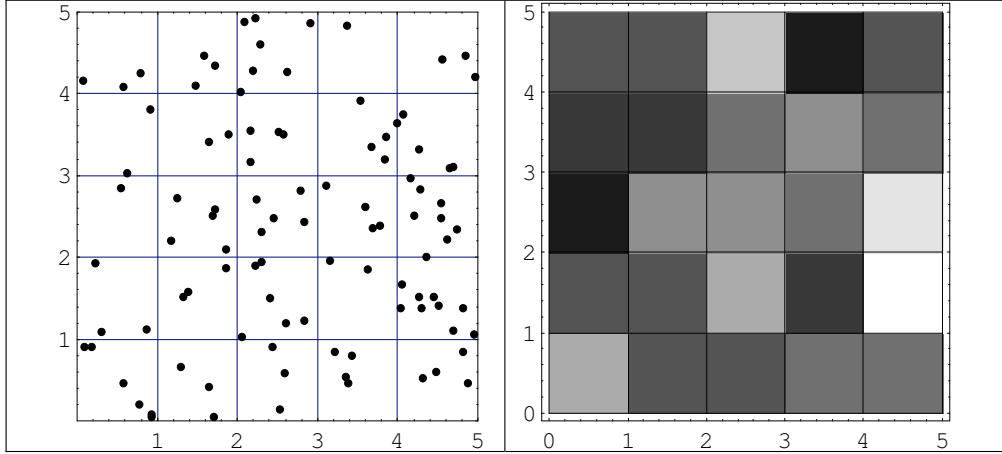
Figure 4.13: Contour plot of number concentrations (right) obtained from the number of tracked particles inside compartments.

a number concentration obtained from Lagrangian (i.e. inertia free) particles that are tracked during the simulation. This approach does not suffer from artificial diffusion, since the position of tracer particles can be resolved with sub-grid-scale accuracy and the velocity field at these particle positions can be obtained by interpolation from the grid values. The artistic view of contour plot as a result of number concentrations obtained from the number of tracked particles inside compartments is shown in Fig. 4.13.

Within this approach, initial positions $\mathbf{x_1},...,\mathbf{x_n}$ for a certain number of n particles are chosen-typically with random positions inside an appropriate subregion such that they form a kind of blob. Then the particles trajectories are computed as the solution of the dynamical system:

$$\dot{\mathbf{x}}(t) = \mathbf{v}(t, \mathbf{x}(t)), \quad \mathbf{x}(0) = \mathbf{x}_i. \tag{4.22}$$

In addition, a certain number m of compartments is defined, where the compartments form a subdivision of the mixing region, i.e.

$$V = \bigcup_{k=1}^{m} V_k, \quad \text{with disjoint} \quad V_k. \tag{4.23}$$

Let $X_k(t)$ denote the number of particles that are inside V_k at time t. Then the
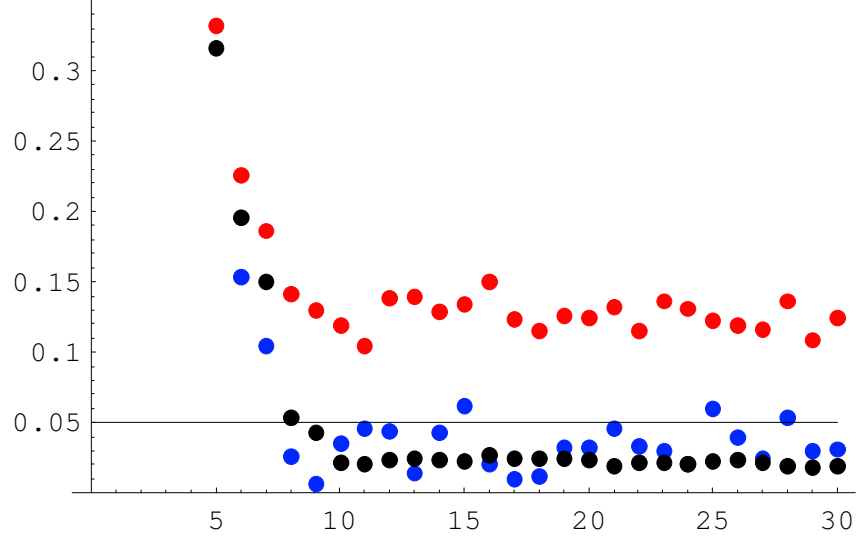
Figure 4.14: Decay of normalised variance under application of the Baker map. Effect of numbers of particles (P) and compartments (C): 100P, 64C (red); 800P, 4C (blue); 3200P, 64C (black).

normalized number concentrations $c_k(t)$ are defined as:

$$c_k(t) = \frac{X_k(t)}{|V_k|} \Big/ \frac{n}{|V|}, \tag{4.24}$$

which reduces to:

$$c_k(t) = \frac{m}{n} X_k(t), \tag{4.25}$$

in the case when all compartments V_k have the same volume. The basic question within this approach is how many particles and how many compartments have to be used to obtain a reliable mixing time from the decay of variance of the normalized number concentrations? A particular time evolution of the variance is of course only a single realisation of a stochastic process. Hence any quantity obtained from it is a random variable that can only be characterized by means of its statistical properties. Furthermore, a state of complete homogenization has a defined meaning only in the statistical sense. Especially, such a state will show a strictly positive variance. Therefore, in order to be able to compute a reasonable mixing time, this "'residual variance"'
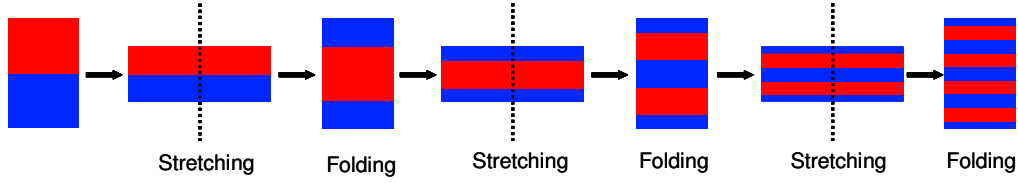
Figure 4.15: Illustration of Baker map
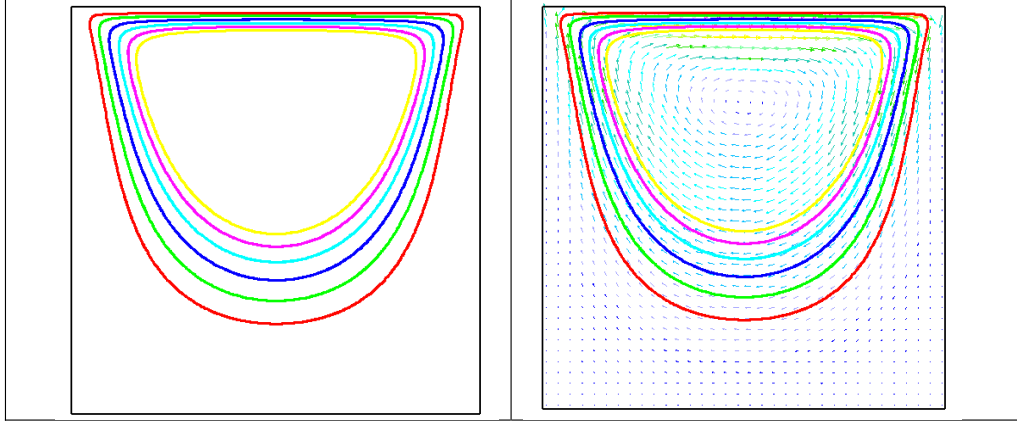
Figure 4.16: Typical particles trajectories in Lid driven cavity.

σ_R^2 has to be much smaller than the threshold $\epsilon s^2(0)$ from above. This is illustarted in Fig. 4.14, which shows the decay of variance under successive applications of the Baker map to a set of n particle positions that are initially close together. Let us note in passing that the Baker map was introduced in the 1930s in [66], probably inspired by Birkhoff. Nowadays, the Baker map is a well-known prototype map that models a simple mixing process composed of stretching and folding. Its definition is implicitly given in Fig. 4.15. In Fig. 4.14, red dots correspond to the variance obtained from 100 particles and 64 compartments. Evidently, the residual variance is too large to reach the threshold for $\epsilon = 0.05$. In case of 800 particles, but only 4 compartments, the residual variance is below the critical value, but the stochastic deviations of these variances from their mean, i.e. the variance of variances, is too large. Reliable results are obtained, e.g., in case of 3200 particles and 64 compartments as shown by the black dots.
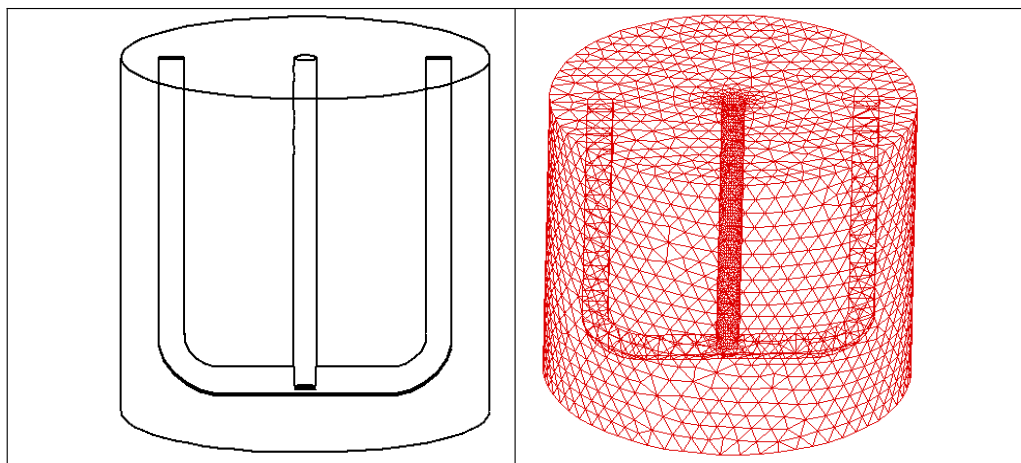
Figure 4.17: Schematic representation of anchor mixer with hybrid (combination of tetra and hexa) mesh. The mesh contains about 100000 control volumes and is generated using Star-Design.
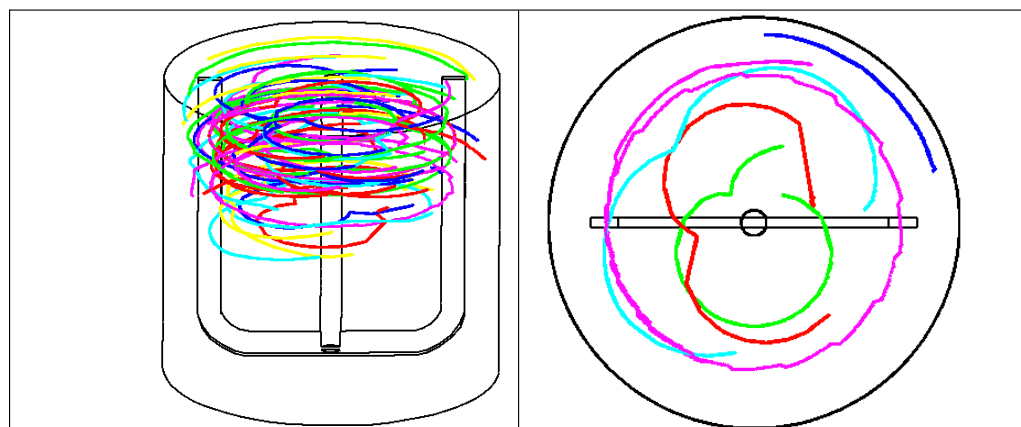
Figure 4.18: Lagrangian particles trajectories in anchor mixer.
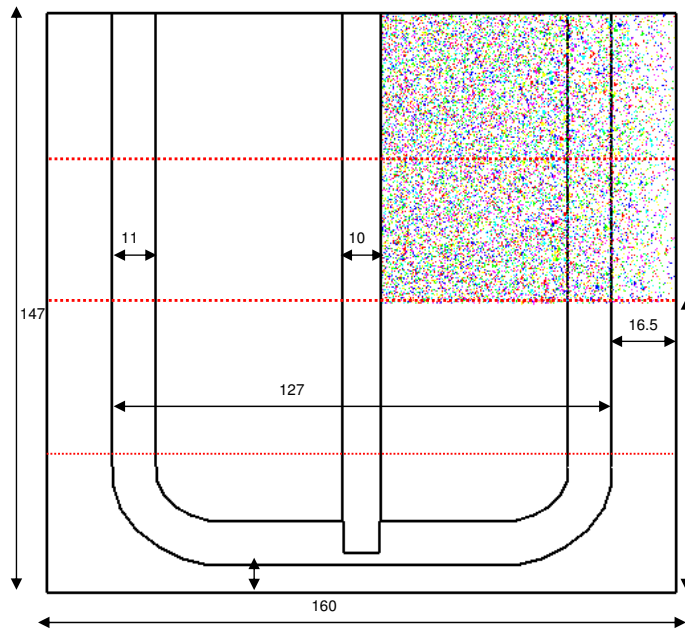
Figure 4.19: Schematic representation of anchor mixer with dimensional configurations (in mm) and it is divided into 4 compartments vertically for particle tracking. A blob of particles also can be seen in the figure.
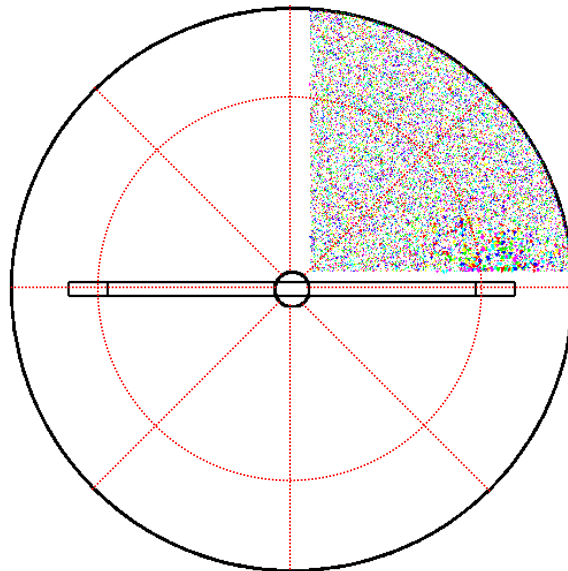
Figure 4.20: Schematic representation of anchor mixer with division of 16 compartments in radial and circumferential cross section.

A similar problem concerning residual variances occurs if mixing times are determined from experimental measurements. In this case σ_R^2 has been calculated under the assumption that the tracer particles are evenly distributed and that the resulting concentrations in individual probes are stochastically independent. The latter assumption is not reasonable if the complete volume is samples by means of all compartments, since then:

$$\sum_{k=1}^{n} p_k c_k(t) = 1 \quad \text{with} \quad p_k = \frac{|V_k|}{|V|} , \tag{4.26}$$

i.e. the random variables c_k (at a fixed time t) are not independent. In fact, if the particles are evenly distributed in V and if X_k denotes the number of particles inside V_k, then their joint distribution is given by the multinomial distribution:

$$P(X_1 = l_1, ..., X_m = l_m) = \frac{n!}{l_1!...l_m!} p_1^{l_1}....p_m^{l_m} , \quad \text{where} \quad n = \sum_{k=1}^{m} l_k . \tag{4.27}$$

We restrict our attention to compartments of equal volume, in which case the above equation simplifies to:

$$P(X_1 = l_1, ..., X_m = l_m) = \frac{n!}{l_1!...l_m!} \frac{1}{m^n} , \quad \text{where} \quad n = \sum_{k=1}^{m} l_k . \tag{4.28}$$

Then, by an elementary calculation yields:

$$\text{Var}[X_k] = n\frac{1}{m}(1 - \frac{1}{m}), \quad \text{hence} \quad \sigma_R^2 = \text{Var}[c_k] = \frac{m}{n}(1 - \frac{1}{m}). \tag{4.29}$$

If, initially, the particles are evenly distributed in l of the m compartments, the initial variance is:

$$\sigma_0^2(X) = \frac{n^2}{m}(1 - \frac{l}{m})\frac{1}{l} . \tag{4.30}$$

This leads to a relative residual variance of:

$$\frac{\sigma_R^2}{\sigma_0^2(c)} = \frac{\text{Var}[X_k]}{\sigma_0^2(X)} = \frac{n}{m}(1 - \frac{1}{m})\frac{1}{\frac{n^2}{m}(1 - \frac{l}{m})\frac{1}{l}} = \frac{(m-1)l}{n(m-l)} \approx \frac{l}{n} \quad \text{for} \quad l \ll m . \tag{4.31}$$

The estimate Eq. 4.31 can now be used to calculate the number of particles needed to compute a reliable mixing time $t_M^{1-\epsilon}$ for a given level $\epsilon > 0$. Indeed, this number n has to chosen such that:

$$\gamma = \frac{l}{\epsilon n} \ll 1 , \tag{4.32}$$

say $\gamma=0.1$. As an example, for $\epsilon=0.05$ and $l=1$, at least 200 particles should be used, but $200^2 = 40000$ particles are required if the mixing time is computed from standard deviations instead of variances. Within the computations, the true variance is estimated by means of:

$$s^2(X) = \frac{1}{m}\sum_{k=1}^{m}(X_k - \frac{n}{m})^2, \quad \text{resp.} \quad s^2(c) = \frac{1}{m}\sum_{k=1}^{m}(c_k - 1)^2. \tag{4.33}$$

To avoid wrong mixing times caused by too much noise contained in the computed variance, one should also check for:

$$\frac{\text{Var}[s^2(c)]}{\sigma_R^2} \leq \gamma, \tag{4.34}$$

say. Again by elementary calculations it follows that:

$$\frac{\text{Var}[s^2(c)]}{\sigma_R^2} = \frac{\text{Var}[s^2(X)]}{E[s^2(X)]} = \frac{\text{Var}[s^2(X)]}{\text{Var}[X]} = \frac{2}{m-1}(1-\frac{1}{n}) \approx \frac{2}{m-1} \tag{4.35}$$

which determines the number of compartments needed. Surprisingly, quite few compartments are sufficient to keep the noise at a small level.

4.4 Results and Discussions

The above developed method has been evaluated using the numerical investigation of one of the oldest and yet widely used mixer configuration which is shown in Fig. 4.19. It consists of a flat bottomed vessel of 147 mm height and a diameter of 160 mm. The tank is equipped with anchor impeller of width 127 mm and height equal to the vessel height of 140 mm. Other important dimensions such as clearance between the wall and anchor, blade width and thickness are shown in Fig. 4.19. Unstructured hybrid (combined hexa and tetra type) mesh consists of approximately 70,000 control volumes was generated using Star-Design software. The working liquid is a Newtonian fluid with material properties density: $\rho=1000$ kg/m3 and viscosity: $\mu= 5$ Pa s. A speed of 50 rotations per minute is set for the rotating reference frame. Since the boundaries of the rotating domain is assumed to be rotating witht the same angular speed, an opposite spin of the same angular speed is defined on the inner walls to make

them stationary. Reynolds number of 2.7 is held which is correspond to laminar flow condition. The time dependent transport equations [Eq. 3.12] are solved in Cartesian co-ordinates for laminar flow. The influence of grid dependency is investigated at 3 different grid sizes and the observation is that the solution has a very little effect based on the velocity field comparison. A compramise in grid size is arrived based on accuracy of the calculation and numerical efforts needed. A second order accurate spatial discretization [Eq. 3.5] scheme is used to solve convective terms. The following section discusses the calculation of intensity of segregation.

4.4.1 Intensity of Segregation

In case of transient species distribution $c(t, \mathbf{x})$, the standard deviation $\sigma = \sigma(t)$ and, hence, the variation coefficient will also depend on time, although the mean value stays constant if no flux of tracer across the domain boundaries occurs. The evolution of $\sigma(t)$ indicates how the quality of mixing changes in the course of time occurs. The evolution of the homogeneity of a scalar field at a given time, it cannot be directly employed for the definition of a mixing time or a mixing length. This is due to the fact that it is not normalized to the range 0...1, say, but can attain any value between zero and infinity. Hence, while an ideally homogeneous mixture has a segregation coefficient of zero, it is not clear which threshold should be reached during a mixing process. An appropriate normalization can be derived more easily in case of non-reactive mixing and for an isolated mixing region. As mentioned above, the expectation μ stays constant then, hence only the variance σ^2 needs to be normalized. This leads to:

$$I = \frac{\sigma^2}{\sigma_{max}^2} \, , \tag{4.36}$$

where σ_{max}^2 denotes the maximum variance. These considerations result in Danckwert's intensity of segregation [16], defined by:

$$I_S = \frac{\sigma^2}{\mu(1 - \mu)} \, . \tag{4.37}$$

Based on Danckwert's intensity of segregation, measures for the intensity of mixing can be derived and a large number of related measures which are similar in the sense
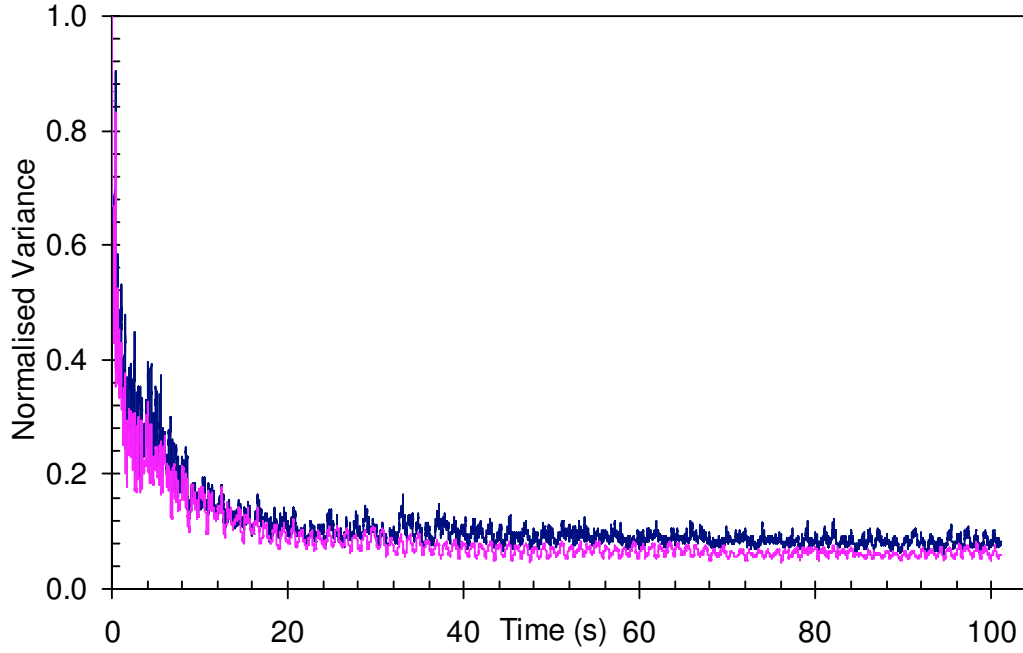
Figure 4.21: Time evolution of normalised variance for anchor mixer. Effect of numbers of particles (P) while compartments (C) kept constant: 100P, 64C (red); 1600P, 64C (blue).

that they depend on statistical parameters are reviewed in [12]. A typical example, which is recommended there, is:

$$I_M = (1 - \sqrt{I_S}) = 1 - \frac{\sigma}{\sigma_{max}}. \tag{4.38}$$

Since I_S is normalized, this measure is zero for completely segregated mixtures and attains the value one in the homogeneously mixed case.

In order to assess the quality of mixing in stirred vessels, the significant task was to compute the tracer particles trajectories and obtain the data for variance evolution. To achieve this, a mass-less Lagrangian particles of 1600 are randomly placed initially in one compartment (sub-volume) such that they form a blob of particles as shown in Fig. 4.19 and Fig. 4.20. This approach does not suffer from artificial diffusion, since the position of tracer particles can be resolved with the sub-grid scale accuracy and the velocity field at these particle positions can be obtained by interpolation from the grid values as mentioned earlier. Notice that the co-ordinates (position) of the particles
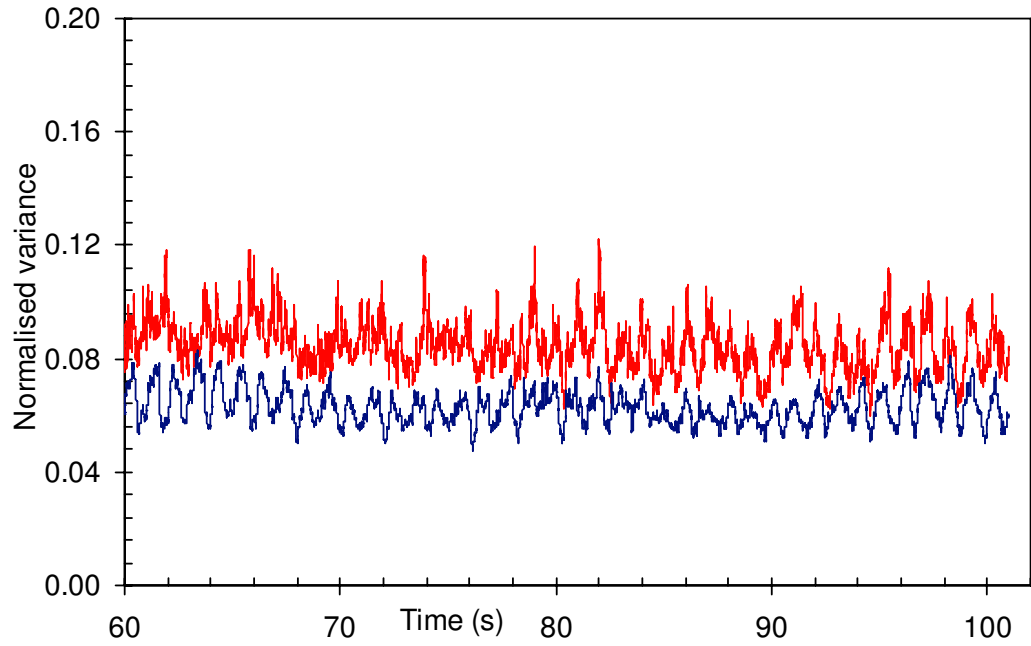
Figure 4.22: Time evolution of normalised variance for anchor mixer. Effect of numbers of particles (P) while compartments (C) kept constant: 100P, 64C (red); 1600P, 64C (blue).
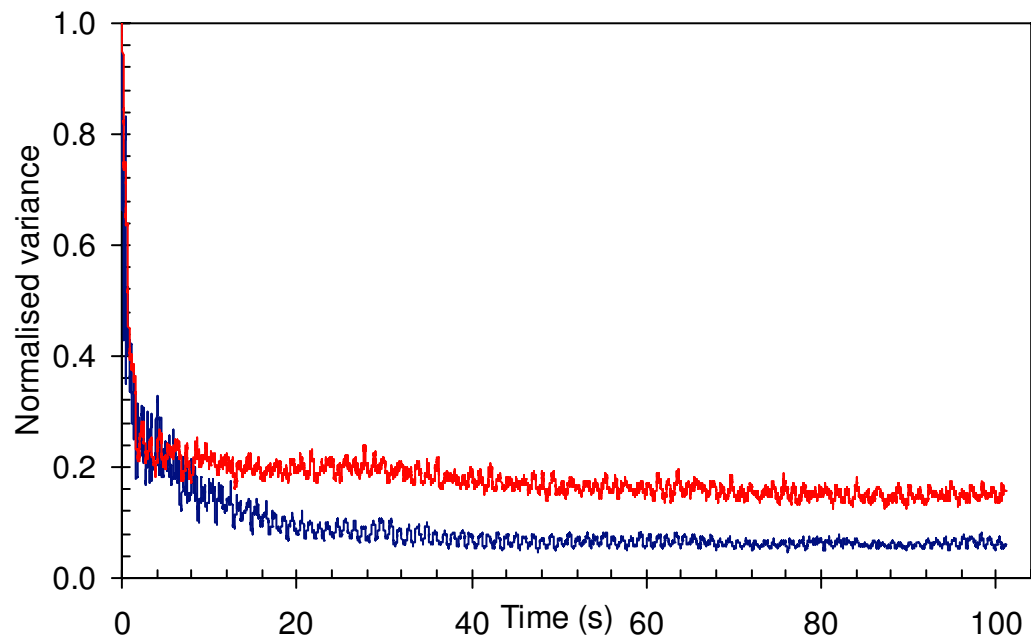
Figure 4.23: Time evolution of normalised variance for anchor mixer. 1600 Particles are initially placed in one compartment (blue), multiple compartments (red).
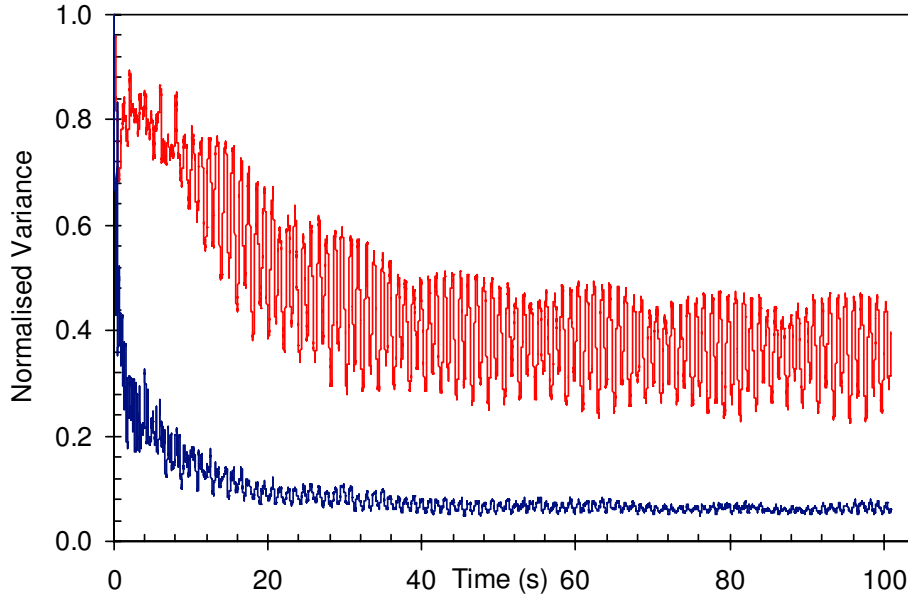
Figure 4.24: Time evolution of normalised variance for anchor mixer. Effect of numbers of compartments (C) while particles (P) kept constant: 1600P, 4C (red); 1600P, 64C (blue).

are in rotating reference frame and it is necessary to transform them to laboratory frame. The particle number information is recorded during the simulation process with the aid of user defined subroutine written in FORTRAN 77 and provided to Star-CD. During the process of particle tracking, the number concentration is calculated according to Eq. 4.24. The evolution of variance can then be computed based on number concentration information as defined in Eq. 4.33.

Time evolution of normalised variance (is also known as intensity of segregation, obtained by dividing computed variance with the initial variance) can be seen in Fig. 4.21. The value on Y-axis varies between one and zero. Intensity of segregation (I_s) equal to 1 means complete segregation and a value of 0 stands for complete homogenisation. To achieve complete homogenisation ($I_s=0$) in numerical studies is very difficult even with the present day computers. In Fig. 4.21, the blue curve correspond to I_s with 1600 particles and the red curve correspond to I_s with 100 particles. In both the cases, particles are initially placed only in one compartment. A

sharp decrease is observed at the beginning of the calculation in these curves which is attributed to the domination of the flow due to kinematical mixing. When time proceeds, a condition of unvarying in the evolution curves occur which is due to the fact that almost even distribution of the particles in the whole domain is obtained. The one of the important observations from this figure is that the red curve possesses more noise than the blue curve (Fig. 4.22), owing to insufficient number of particles. In the case of anchor mixer, it is well known fact that the velocity gradients are poor in vertical direction. Hence 1% of initial variance is achieved only after expensive numerical simulation.

In Fig. 4.23 we illustrate the effect of number of compartments where particles are initially placed. It shows two curves with different colours, the one in blue is the result of time evolution of I_s when the particles are initially placed in one compartment and the other in red colour is the result of I_s when the particles are placed initially in multiple compartments. Remarkable difference can be seen in the magnitude of I_s between these two curves. If particles are initially placed in more than one compartment, there is a possibility of attaining I_s greater than one, since after certain time elapses particles may be advected to the compartments which are less than the compartments in which particles are placed initially. The other important observation in the current investigations is that the number of compartments required for reasonable mixing quality. This phenomenon is depicted in Fig. 4.24. If the total computational domain is divided into few compartments, the residual variance is too large and also the fluctuations in I_s are too high even with more particles.

4.4.2   Mixing Time

A general definition of σ_{max}^2 is problematic, since a universal maximum value for the molar concentration does not exist. One possible adaptation to molar concentrations or, more generally, intensities is to let σ_{max}^2 be the variance of a totally segregated distribution composed of the same amount of substance or the same total intensity and the same maximum value c_{max}. Again, this variance is independent of the concrete

structure of the segregated field and leads to $\sigma^2_{max} = \mu(c_{max} - \mu)$. This reference value allows for a normalization of the variance of the distribution based on the scalar field itself., i.e. without need for an additional external value. This is useful for assessing a species distribution by itself, but, since c_{max} will usually change with time or space it cannot be employed for defining a mixing time or a mixing length. On the other hand, if a mixing time or length is to be defined, a mixing process instead of a single mixture is to be evaluated. In this case, mixing evolves in the course of time or along a spatial direction and, hence, the variance σ^2_0 at the initial time or the entrance of the mixing channel can be used instead of σ^2_{max}. For instance, a mixing time t_{mix} is obtained as the first time t_0 such that:

$$s^2(t) \leq \epsilon s^2(0) \quad \text{for all} \quad t \geq t_0 \,, \tag{4.39}$$

where ϵ (with $0<\epsilon<1$) is a given fraction; typical values are $\epsilon=0.05$ or $\epsilon=0.01$. This criterion corresponds to the condition $\sigma^2/\sigma^2_0 \leq \epsilon$ or to $I_S \leq \epsilon$ with I_S from Eq. 4.37 in case of a completely segregated initial state. Of course, these mixing times strongly depend on the choice of ϵ. As a variant of the later definition above, a mixing time is also defined as the first time from which on I_M from Eq. 4.38 stays above 1-ϵ.

The determination of mixing times from numerical tracer experiments with the help of CFD simulations can be difficult, since a value of $I_M=0.99$, say, will often be only reached after long and expensive calculations. This is especially true for highly resolved simulations which need to be used in case of high Schmidt numbers. On the other hand, there are several references, apparently starting with [40] in which an exponential asymptotic behavior of the type:

$$\sigma^2(t) \sim \exp(-t/\tau^{\infty}_{mix}) \quad \text{for large} \quad t \,, \tag{4.40}$$

with an assymptotic mixing time τ^{∞}_{mix} is assumed. In case of a continuous mixing process, this type of behaviour with more time replaces by axial position is employed in [31] to define a mixing length. While Eq. 4.40 is often used without justification, there is increasing mathematical evidence for Eq. 4.40 to be valid in several situations [44] and [75]. In situations where Eq. 4.40 holds, this can of course be used to reduce
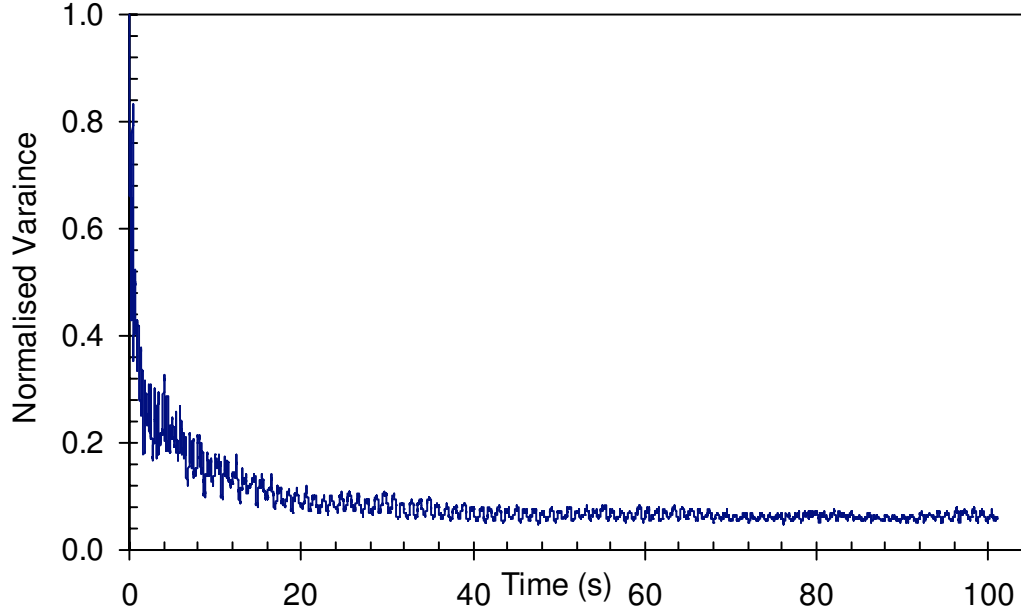
Figure 4.25: Time evolution of normalised variance for anchor mixer with 1600 parti-
cles and 64 compartments.

the computational effort needed for numerical mixing time calculation. Indeed, it then
suffices to run a numerical tracer experiment until a linear dependence of $\log\sigma$ versus
time is reached and the mixing time can then be obtained by extrapolation [29].

In the case anchor mixer, the mixing time is computed based on the procedure
mentioned above and let us consider the value of $\epsilon = 0.05$. As it can be seen from
Fig. 4.25, normalised intensity never reaches a value of $\epsilon = 0.05$. If we consider
$\epsilon = 0.1$, normalised intensity achieves certain minimum but again increases. Hence the
appropriate definition of mixing time in anchor mixer is difficult and even after a long
and expensive computations. These observations reveal the poor mixing characteristics
of anchor mixer. It is well known that anchor mixer is good for heat transfer between
wall and the fluid rather than its mixing capabilities. Numerical investigation of
mixing in a specific kneader element is presented in the next chapter.

Chapter 5

Mixing in a Kneader Element

5.1 Introduction

Synthesis of highly viscous materials such as polymers, rubber and food etc requires suitable machines and screw extruders are well known for this purpose. However, screw extruders are no more efficient when longer residence time and little axial dispersion is needed. Hence, several investigations were made in the early 20th century to modify screw extruders to achieve longer residence time and little axial dispersion. One of the such maschines is kneader reactor which is used for mixing of highly viscous liquids especially paste like materials and these maschine has a construction similar to screw extruders. During this time the idea of using extrudes with pins on a barrel, reciprocating screws and self-cleaning action evolved. The purpose of pins [3, 84] on barrel is to agitate and knead the material being processed to remove air from it. The reciprocating action of screws yield better injection molding for highly viscous polymers. The term self cleaning means here every surface which is in contact with the reacting product is mechanically wiped by another surface with a well defined closed distance. The principle of rotating and oscillating action of single shaft Kokneader is shown in Fig. 5.1. Keeping the screws clean to avoid collection of dirt and sticky nature of polymers to the kneading pins and barrel can be achieved by self cleaning mechanism [Fig. 5.2] of the extruder.
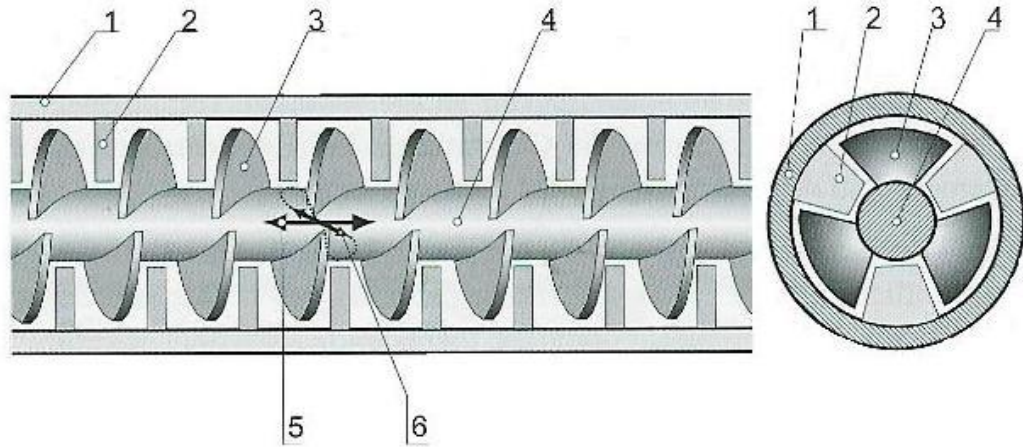
Figure 5.1: Single shaft kokneader with oscillating and rotating mechanism; 1. Barrel, 2. Kneading pin, 3. Kneading element, 4. Shaft, 5. Oscillation and 6. Rotation.

Heinz List [43] invented kneader by combining the better kneading, injection and self cleaning mechanisms. Further developments were intensely took place between 1960-70 to further modify kneaders for various applications. For more detailed overview on the literature related to kneader development can be found in [83] and the references given there. Few experimental investigations on buss kneader characteristics were done between 1955-95. However, the first basic and detailed experimental study is reported by [20]. They used silicone oil ($\mu = 1$ Pas) and a parafanic oil (0.2 Pas) under isothermal conditions at room temperature to measure throughput versus screw speed, pressure and fill lengths. Little later, Lyu and White [45, 46] published their findings on fill factor and temperature profiles, melting conditions and residence time distribution as a function of screw configuration and processing conditions for List/Buss kneader. More recent studies [76, 77] concerning Buss kneader as a polymerization reactor shows the good mixing properties of kneader in radial as well as axial directions for exothermal reactions. Simulations of fluid flow in a Buss kneader started in the late 80s to model flow and pressure field distributions. A detailed investigations on total machine characteristics of Buss kneader were published by Elemans and Meijer [20], Lyu and White [45–48]. A 3-D computational study reported by Mehranpour et al. [53] to predict the velocity field in the conveying element of a Ko-kneader shows
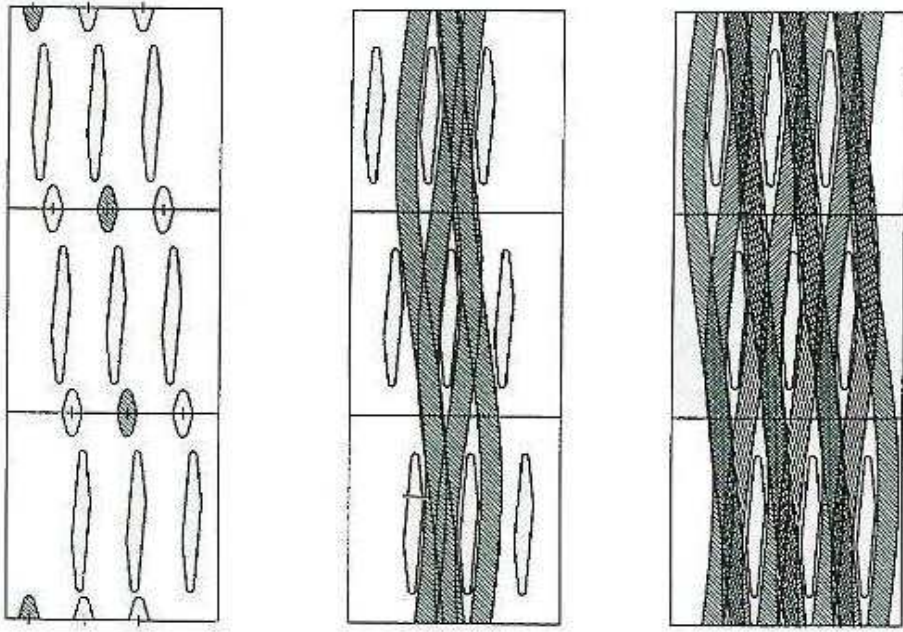
Figure 5.2: Schematic of the self-cleaning mechanism of kneader by movements of the pins [83].

that the reciprocating action of Kokneader enhances the mixing performance by means of periodically changing the flow field and shear rate distribution.

In addition to single shaft, kneaders with double shaft are also gained much attention in the recent years. The advantage being large length to diameter ratio and shows clear analogous to twin screw extruder. A typical configuration of double shaft kneader is shown in Fig. 5.3 which has large length to diameter ratio and also the incident angle of the two shafts. The angle formed by the surface of each kneading element with the shaft of the rotor towards the bottom of the tank is designated by α where as the angle formed by the surface of each kneading element with the shaft of the rotor against the bottom of the tank is designated as β. Similar to twin screw extruder, the flexibility of double shaft kneader is also that it can be corotating or counter rotating. The experimental works are mainly limited to determination of integral, characteristic features of the whole reactor, such as mean residence time or mean degree of filling [5, 63]. The experimental investigation of residence time in kneader, single as well as twin screw extruders are carried out by several researchers

using different tracer materials, for example using aluminium flakes [49, 67], coloured materials [5, 15, 62, 69, 73], iron powder [63], salts [17, 19, 78, 79] and light emission of flourescent tracer [15]. However, local phenomena and fundamental mechanisms are not studied. The recent master thesis [65] reports on experimental investigation of double shaft intermeshing kneader. Their results include investigation of power dissipation, fill level, residence time distribution (RTD) and heat transfer for the better understanding of the basic mechanisms in the kneader.

For the description of the process, simple cumulative models such as the cascade model [48, 54], dimensionless numbers relations or even regression approaches [51] are employed but cannot contribute to a thorough understanding. Only very little work is based on continuum mechanical models. These are mainly devoted to twin screw extruders. In that case, flow geometry make the use of lubrication theory relevant to fully filled parts, resulting in 1D-models for RTD, average temperature and pressure. For simplified materials rheology, these models, together with specific optimization algorithms, can help to optimize compounding processes up to a limited level only [25, 42]. Recent progresses using 3D local approaches have also been made [7] using fluid-structure interaction techniques [28]. Admittedly, according to the knowledge of the author of the present thesis, there are no numerical investigations reported in the literature on the investigation of double shaft kneaders. In particular, essential aspects of kneaders such as interpreting geometries of the rotating shafts, the appearance of free surfaces and, above all, an adequate modelling of mixing and mass transfer are still missing. The reason is that the limited capability of numerical simulation techniques to handle intermeshing or ovelapping grid problems. Basic numerical investigation of a particular unit cell of a kneader element is presented in this chapter. The geometry used in the current investigation is a cylindrical stirred tank equipped with complicated kneading disks and pins as shown in Fig. 5.4. This geometrical configuration contains kneading disks attached to the shaft and kneading pins mounted on the kneading discs for the purpose of cleaning the barrel if any material is sticked to it especially during highly viscous polymer mixing. Simulation procedure in this stirred tank is explained

Figure 5.3: Two shaft intermeshing Reacom 60L kneader reactor.

in the following section.

5.2 Simulation

For the computations presented here, a general purpose finite-volume based commercial CFD package from CD-Adapco has been used. This package includes tools for parametric geometry definition, automatic mesh generation, flow-field solution and postprocessing the results.

5.2.1 Flow Computation

Time dependant simulations were performed for the flow created by kneading element in a tank. The tank itself is a vertical, cylindrical vessel with a diameter of 130 mm and height of 90 mm. The concentrically located shaft extends the entire height of the tank and has a diameter of 60 mm. Each of three kneading disks are spaced at 120° in circumferential direction and each of three kneading disks in vertical direction are spaced at 40° each in vertical direction corresponding to equally sized nine kneading disks. Kneading pins are appropriately mounted on the kneading disks without losing

symmetry. It should be noted that the computational model of this system represents the exact geometry including the small and angled pins. The unstructured mesh is generated using Star-Design and contains approximately 100,000 hybrid (hexa and tetra) computational cells. The mesh is exported to Pro-Star where the parameters of simulation are provided. The properties of the working liquid in this case are constant viscosity (μ) of 1 Pas and constant density (ρ) of 1000 kg/m3. The laminar, incompressible and time dependant momentum conservation equation in rotating reference frame [Eq. 3.12]:

$$\frac{\partial \mathbf{u}}{\partial t} + (\mathbf{u} \cdot \nabla)\mathbf{u} + \mathbf{\Omega} \times (\mathbf{\Omega} \times \mathbf{r}) + 2\mathbf{\Omega} \times \mathbf{u} = -\frac{1}{\rho}\nabla p + \nu\nabla^2\mathbf{u} + \mathbf{g}, \qquad (5.1)$$

is solved, where $\mathbf{g}$ is the acceleration due to gravity. The continuity equaion ($\nabla \cdot \mathbf{u} = 0$) is invariant regardless of the reference frame. The whole computational domain is rotated (solid-body rotation) with an angular velocity of 60 rotations per minute. The velocity boundary conditions for all cells on the kneading disks, pins together with shaft are set to zero by defining equal and opposite magnitude of angular velocity used for solid-body rotation. The velocity boundary conditions for all computational cells on the cylindrical vessel surface, top and bottom walls are set to correspond to the solid-body rotation. The initial velocities of the fluid cells are assumed to correspond to the same solid-body rotation as the tank walls. A time step of 0.0005 sec is set and several time steps were carried out resulting adequate rotations of the impeller.

5.2.2   Particle Tracking

In the present study, mass-less fluid particles are introduced in the flow is followed using a Lagrangian particle tracking method in order to quantify the mixing quality. A randomly distributed 1600 particles are placed in small volume in the middle of the vessel at the beginning of the simulation process. As discussed earlier, particle tracking approach avoids the introduction of numerical diffusion which results if a scalar variable is tracked, which confuses the actual mixing behaviour of equipment. The movement of the particle tracers in the flow is tracked by the integration of the

(a)   (b)
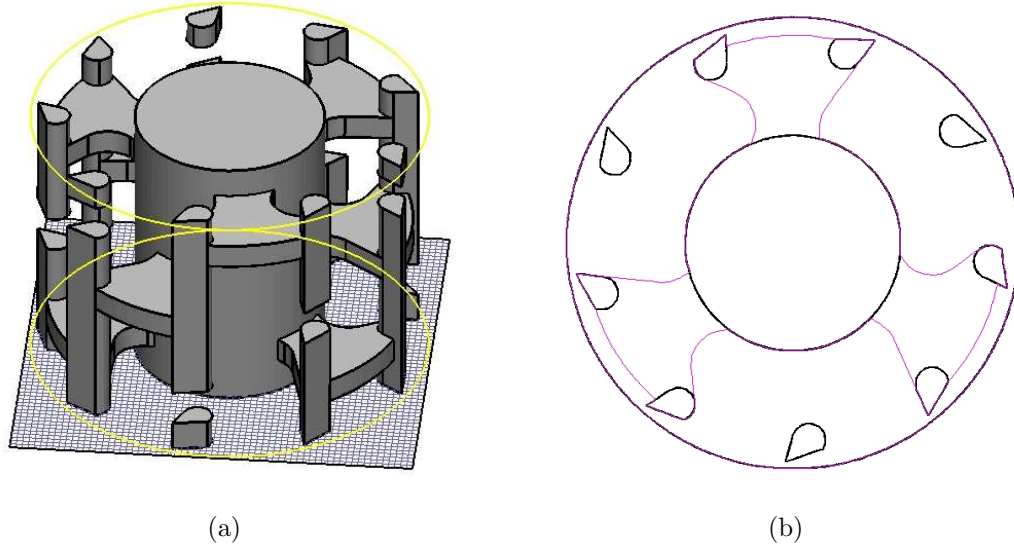
Figure 5.4: Schematic of (a) unit cell of a specific kneader and (b) the top view of kneader element (CAD data from BASF AG, Ludwigshafen).

vector equation of motion of each particle [Eq. 4.22]. A rebound condition given to the particles to avoid trajectories being trapped near the walls where the local velocity is close to zero.

5.3 Results and Discussions

Simulations are performed in a kneader element as explained in the previous sections and the post processing of the results are discussed below.

5.3.1 Flow Patterns

In order to understand the flow inside the kneading element, velocity magnitude section plots are discussed here. Fig. 5.5(a) shows the velocity contour plot in horizontal cross section. Red colored regions denote high velocity magnitudes, blue colored regions denote low velocities while the regions between red and blue color denotes the intermediate velocity magnitudes. The highest velocities are observed near the tip of the kneading disk, while velocities are lowest near the walls. Fig. 5.5(b) shows the

velocity vectors in 3-D horizontal cross section made at the middle of the vessel. The vectors point in the direction of liquid velocity at the point where they originate. The length of the vectors is proportional to the magnitude of the liquid velocity. The flow is weak near the walls and strong around the kneading disks. It is also found in both the plots that the regions with low velocities are minor and hence the high mixing behaviour of kneading element is justified.

(a)   (b)
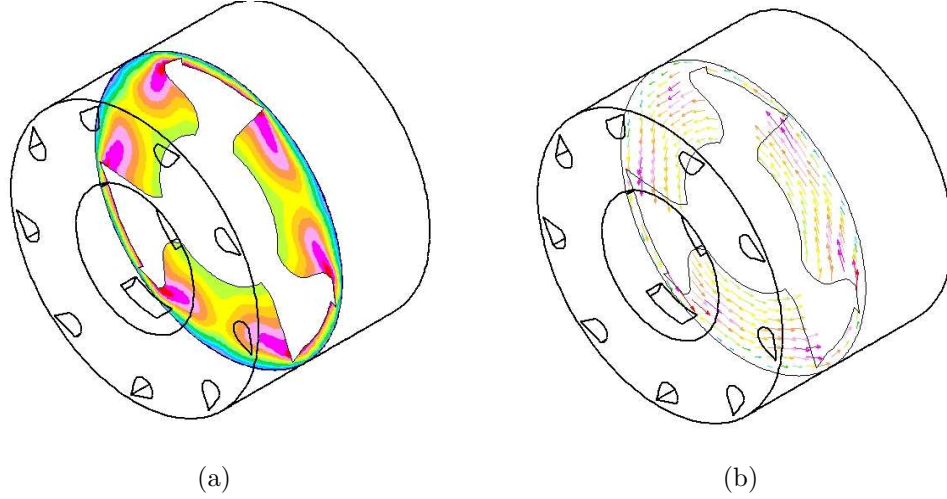
Figure 5.5: Horizontal section plots of velocity fields. (a) Contour plot and (b) vector plot.

5.3.2 Mixing Quality

It follows the same method as discussed in previous chapter. In order to quantify the homogeneity of a mixture, a statistical analysis of the concentration in samples from the mixture, which is based on Danckwert's intensity of segregation concept [16] can be used. The intensity of segregation approach is based on the variance of the concentration at different regions in space with respect to the mean concentration. In the case of massless tracer particles, a number based variance is calculated by dividing whole computational domain into small compartments. The intensity of segregation is then variance divided by its maximum value.

An intensity value of 1 corresponds to complete segregation and a value of 0 in-
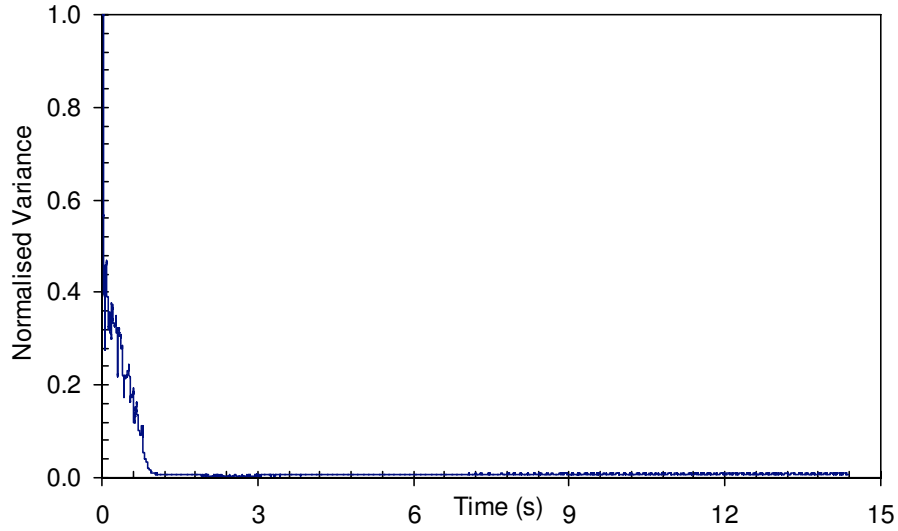
Figure 5.6: Time evolution of normalised variance for kneader element with 1600 particles and 64 compartments.

dicates complete mixing. To determine the mixing quality, the most important task was to compute the tracer particles trajectories. This has been usually done based on the velocity integration over time. To do this, total computational domain was divided into 64 compartments (sub-volumes) of approximately equal volume and 1600 particles are randomly distributed initially in one of the compartments. Then the variance and also the intensity of segregation is computed. The results obtained are presented in Fig. 5.6 where the evolution of intensity of segregation is plotted against time. The value of I_s starts at 1 where the particles are completely segregated and reaches close to zero corresponding to the optimal dispersion. It can be seen that the intensity of segregation is decreasing in unordered manner with random periods at the beginning of the simulation. This is due to the fact that the tracer particles are still need to undergo significant stretching. It can also be observed that the level off of the intensity of segregation curve occurs at time 8s. This time can be defined as the mixing time as it indicates when the tracer concentration stabilizes. The intensity of segregation values after reaching this mixing time is $\epsilon = 0.05$. However, we still can go below this value to about $\epsilon = 0.007$, but again the intensity of segregation starts

to increase.

5.4   Mapping Method

In the following section, mapping matrix approach is described for the simulation of mixing in a specific kneader element. The method is based on a spatial discretization of the locally averaged concentration of fluid components in the mixture. A distribution matrix, that describes the changes in a component concentration, is composed. This mapping matrix approach makes it possible to rapidly predict the mixing performances. Introduction and basic principle of this approach is given in the following subsection.

5.4.1   Introduction

As already mentioned in the previous chapters, mixing of fluids is a topic of significant interest, because of wide applications in process industries. One of the simple but important class of mixing phenomena is laminar mixing. Inspite of considerable achievements in the understanding of its mechanisms, numerical mixing remains computationally expensive and requires special methods. Further, determination of the accurate velocity field is a very important step. Once the velocity field is known, a variety of techniques is available to study mixing based on the tracking of deforming individual fluid volumes such as front capturing and front tracking. Front capturing technique describe the advection of a special material function and accordingly use post-processing techniques to restore the interface shape. In contrast to this, front tracking techniques rely on an explicit description of the interface shape for which an auxiliary surface mesh is used. This approach yields an accurate description of strongly deforming fluid volumes and is capable to deal with the mixing of different fluids (distributive mixing). But the amount of data produced increases exponentially in case of efficient mixing flows. Most spatially bound mixing flows exhibit temporal or spatial periodicity, dynamical system methods [58] such as Poincaré maps, peri-

odic points and analysis of their manifolds are useful. Poincaré maps help to reveal zones of chaotic mixing and regular motion where as periodic points are regarded as chaos or regularity. However, they do not provide information on the rate of mixing and concentration distribution. Numerical tracer experiments are of increasing importance to analyze mixing, but the accurate solution is spoiled by numerical diffusion. Lagrangian particle tracking can give the particle distribution concentration during the course of the mixing, but requires lot of computational memory and time. A way to avoid these problems is using of mapping matrix method.

Since chaotic mixing of viscous liquids in laminar flows (ex. kneaders, static and micro mixers) is usually based on the situation where the Baker's transformation is applied a number of times on a specified volume of material, distribution of material in such flows can be handled quite well by distribution matrix method. The mapping method is essentially the transport of a conservative quantity by means of mapping matrix, describing the transport of fluid from an initial cross section to final one in the case of space periodic flows or from an initial time to final time in the case of time periodic flow (in the present case). The advantage of using mapping method is that it requires just one-time computation of the deformation induced by the flow during fixed flow in time Δt and the effect of flow for any number of combination of cycles can then be evaluated by a repeated multiplication of the distribution matrix with a prescribed initial concentration distribution vector. Since these multiplications take only a few CPU seconds, this brings a huge benefit over conventional tracking method in which the tracking is repeated from the first to last period to analyze mixing which results in lot of computational time. The basics and the mechanism of the mapping method is described below.

5.4.2 Basic formulation

Laminar, highly viscous liquid mixing is typically based on a repetetion of the same motion characterized by three simple steps: streching, cutting and folding a specified volume of material. The dustribution of the material in such flows can be handled
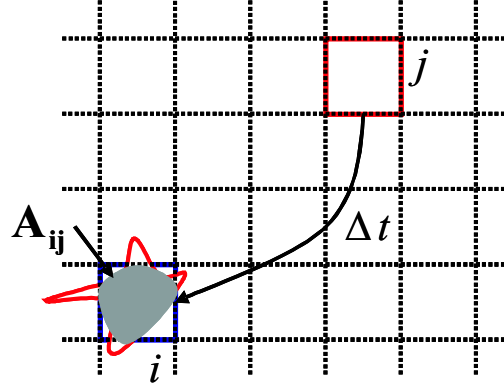
Figure 5.7: Schematic of the mapping matrix method: stretching of fluid element.

quite well by the use of mapping matrix methods as originally proposed by [71] and
was redefined in a computationally efficient way by [37]. In this section we describe the
formulation of mapping method by considering two cases. One is based on the tracking
of boundaries of a sub-volumes which cover the entire fluid volume and the other is
based on the tracking of particles in the compartments of the complete computational
domain.

Case-1: Let us consider an arbitrary fluid region V is divided into a number of
sub-regions V_k that covers the entire fluid volume. The boundaries of the sub-voulmes
are tracked from $t = t_0$ to $t = t_0 + \Delta t$. The two grids are superimposed (Fig. 5.7) and
the intersection $\mathbf{A}_{ij}$ is computed as:

$$\mathbf{A}_{ij} = \int_{V_j(t=t_0+\Delta t) \bigcap V_i(t=t_0)} dS / \int_{V_j(t=t_0)} dS \,, \tag{5.2}$$

where $\mathbf{A}_{ij}$ is the fraction of sub-volume V_j at $t = t_0$, that is tracked to $t = t_0 + \Delta t$ and
found in the sub-volume V_i. These intersections are stored in a matrix called mapping
matrix or distribution matrix $\mathbf{A}$. To obtain the intersection points of the distribution
matrix, the total cross section of the flow domain is sub-divided into a large number of
discrete cells (N) of identical cells. During the flow, the material from a donor cell is
advected to different recipient cells. The fraction of material that is transferred from
the donor cell to a recipient cell gives the distribution coefficient of the donor cell with
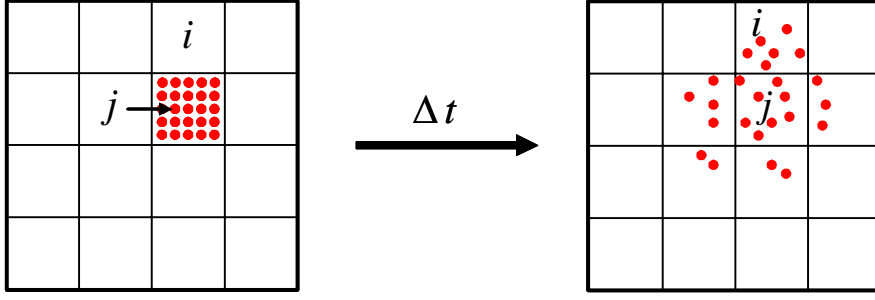
Figure 5.8: Schematic of the mapping matrix method: particle distribution.

respect to the recipient cell. Therefore, in total N cells from mapping matrix $\mathbf{A}$ of the order NXN. For further information on this method please refere to [37]. But tracking all interfaces of all N cells during a flow over a time Δt is cumbersome to track interfaces experiencing complicated deformation patterns. Thus, an alternative approach that is much simpler is presented below.

Case-2: Similar manner is followed as above to generate a mapping matrix using particles number concentrations to compute variance. A detailed formulation of the mapping method based on the particle number concentration is given in [68]. In this case, the coefficients of the mapping matrix $\mathbf{A}$ are calculated in the formulation given here. A schematic representation of the particle distribution in the sub-volumes are shown in Fig. 5.8. Particles inside all sub-volumes are tracked to approximate the coefficients of $\mathbf{A}$. The particles are uniformly distributed in the sub-volumes. If the number of particles in sub-volume V_j is B_j at $t = t_0$ and the number of particles found after tracking in the sub-volume V_i is B_{ij} at $t = t_0 + \Delta t$, then the mapping coefficient $\mathbf{A}_{ij}$ is computed as:

$$\mathbf{A}_{ij} = \frac{B_{ij}}{B_j} \; . \tag{5.3}$$

In general, the coefficient $\mathbf{A}_{ij}$ is the measure of the fraction of total flux of the sub-volume V_j donated to the sub-volume V_i. Since the majority of the efficient mixers show periodicity either in space or time, the same matrix is repeated with itself to obtain $\mathbf{A}^n$ in order to account for the periodicity of the flow as suggested by [71].

By studying the properties of $\mathbf{A}^n$, mixing can be analyzed by its evolution in time or space. However, this procedure is not so attractive and feasible especially in 3D-situation where $\mathbf{A}^n$ (dense matrix) generates large data and hence require huge storage capacity. Instead of analyzing the evolution of the matrix, the concentration C of a fluid in each sub-volume is computed as proposed by [24, 37, 38]. Thus, alternatively C^n is computed by the sequence for $i=1$ to n:

$$C^i = \mathbf{A}\, C^{i-1}\,. \tag{5.4}$$

This procedure eliminates the necessity to compute $\mathbf{A}^n$ and therefore, much cheaper in numbers of operations as well as computer memory. The mapping matrix calculations are easily parallelized [23].

5.4.3   Application to a Kneader Element

Here, we consider unit cell of a single shaft specific kneader element for the application of mapping method. First, computations are performed using 1600 mass-less particles placed initially in one of the 64 sub-volumes (compartments) and collected information regarding the particle distribution in each compartment at regular time intervals. Once all the compartments are occupied with approximately equal number of particles, simulations restarted and tracked the trajectories of each particle. Each particle can be identified with particle ID number. This means, for example a particle with number 1 in compartment 1 at $t = t_0$, advected to some other compartment after $t = t_0 + \Delta t$. Here, Δt can be the time required for one or and one-third rotation of the impeller. Likewise, positions of all 1600 particles are identified after one rotation and stored them in a matrix of an order 64X64. The stored data contains one starting position and the end position for each numbered particle. Matrix coefficients are created by comparison of starting and ending position. For every particle starting in compartment m and reaching the compartment n, the coefficient in the mapping matrix is raised by one. Then, each row of the matrix is normalized with the total number of particles in the complete row. Multiplication of the resultant matrix with the matrix vector

Figure 5.9: Time evolution of variance in a kneader element: Comparison of simulated data with data obtained from mapping matrix.

containing single distribution (at $t = 0$, single column matrix) yields mapping matrix. First case, time evolution of variance is computed with the use of the resulting mapping matrix at this particular time step. This procedure is repeated without using CFD software further to obtain the variance at each time step for up to 10 rotations. On the other hand, CFD simulation is performed for the same case file and computed the time evolution of variance for each rotation of the impeller. Fig. 5.9 verifies the variance values computed using mapping matrix method and simulation using CFD software. The solid line represent the variance values obtained using tracking where as the points correspond to mapping. In this case, mapping matrix at corresponding rotation is multiplied with the matrix from the previous rotation.

Next, we consider the mapping matrix obtained only after one rotation and used to compute the particle distribution with base matrix with a vector containing the initial distribution. The distribution after n rotations can be obtained by multiplying the initial distribution vector with the matrix for n times. Although one can use every desired initial position of the particles, simulation data by tracking is needed for comparison. The comparison of the time evolution of normalised variance computed

Figure 5.10: Time evolution of normalised variance in a kneader element. Comparison of simulated data with data obtained from mapping matrix after every rotation of the impeller.

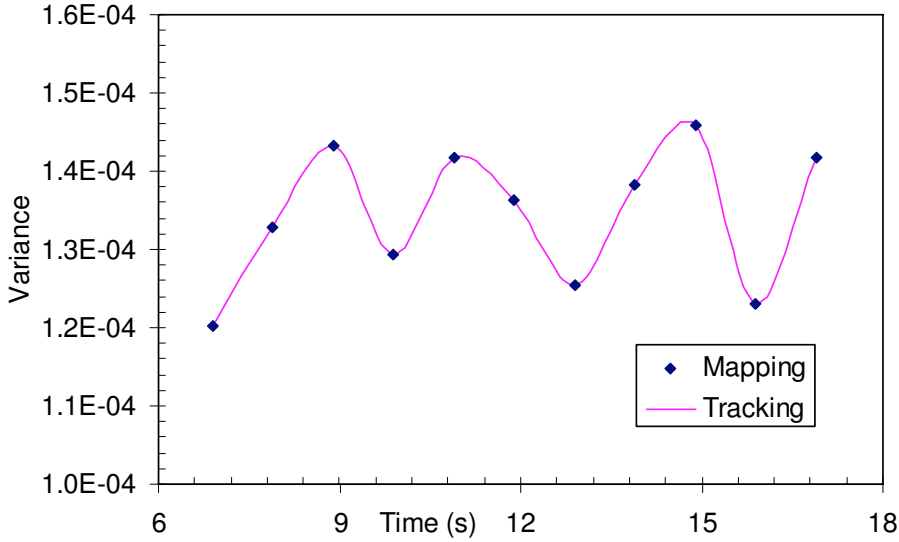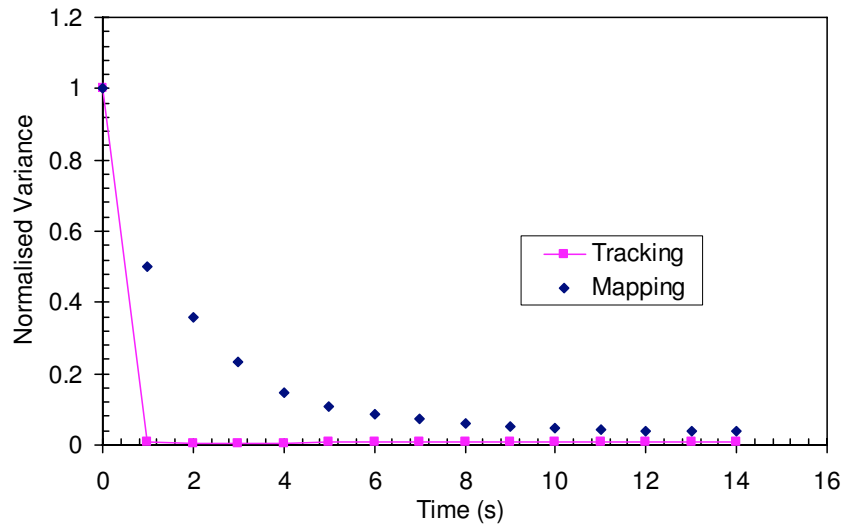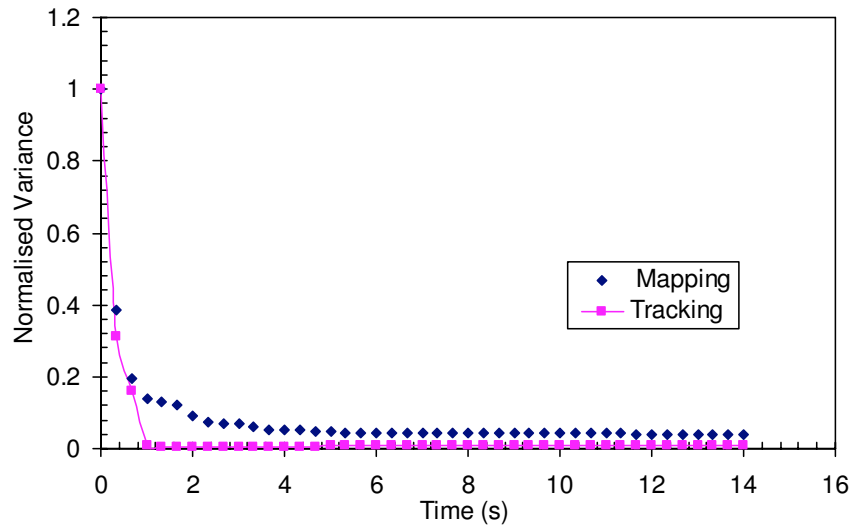Figure 5.11: Time evolution of normalised variance in a kneader element. Comparison of simulated data with data obtained from mapping matrix after every one-third rotation of the impeller.

based on mapping method and CFD simulation is shown in Fig. 5.10. Each marked point in this figure represents corresponding values at each rotation of the impeller. In this case one rotation needs one second of real time. It can be seen that, the normalised variance computed based on mapping method deviates at the beginning but afterwards approaches the CFD simulation values.

Fig. 5.11 shows the time evolution of normalised variance computed based on mapping method and CFD simulation. Each marked point in this figure represents corresponding values at each one third rotation of the impeller. Based on the geometrical configuration of this particular kneader element we assume that the flow is periodic after each one third rotation. It can be observed here that, the deviation between the normalised variance computed based on mapping matrix and simulation, is minimised. However, this deviation is caused by the different flow fields used for mapping and tracking. The tracking data us created by introducing the particles at $t = 0$ and then start the run. Where as the mapping data is created for the simulation after the particles are uniformly distributed (after few impeller rotations) inside all compartments. This means the flow field used for mapping is developed and the flow field used for tracking is transient.

This is verified from the computations from Maxisch [52]. In Fig. 5.12 four data sets Matrix1, Matrix2,... can be seen. Each data set represents the time evolution of normalised variance for 1600 particles initially placed in one compartment. The difference here is the creation of the matrix. All matrices are created for initially randomly placed particles. The Matrix1 is created after the first rotation, Matrix2 is created after the second rotation and so on. As one can see, the ability of mixing decreases when the flow field develops. In the simulation of the current thesis, the mapping data is generated for a developed flow which according to the Fig. 5.12, shows lower mixing effect. So the deviation between mapping and tracking (Fig. 5.10, Fig. 5.11) can be seen. Better would be to compare tracking and mapping data for either constant flow field or for transient flow field. In Fig. 5.13, the comparison of tracking and mapping data was done for transient flow field. The agreement between
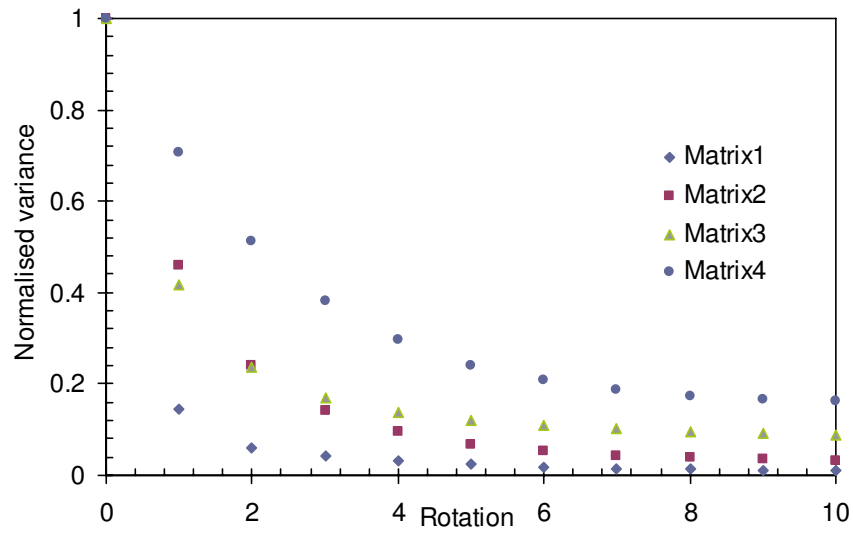
Figure 5.12: Time evolution of normalised variance in a kneader element. Effect of mapping matrices [52].
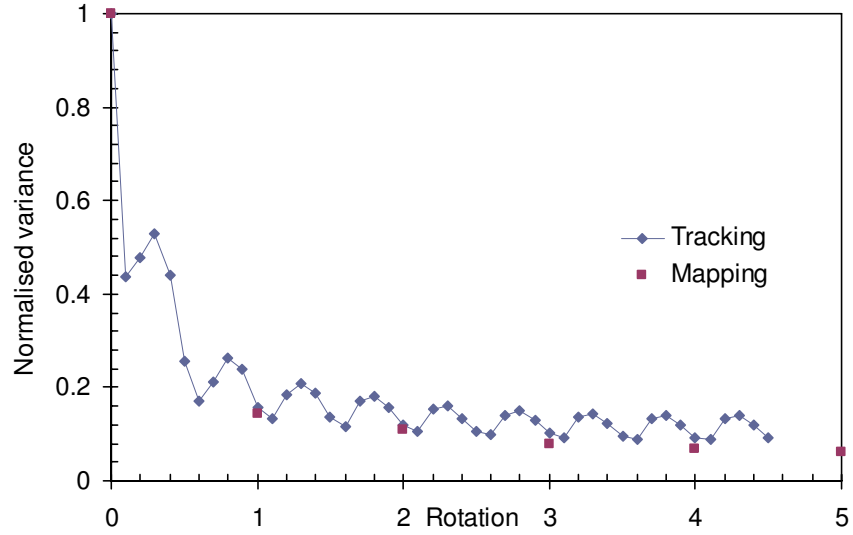
Figure 5.13: Time evolution of normalised variance in a kneader element. Comparison of simulated data with data obtained from mapping matrix [52].

tracking and mapping data is very good. The evolution of normalised variance is not decreasing as much as in the current thesis since the boundary conditions of the simulations [52] are different in this particular case.

Thus, it can be concluded here that the mapping method is used to analyze the mixture quality and optimize the mixers with less efforts since the matrix-vector multiplications only take a few seconds on a personal computer. Therefore, mapping method can be used as an alternative engineering tool to conventional mixing measures.

Chapter 6

Conclusions and Outlook

Modeling and simulation of mixing in stirred vessels is very challenging task because of complex design of impellers. It will be further complicated if the operation involves highly viscous medium. The present contribution addressed the problems showed up during the numerical simulation of highly viscous liquid mixing and recommended a novel approach to overcome it.

Since this study deals with mixing in stirred vessels, various possible numerical methods were discussed and validated by applying them to a simple rotating reference goemetry. The two well known, rotating reference frame and moving mesh simulations were explained comprehensively and discussed the advantages and disadvantages. These two methods were employed on a model geometry and showed that they both yield the same results. Further simulations were accomplished using the rotating reference frame, because the efforts needed to set up rotating reference frame are less compared with the moving mesh case set up and also moving mesh calculations needs longer computational time. Additionally, a test case simulations were performed in a flow between two concentric rotating cylinders (Couette-flow) to assess the capabilities of Star-CD in handling highly viscous liquids. The torque computations for highly viscous liquids in Coette-flow show remarkable agreement with the analytical calculations.

Volume of Fluid (VOF) simulations in a partly filled anchor mixer reveals the flow

field distribution inside the mixing domain. The results show high velocity magnitudes around the anchor arms as the flow is purely induced by the impeller. High pressure in the front and low pressure behind the anchor arms attributes to the maximumu forces acting on anchor arms against the flow. In addition, the systematic procedure to calculate torque and power number in rotating systems is given with detailed mathematical expressions. Time evolution of torque in anchor mixer is shown for highly viscous liquids Newtonian. The results show that torque is maximum at the onset of motion due to the fluid at rest. However, it decreases abruptly and attains constant value within a short period of time. Further, torque computations at different viscosities also presented and discussed. It has to be noted that the power number calculation also show the similar trend as torque, since power number is a function of torque for a particular geometrical design.

Since the past two decades CFD has become a widely used tool for analysing, optimising and supporting the design of mixing processes. There exists several ways for the numerical investigation of mixing in stirred vessels. The well known among them are numerical tracer experiments, Lagrangian particle tracking and entropy based measures. While numerical tracer experiments are of increasing importance as a means to analyse mixing processes, there is a principle problem which is the so-called numerical diffusion, i.e. the artificially generated smoothing of a tracer profile due to errors from the discretization, and this numerical diffusion can be much stronger than the true physical diffusion. The effect of numerical diffusion was accentuated with a proto type lid driven cavity flow and highlighted the influence of solver settings and grid refinement. A way to avoid this problem is to replace the continuous tracer concentration by a number concentration obtained from Lagrangian (i.e. inertia free) particles that are tracked during the simulation. This approach does not suffer from artificial diffusion, since the position of tracer particles can be resolved with sub-grid-scale accuracy and the velocity field at these particle positions can be obtained by interpolation from its values at grid points.

In this investigation, the method of calculating intensity of segregation and hence

the intensity of mixing and mixing time are discussed based on the Lagrangian particle tracking method. The total computational domain is divided into smaller compartments (sub-volumes) and particles are initially placed in one compartment, say. During the process of particle tracking the resulting number concentrations are recorded and allow for computation of the evolution of its variance. A fundamental question in this approach is how many compartments and particles are needed for a reliable assessment of the mixing quality. Based on elementary statistics, it can be shown that a reliable mixing time $t_M^{1-\tau}$ for a given level $\epsilon > 0$ requires $100/\epsilon^2$ particles (if standard deviations instead of variances are employed) while a surprisingly small number of about 20 compartments is sufficient.

This method has been evaluated using the numerical investigation of mixing in a vessel stirred with an anchor impeller as well as a specific kneader element. It was shown that even after a very long and expensive simulation, anchor mixer exhibits poor mixing behaviour. It is known that anchor is very good for heat transfer between vessel wall and fluid rather than its mixing capabilities. However, the simulations in a specific kneader shows its excellent mixing characteristics within a short time. It is due to the complex impeller design with pins on the kneading discs. It is believed that the material inside the mixing chamber undergoes Baker transformation i.e., stretching and folding.

Finally, we elaborated a mapping method to evaluate the quality of mixing. This mapping method employs a transition matrix, which describes how many particles are advected from one sub-volume to the other sub-volume in a particular period of time. With the aid of this transition matrix one can compute variance evolutions and mixing times using matrix-vector multiplications with significantly less computational effort. Preliminary results of mapping method for a kneader element are discussed and compared with the simulation results. The evolution of variance from both methods (simulation and mapping) show good agreement between them. Therefore, the mapping method can be considered as an engineering tool to analyze the mixture quality and optimize the mixers within few seconds on a personal computer. Nevertheless,

CFD simulation is performed to get the approximately equal particle distribution in each compartments after one rotation.

In the present numerical investigations, it has been showed that Lagrangian particle tracking method is a novel approach to assess the mixing quality. The initial position of blob of particles can be varied and checked for the influence on mixing characteristics. Here, we restricted ourself to simple geometries. Generally, computation of mixing mechanisms in kneaders are difficult. Single shaft kneaders can be calulated using appropriate moving or rotating reference frame as shown in this work. But, the flow computation in double shaft kneaders cannot be modelled using the sliding mesh technique because of the ovelapping of kneading discs as well as the close clearance kneading pins. New techniques have been developed recently for the numerical treatment of overlapping meshes. The above mentioned Lagrangian particle tracking method can be extended to investigate mixing in double shaft kneaders and also twin srew extruders.

Bibliography

[1] *User Guide: Star-CD v 3.22, CD-Adapco (2004).*

[2] ABID, M., XUEREB, C., AND BERTRAND, J. Hydrodynamics in vessels stirred with anchors and gate agitators: Necessity of a 3-d modelling. *Trans IChemE 70* (1992), 377–384.

[3] ANDERSON, F. B. *U.S. Patent* (1930).

[4] ANDERSON, J. D. *Computational Fluid Dynamics: The basics with applications.* McGraw-Hill, Inc., 1995.

[5] APRUZZESE, F., PATO, J., BALKE, S. T., AND DIOSADY, L. L. In-line measurement of residence time distribution in a co-rotating twin-screw extruder. *Food Research International 36* (2003), 461–467.

[6] AUBIN, J., AND XUEREB, C. Design of multiple impeller stirred tanks for the mixing of highly viscous fluids using cfd. *Chem. Eng. Sci. 61* (2006), 2913–2920.

[7] AVALOSSE, T., AND RUBIN, Y. Analysis of mixing in corotating twin screw extruders through numerical simulation. *Int. Poly. Process. XV-2* (2000), 117–123.

[8] BARAILLER, F., HENICHE, M., AND TANGUY, P. A. Cfd analysis of a rotor-stator mixer with viscous fluids. *Chem. Eng. Sci. 61* (2006), 2888–2894.

[9] BECKNER, J. L., AND SMITH, J. M. Anchor-agitated systems: Power input with newtonian and pseudo-plastic fluids. *Trans. Instn. Chem. Engrs. 44* (1966), T224–T236.

[10] BERTRAND, F., TANGUY, P. A., AND BRITO-DE LA FUENTE, E. A new perspective for the mixing of yield stress fluids with anchor impellers. *Journal of Chemical Engineering of Japan 29* (1996), 51–58.

[11] BIRD, R. B., STEWART, W. E., AND LIGHTFOOT, E. N. *Transport Phenomena.* Wiley, 1962.

[12] BOSS, J. Evaluation of the homogeneity degree of a mixture. *Bulk Solids Handling 6 6* (1986), 1207–1215.

[13] BOTHE, D. *Lecture Notes: Modelling of Chemical Reaction Systems.* University of Paderborn, WS 2004/05.

[14] BOTHE, D., AND WARNECKE, H.-J. Berechnung und beurteilung strömungs-basierter komplex-laminarer mischprozesse. *Chem. Ing. Tech. 79* (2007), 1001–1014.

[15] CARNEIRO, O. S., COVAS, J. A., FERREIRA, J. A., AND CERQUEIRA, M. F. On line monitoring of the residence time distribution along a kneading block of a twin screw extruder. *Polymer Testing 23* (2004), 925–937.

[16] DANCKWERTS, P. V. The definition and measurement of some characteristics of mixtures. *Appl. Sci. Res. A3* (1952), 279–296.

[17] DE GRAAF, R. A., ROHDE, M., AND JANSSEN, L. P. B. M. A novel model predicting the residence time distribution during reactive extrusion. *Chem. Eng. Sci. 52* (1997), 4336–4345.

[18] DEMIRDZIC, I., AND PERIC, M. Space conservation law in finite volume calculations of fluid flow. *Int. J. Num. Meth. Fluids 8* (1988), 1037–1050.

[19] EBRAHIMI-MOSHKABAD, M., AND WINTERBOTTOM, J. M. The behaviour of an intermeshing twin screw extruder with catalyst immobilised screws as a three phase reactor. *Catalysis Today 48* (1999), 347–355.

[20] ELEMANS, P. H. M., AND MEIJER, H. E. On the modeling of continuous mixers. part ii: The cokneader. *Poly. Eng. Sci. 30* (1990), 893–904.

[21] FERZIGER, J. H., AND PERIC, M. *Computational Methods for Fluid Dynamics.* Springer, 1999.

[22] FOGIEL, M. *The transport phenomena problem solver: Momentum, Mass and Energy.* Research and Education Association, 1986.

[23] GALAKTIONOV, A. S., ANDERSON, A. D., AND PETERS, G. W. M. Mixing simulations: tracking strongly deforming fluid volumes in 3d flows. In *M Bubak JD, Wasniewski J (eds) Lecture notes in computer science, volume 1332 of Recent advances in parallel virtual machine and message passing interface. Springer, Heidelberg. 463-469* (1997).

[24] GALAKTIONOV, O. S., ANDERSON, P. D., KRUIJT, P. G. M., PETERS, G. W. M., AND MEIJER, H. E. M. A mapping approach for three-dimensional distributive mixing analysis. *Computers & Fluids 30* (2001), 271–289.

[25] GASPAR-CUNHA, A., POULESQUEN, A., VERGNES, B., AND COVAS, J. A. Optimization of processing conditions for polymer twin-screw extrusion. *Int. Poly. Process. XVII-3* (2002), 201–213.

[26] GIGUERE, R., BERTRAND, F., AND TANGUY, P. A. A three-dimensional mesh refinement strategy for the simulation of fluid flow with fictitious domain method. *Comp. & Chem. Eng. 30* (2006), 453–466.

[27] GLOWINSKI, R., PAN, T., AND PERIAUX, J. A fictitious domain method for dirichlet problem and applications. *Comp. Meth. Appl. Mech. Eng. 111* (1994), 283–303.

[28] GLOWINSKI, R., PAN, T.-W., HELSA, T., AND JOSEPH, D. A distributed lagrange multiplier/fictitious domain method for particulate flows. *Int. J. Multiphase Flows 25 25* (1999), 755–794.

[29] GREBE, T. *Simulation und Modellierung des Mischverhaltens von Taylor-Couette Reaktoren.* PhD thesis, University of Paderborn, 2004.

[30] HADZIC, H. *Development and Application of a Finite Volume Method for the Computation of Flows Around Moving Bodies on Unstructured, Overlapping Grids.* PhD thesis, Technical University of Hamburg-Harburg, 2005.

[31] HARNBY, N., EDWARDS, M. F., AND NIENOW, A. W. *Mixing in the Process Industries.* Butterworth-Heinemann, 1992.

[32] IRANSHAHI, A., HENICHE, M., BERTRAND, F., AND TANGUY, P. A. Numerical investigation of the mixing efficiency of the ekato paravisc impeller. *Chem. Eng. Sci. 61* (2006), 2609–2617.

[33] KAMINOYAMA, M., ARAI, K., AND KAMIWANO, M. Numerical analysis of power consumption and mixing time for a pseudoplastic liquid in geometrically similar stirred vessels with several kinds of plate-type impellers. *Journal of Chemical Engineering of Japan 27* (1994), 17–24.

[34] KAMINOYAMA, M., SAITO, F., AND KAMIWANO, M. Flow analogy of pseudoplastic liquid in geometrically similar stirred vessels based on numerical analysis. *Journal of Chemical Engineering of Japan 23* (1990), 214–221.

[35] KANG, T. G., AND KWON, T. H. Colored particle tracking method for mixing analysis of chaotic mixers. *Journal of Micomech. Microeng. 14* (2004), 891–899.

[36] KRESTA, S. M., KREBS, R., AND MARTIN, T. Review: The future of mixing research. *Chem. Eng. Tech. 27* (2004), 208–214.

[37] KRUIJT, P. G. M. *Analysis and optimization of laminar mixing: design, development and application of the mapping method.* PhD thesis, Eindhoven Universtiy of Technology, 2000.

[38] KRUIJT, P. G. M., GALAKTIONOV, O. S., ANDERSON, P. D., PETERS, G. W. M., AND MEIJER, H. E. M. Analyising fluid mixing in periodic flows by distribution matrices: the mapping method. *AIChE Journal 47* (2001), 1005–1015.

[39] KURIYAMA, M., INOMATA, H., ARAI, K., AND SAITO, S. Numerical solution for the flow of highly viscous fluid in agitated vessel with anchor impeller. *AIChE Journal 28* (1982), 385–391.

[40] LACELY, P. M. C. Development in the theory of particle mixing. *Journal of Applied Chemistry 4* (1954), 257–268.

[41] LEONARD, B. P. A stable and accurate convective modelling procedure based on quadratic upstream interpolation. *Comp. Meth. Appl. Mech. Eng. 19* (1979), 59–98.

[42] LERTWIMOLNUN, W., AND VERGNES, B. Effect of processing conditions on the formation of polypropylene/organoclay nanocomposites in a twin screw extruder. *Poly. Eng. Sci. 46* (2006), 314–323.

[43] LIST, H. *Swiss Patent* (1945).

[44] LIU, W., AND HALLER, G. Strange eigenmodes and decay of variance in the mixing of diffusive tracers. *Physica D 188* (2004), 1–39.

[45] LYU, M. Y., AND WHITE, J. L. Models of flow and experimental studies on a modular list/buss kneader. *Int. Poly. Process. 10* (1995), 305–313.

[46] LYU, M. Y., AND WHITE, J. L. Modeling of a viscous non-newtonian polymer melt in a list/buss kneader and comparison to experiment. *Int. Poly. Process. 11* (1996), 208–221.

[47] Lyu, M. Y., and White, J. L. Simulation of linear viscoelastic flow behavior in the buss kneader. *Poly. Eng. Sci. 37* (1997), 623–635.

[48] Lyu, M. Y., and White, J. L. Simulation of non-isothermal flow in a modular buss kneader and comparison with experiment. *Int. Poly. Process. 12* (1997), 104–109.

[49] Lyu, M. Y., and White, J. L. Residence time distribution and basic studies of flow and melting in a modular buss kneader. *Poly. Eng. Sci. 38* (1998), 1366–1377.

[50] Mackley, M. R., and Saraiva, R. M. C. N. The quantitative description of fluid mixing using lagrangian- and concentration-based numerical approaches. *Chem. Eng. Sci. 54* (1999), 159–170.

[51] Maridass, B., and Gupta, B. R. Performance optimization of a counter rotating twin screw extruder for recycling natural rubber vulcanizates using response surface methodology. *Polymer Testing 23* (2004), 377–385.

[52] Maxisch, T. Private communication. Tech. rep., Institute of Technical Chemistry and Chemical Process Engineerng, University of Paderborn, 2008.

[53] Mehranpour, M., Nazokdast, H., and Dabir, B. Computational study of the velocity field in the conveying element of a ko-kneader with cfd method. *Int. Poly. Process. 17* (2002), 108–114.

[54] Meijer, H. E., and Elemans, P. H. M. The modeling of continuous mixers. part i: The corotating twin-screw extruder. *Poly. Eng. Sci. 28* (1988), 275–290.

[55] Mezaki, R., Mochizuki, M., and Ogawa, K. *Engineering data on mixing.* Elsevier, 2000.

[56] Motzigemba, M., Bothe, D., Broecker, H.-C., Prüss, J., and Warnecke, H.-J. A contribution to simulation of mixing in screw extruders em-

ploying commercial cfd-software. In *10th European conference on mixing, Delft* (2000).

[57] MURALIDHAR, K., AND BISWAS, G. *Advanced Engineering Fluid Mechanics.* Narosa Publishing House, 1999.

[58] OTTINO, J. M. *The kinematics of mixing: streching, Chaos, and Transport.* Cambridge University Press, Cambridge, 1989.

[59] PEDROSA, S. M. C. P., AND NUNHEZ, J. R. The behavior of stirred vessels with anchor type impellers. *Comp. & Chem. Eng. 24* (2000), 1745–1751.

[60] PETERS, D. C., AND SMITH, J. M. Fluid flow in the region of anchor agitated blades. *Trans. Instn. Chem. Engrs. 45* (1967), T360–T366.

[61] PHELPS, J., AND TUCKER III, C. L. Lagrangian particle calculations of distributive mixing: Limitations and applications. *Chem. Eng. Sci. 61* (2006), 6826–6836.

[62] PRAT, L., GUIRAUD, P., RIGAL, L., AND COURDON, C. Two phase residence time distribution in a modified twin screw extruder. *Chem. Eng. Processing 38* (1999), 73–83.

[63] PUAUX, J. P., BOZGA, G., AND AINSER, A. Residence time distribution in a corotating twin-screw extruder. *Chem. Eng. Sci. 55* (2000), 1641–1651.

[64] SCHÜTZ, S., BIERDAL, M., AND PIESCHE, M. Charakterisierung des mischverhaltens von gegenstrom-injektions-mischern. *Chem. Ing. Tech. 77* (2005), 398–405.

[65] SECK, O., AND MAXISCH, T. Verfahrenstechnische charakterisierung eines kneters. Master's thesis, University of Paderborn, 2006.

[66] SEIDEL, W. Note on a metrically transitive system. In *Proceedings of National Academy of Science USA 19* (1933).

[67] SHON, K., CHANG, D., AND WHITE, J. L. A comparative study of residence time distribution in a kneader, continuous mixer, and modular intermeshing co-rotating and counter rotating twin screw extruders. *Int. Poly. Process. 14* (1999), 44–50.

[68] SINGH, M. K., KANG, T. G., MEIJER, H. E. H., AND ANDERSON, P. D. The mapping method as a toolbox to analyze, design, and optimize micromixers. *Microfluidics and Nanofluidics DOI 10.1007/s10404-007-0251-7.*

[69] SOMBATSOMPOP, N., AND PANAPOY, M. Comments on temperature profiles of pp melt in the barrel of a twin screw extruder. *Polymer Testing 20* (2000), 217–221.

[70] SOMMERFELD, M., AND DECKER, S. State of the art and future trends in cfd simulation of stirred vessel hydrodynamics. *Chem. Eng. Tech. 27* (2004), 215–224.

[71] SPENCER, R. S., AND WILEY, R. M. The mixing of very viscous liquids. *Journal of Colloid Science 6* (1951), 133–145.

[72] SPURK, J. H., AND AKSEL, N. *Strömungslehre.* Springer, 2005.

[73] STUBER, N. P., AND TIRRELL, M. Continuous polymerization studies in a twin screw extruder. *Poly. Proc. Eng. 3* (1985), 71–83.

[74] SUMI, Y., AND KAMINAWO, M. Development and mixing characteristics of a multistage impeller for agitating highly viscous fluids. *Journal of Chemical Engineering of Japan 34* (2001), 485–492.

[75] THIFFEAULT, J.-L. Scalar decay in chaotic mixing. transport in geophysical flows: Ten years after. In *Proceedings of the Grand Combin Summer School* (2004).

[76] TROLESTRA, E. J., VAN DIERENDRONCK, L. L., AND JANSSEN, L. P. B. M. Modeling of a buss-kneader as a polymerization reactor for acrylate. parti: Model validation. *Poly. Eng. Sci. 42* (2002), 230–239.

[77] Trolestra, E. J., Van Dierendronck, L. L., and Janssen, L. P. B. M. Modeling of a buss-kneader as a polymerization reactor for acrylate. partii: Methyl methacrylate based resins. *Poly. Eng. Sci. 42* (2002), 240–247.

[78] Unlu, E., and Faller, J. F. in twin screw food extrusion. *Journal of Food Engineering 53* (2002), 115–131.

[79] van Zuilichem, D. J., Kuiper, E., Stolp, W., and Jager, T. Mixing effects of constituting elements of mixing screws in single and twin screw extruders. *Powder Technology 106* (1999), 147–159.

[80] Vanyo, J. P. *Rotating Fluids in Engineering and Sciences.* Butteworth-Heinemann, 1993.

[81] Versteeg, H. K., and Malalasekara, W. *An Introduction to Computational Fluid Dynamics.* Longman Scientific & Technical, 1995.

[82] Wang, W., Manas-Zloczower, I., and Kaufman, M. Entropic characterisation of distributive mixing in polymer processing equipment. *AIChE Journal 49* (2003), 1637–1644.

[83] White, J. L., and Potente, H. *Screw Extrusion.* Carl Hanser Verlag, 2003.

[84] Wurster, C. *German Patent* (1901).